GL02145

USGS-OFR-96-28

U.S. DEPARTMENT OF THE INTERIOR
U.S. GEOLOGICAL SURVEY

HYBRID-SOURCE SEISMIC REFLECTION PROFILING ACROSS YUCCA MOUNTAIN, NEVADA: REGIONAL LINES 2 and 3

By

Thomas M. Brocher[1], Patrick E. Hart[2], W. Clay Hunter[3], and Victoria E. Langenheim[4]

Open-File Report 96-28

[1]U.S. Geological Survey, 345 Middlefield Road, M/S 977, Menlo Park, CA 94025
[2]U.S. Geological Survey, 345 Middlefield Road, M/S 999, Menlo Park, CA 94025
[3]U.S. Geological Survey, 755 Parfet Street, M/S 425, Lakewood, CO 80215
[4]U.S. Geological Survey, 345 Middlefield Road, M/S 989, Menlo Park, CA 94025

Prepared in Cooperation with the
Nevada Operations Office
U.S. Department of Energy
(Interagency Agreement DE-A108-92NV10874)

Menlo Park, California
1996

ABSTRACT

This report describes the acquisition, processing, and preliminary interpretation of regional intermediate-depth seismic reflection lines collected across Yucca Mountain, Nevada, during the fall of 1994. Northern Geophysical of America, under contract to the U.S. Geological Survey (USGS), acquired 37 km of high-fold seismic reflection lines across Yucca Mountain. The principal objectives of this profiling were (1) to track the pre-Tertiary/Tertiary boundary beneath Yucca Mountain, (2) to determine the geometry of faults in the subsurface, and (3) to provide subsurface data to limit the number of structural models for Yucca Mountain. For this reason the reflection lines were run through several existing wells including UE-25 p#1, which penetrated Paleozoic carbonate rocks, and USW VH-1 in Crater Flat. A subsidiary objective was to look for seismic bright spots that could indicate the existence of magma chambers in the middle and lower crust. Geologic mapping, gravity and magnetic data acquired along the lines, several Vertical Seismic Profiles (VSPs), and a seismic refraction model support interpretation of the seismic reflection data.

After testing of field parameters, two seismic lines crossing Yucca Mountain were acquired. Line 2 ran 26 km northeast from Amargosa Desert through Steve's Pass across Crater Flat and Yucca Mountain ending in the vicinity of well UE-25 UZ-16. Line 3, totaling 11 km, trended easterly from well USW H-6 across Yucca Mountain, through well UE-25 p#1, across Fortymile Wash and into Jackass Flats. Lines 2 and 3 intersect several hundred meters east of the crest of Yucca Mountain in the vicinity of well USW SD-7. The seismic data were acquired using a hybrid mix of seismic sources including vibrators, Poulter shots, minihole patterns, and explosive shot holes. The vibrator, Poulter, and minihole sources were used to provide high-fold (60- to 125-fold) sections for the upper 5 seconds of the crustal section; the shot holes were used to provide low-fold (up to 8-fold) images of the middle to lower crust (5 to 10 s).

The inferred top of the Paleozoic section may be traced discontinuously in the reflection data beneath Yucca Mountain, where it is offset by moderate- to high-angle faults. Offset of the Paleozoic/Tertiary contact beneath Yucca Mountain by high- to moderate-angle faults suggests that this contact does not represent an active detachment surface, as proposed by others. Discontinuous reflections along Lines 2 and 3 and VSPs at several wells indicate that a reflector within the Miocene tuffs, probably at or near the top of the Prow Pass Tuff of the Crater Flat Group, subparallels the topographic surface of the east flank of Yucca Mountain at a depth of about 500 m, near the static water level. This reflection appears to have been offset down to the west most noticeably at the Solitario Canyon fault. Westward stratal dips are noted only in the immediate vicinity of the Solitario Canyon fault.

Seismic reflection Line 2 shows remarkably different images, respectively, for the western and eastern halves of Crater Flat. The seismic and magnetic data show much more lateral continuity of structure and greater Tertiary thicknesses in the western half of the basin than in the eastern half. The seismic data image the Amargosa Desert structural trough, a fault-bounded graben-like structure beneath Crater Flat and Yucca Mountain with a maximum depth of about 3.5 to 4 km. The structural trough is asymmetric: one of a series of northeast-dipping (42°) reflections is interpreted as the western bounding fault, the Bare Mountain range-front fault, truncating a series of west-dipping reflections within the Tertiary fill in Crater Flat to a depth of at least 3.5 km. The eastern boundary is defined by a series of antithetic down-to-the-west normal faults, between the Solitario Canyon and Paintbrush Canyon faults, which together are inferred to drop the top of the Paleozoic sequence between 750 and 1000 m beneath Yucca Mountain.

Gently dipping, shallow reflections between Little Cones and Red Cone, inferred to be basaltic flows dated between 3.7 to 11 Ma, indicate that only minor (less than 12 m) faulting of the southwestern part of Crater Flat has occurred since the basaltic flows erupted. In the eastern half of Crater Flat, reflections are much more highly disturbed, being offset at intervals of about 1 and

2 km, in agreement with the mapping of numerous faults at the surface and the 1- to 2-km wavelength of magnetic and gravity anomalies.

The uppermost sedimentary sequences in southwestern Crater Flat lie above a major unconformity that deepens westward to over 1 kilometer beneath the surface. The unconformity lies above rocks of the Tiva Canyon Tuff of the Paintbrush Group at well USW VH-1, where the unconformity appears to roll over. This entire sequence is underlain at a depth of nearly 5 km by a subhorizontal, west-dipping reflection within the Precambrian/Paleozoic section, possibly from the Eleana Formation, or, more speculatively, from a mafic intrusion beneath it. Either lithology could produce the broad magnetic anomaly high over Crater Flat, but the anomaly is inconsistent with models incorporating a magnetic source within the Tertiary basin fill.

A reflective lower crust is imaged only on the southwest end of Line 2, in the vicinity of the Amargosa Desert and Steve's Pass. The top of the reflective lower crust is about 15 km deep, and the base of the crust, or Moho, is between 27 and 30 km deep. Neither the explosion nor vibrator sources provided an image of the lower crust in the vicinity of Yucca Mountain or along Line 3. No evidence for a lower-crustal magma chamber (bright spot reflection) was observed in the Amargosa Desert.

Better interpretation of the seismic reflection data will require additional deep boreholes along the seismic reflection lines. In particular, deep boreholes sampling the Paleozoic/Tertiary contact are necessary to test the interpretations presented here.

CONTENTS

Abstract	1
Introduction	5
Geologic Setting	6
Data Acquisition Parameter Testing	8
Acquisition of Seismic Reflection Lines 2 and 3	11
Comparison of Field Shot Records	20
Data Processing	21
VSPs and Well Logs	24
Geologic Interpretation of Seismic Sections	28
Discussion	36
Conclusions	39
Acknowledgments	39
References Cited	41
Appendix 1. NGA Crew List for Crew 110	46
Appendix 2. NGA Instrumentation	48
Appendix 3. Survey Coordinates for Lines 2 and 3	50
Appendix 4. Observer's Log for Noise Test	63
Appendix 5. Observer's Log for Line 2	66
Appendix 6. Observer's Log for Line 3	76

FIGURES

Figure 1A. Regional map of Yucca Mountain area, Nevada, showing seismic lines	83
Figure 1B. Detailed map of Yucca Mountain, Nevada, showing seismic Lines 2 and 3	84
Figure 2. Geophone and source patterns tested during noise study	85
Figure 3. Common source gather from noise test, St. 752	86
Figure 4. Common source gather from noise test, St. 652	88
Figure 5. Wind-speed data recorded at Yucca Mountain during seismic field work	90
Figure 6. Comparison of vibrator and Poulter records from Line 2, St. 941	92
Figure 7. Comparison of vibrator and minihole records from Line 3, St. 416	93
Figure 8. Stacking velocities for Lines 2 and 3	94
Figure 9. Well logs and synthetic seismograms for seven wells	96
Figure 10. Final, uninterpreted section for Line 2	98
Figure 11. Final, uninterpreted section for Line 3	99
Figure 12. Final depth-converted section for Line 2, uninterpreted	100
Figure 13. Final depth-converted section for Line 3, uninterpreted	101
Figure 14. Final migrated, depth-converted section for Line 2, uninterpreted	102
Figure 15. Final migrated, depth-converted section for Line 3, uninterpreted	103
Figure 16. Final migrated, depth-converted section for Line 2, interpreted	104
Figure 17. Final migrated, depth-converted section for Line 3, interpreted	105
Figure 18. Intermediate, uninterpreted section for Line 2 showing deep events	106
Figure 19. Isostatic gravity anomaly model for Line 2	107
Figure 20. Ground magnetic anomaly model for Line 2	108
Figure 21. Isostatic gravity anomaly model for Line 3	109
Figure 22. Ground magnetic anomaly model for Line 3	110

TABLES

Table 1. Data acquisition parameter tests 10
Table 2. Well ties to Lines 2 and 3 12
Table 3. Acquisition parameters for Line 2 13
Table 4. Look-ahead tests (LATs) of the RSX Units 15
Table 5. Shot hole information for Lines 2 and 3 15
Table 6. Shot hole shooting systems, shooters, and wind conditions 16
Table 7. Comparison of actual and design shot hole locations for Lines 2 and 3 16
Table 8. Shot hole lithologies for Lines 2 and 3 17
Table 9. Acquisition parameters for Line 3 18
Table 10. Data processing scheme for Lines 2 and 3 23
Table 11. VSP data 25
Table 12. VSP data versus synthetic seismograms 26
Table 13. Digital well log data for synthetic seismograms 27
Table 14. Line 2 and 3 markers 29
Table 15. Line 2 and 3 sources 29

INTRODUCTION

In October and November 1994, Northern Geophysical of America (NGA), under contract to the U.S. Geological Survey (USGS), acquired 37 km of high-fold seismic reflection data across Yucca Mountain, Nevada. Yucca Mountain is the site of a potential high-level nuclear waste storage facility currently under evaluation for long-term geological stability (fig. 1A). General objectives of the regional seismic reflection profiling included acquisition of images to describe the boundary between the Tertiary and underlying Paleozoic rocks, to evaluate the presence of a postulated west-dipping subhorizontal detachment surface beneath Yucca Mountain [e.g. Scott, 1990] and possible magma centers in the middle to lower crust [Evans and Smith, 1992], and to identify structural features in the shallow stratigraphic sequence, if possible. Hybrid seismic sources including vibrators, surface-mounted explosive (Poulter) charges [Poulter, 1950], and conventional shallow minihole and deep shot holes were used for data collection in response to environmental, operational, and topographic limitations. Interpretations derived from the seismic reflection profiling will feed into investigations of probabilistic seismic hazards and probabilistic volcanic hazards, and this work may help to discriminate between alternate tectonic models for the Yucca Mountain region. The reflection lines were run through existing wells USW VH-1, USW WT-7, USW UZ-6, USW WT-2, USW SD-7, UE-25 UZ-16, USW H-6, and UE-25 p#1, and close to well USW H-4. In addition, closely spaced measurements of gravity and magnetic fields were made along the seismic lines. This report provides a detailed account of the acquisition, processing, and preliminary interpretation of these seismic reflection data.

Similar seismic reflection testing and profiling were conducted in Amargosa Desert about 20 km south of Yucca Mountain in January 1988 [Brocher and others, 1990]. These tests and success in acquiring Line AV-1 in the Amargosa Desert (fig. 1A) demonstrated that vibrator sources could provide very useful images of the upper crust (0 to 5 seconds of reflection record), and that 45- and 91-kg charges should provide useful images of the lower crust (5 to 10 seconds of record). A detailed comparison of data acquired using vibrator and 91-kg shot hole sources along Line AV-1 was presented by Brocher and Hart [1991]. Brocher and others [1993] presented a geologic interpretation of Line AV-1 and comparison to existing well control and other geophysical profiling. Based partially on these results, further seismic work in the vicinity of Yucca Mountain was recommended [Seismic Methods Peer Review Panel, 1991]. Short, shallow, high-resolution seismic reflection lines acquired on Yucca Mountain in 1993 successfully imaged horizons within the Miocene volcanic tuffs [Daley and others, 1994].

The regional seismic reflection data described in this report were acquired in three stages from October 24 to November 11, 1994. First, we conducted parameter (noise) testing in Crater Flat northeast of USW VH-1, then Line 2 & 2SW, totaling 26 km (16.1 mi), was acquired (fig. 1B). Line 3, totaling 11 km (6.9 mi), was acquired last. The line name, Line 2 & 2SW, resulted from a major change in the planning of Line 2. Line 2 was originally planned to incorporate Stations 646 to 1133. Line 2SW, stations 101 to 645, was added to extend the line across Crater Flat and into the Amargosa Desert (fig. 1B). Hereinafter we refer to Line 2 & 2SW simply as Line 2.

NGA Crew 110 (enumerated in Appendix 1 along with subcontractors) provided an I/O System Two recording system, 100 RSX units (which each control 6 geophone groups) and cables, and 695 24-element geophone strings. During our work all data were recorded as 24-bit words at a 2-millisecond sample rate in demultiplexed SEG-D format [Barry and others, 1975]. A complete list of quality-affecting equipment provided by the NGA Crew and their subcontractors is provided in Appendix 2. Survey coordinates for Lines 2 and 3, given as Nevada State Coordinates accurate to a foot in latitude and longitude, are listed in Appendix 3. Horizontal locations in Nevada State Coordinates and elevations, accurate to a tenth of a foot and a hundredth of a foot, respectively, were provided by the surveyors, and were used in data processing. Within this report measurements are first presented in the units in which they were measured; we have

converted non-metric units to metric units, typically shown in this report in parentheses after the original measurement.

GEOLOGIC SETTING

Structure

Yucca Mountain is located within the Walker Lane (fig. 1A), a complex northwest-trending zone of oroclinal bending and strike-slip faulting that has been interpreted as dividing the southern Great Basin into two parts: an area to the northeast dominated by extensional faulting, and an area to the southwest in which both strike-slip and extensional faulting are important [e.g., Fox and Carr, 1989; Carr, 1990]. Near Yucca Mountain, steeply westward-dipping extensional faults mapped at the surface have been postulated to be listric normal faults that merge into a west-dipping detachment fault within the upper crust [Scott, 1986, 1990; Fox and Carr, 1989]. Others suggest that steeply-dipping focal mechanisms of deep earthquakes in the Basin and Range and geometrical considerations make it very unlikely that detachment surfaces underlie Yucca Mountain at a shallow level [Carr and others, 1986; W. B. Hamilton, unpublished manuscript entitled "Detachment faulting and tectonic modeling in the Yucca Mountain region, dated 30 June 1994, hereinafter cited as Hamilton, written commun., 1994; C. J. Fridrich, unpublished manuscript entitled "Tectonic evolution of Crater Flat structural basin, Yucca Mountain, Nevada", dated 24 Sept. 1995, hereinafter cited as Fridrich, written commun., 1995].

Yucca Mountain itself is formed by stratiform, gently east-dipping Miocene ash-flow tuffs that are broken by north-trending, west-dipping normal faults [e.g., Scott and Bonk, 1986; Fox and Carr, 1989; Scott, 1990]. The bulk of the tuffs comprising Yucca Mountain has been dated at 12.7 to 12.8 $\pm$ 0.3 Ma by the $^{40}Ar/^{39}Ar$ method [Sawyer and others, 1994]. Most of the offset of the Miocene tuffs along the normal faults is relatively modest, although a few of these faults have been mapped with up to 400 m of offset near the surface [Simonds and others, 1996]. Fault dips measured at the surface are typically between 60 and 80 degrees.

Seismic reflection Lines 2 and 3 cross a structural trough that trends northward across the southern Great Basin (fig. 1A). This trough, called the "Amargosa Desert rift zone" by Wright [1989] and the "Kawich-Greenwater rift" by Carr [1990], was first defined on the basis of gravity studies [Healey and Miller, 1965; Healey and others, 1980; U.S. Geological Survey, 1984]. Carr [1990] proposed that this trough represents "a pull-apart at a right-step in the Walker Lane and that the rift was the headwall or breakaway zone for detachment faulting to the west". The structural trough underlies Yucca Mountain and Crater Flat, and its outline has been refined using seismic reflection profiling along Line AV-1 and geological mapping, as well as drill-hole, seismic refraction, electrical, and additional gravity data.

Crater Flat is an elliptical basin bounded on the west by Bare Mountain and on the east by Yucca Mountain (fig. 1A). Gravity and seismic refraction data indicate that the basin fill reaches a thickness of 3 to 4 km [V.E. Langenheim, written commun., 1995; Mooney and Schapper, 1995]. Three main hypotheses have been proposed for the formation of Crater Flat: (1) caldera or volcano-tectonic development [Snyder and Carr, 1984], (2) detachment faulting [Hamilton, 1988], and (3) graben formation [Fridrich and others, 1994b]. Gravity models consistent with the first two models have been proposed [Snyder and Carr, 1984; Oliver and Fox, 1993; Langenheim, written commun., 1995]. More recently, Fridrich [written commun., 1995] has proposed a hybrid origin for Crater Flat structural basin, and he proposed that Crater Flat and Yucca Mountain form a single structural domain.

Stratigraphy

The oldest rocks exposed in the vicinity of seismic Lines 2 and 3 are upper Proterozoic and Paleozoic rocks exposed at Bare Mountain, the Calico Hills, the Striped Hills, and the Specter Range (fig. 1A) [Cornwall and Kleinhampl, 1961; Burchfiel, 1964, 1965; McKay and Williams, 1964; Maldonado, 1985; Monsen and others, 1992] and in the subsurface at UE-25 p#1 [Carr and others, 1986]. The Proterozoic and lower Paleozoic (Cambrian) section consists mostly of clastic and carbonate rocks and is estimated to be at least 2400 m thick at Bare Mountain [Monsen and others, 1992] and over 2800 m thick in the Specter Range [Burchfiel, 1964]. It is likely that the upper Proterozoic and lower Paleozoic sequence rests unconformably on Early Proterozoic crystalline basement rocks at depth in the vicinity of Lines 2 and 3 [Wright and Troxel, 1967].

A sequence of Middle Cambrian through Devonian continental-shelf dolostone and limestone, more than 4000 m thick in the Specter Range [Burchfiel, 1964], was deposited conformably above the upper Proterozoic and lower Cambrian clastic rocks. The thickness of Middle Cambrian (Bonanza King Formation) through Devonian (Eleana Formation) rocks is estimated to be more than 4300 m at Bare Mountain [Monsen and others, 1992]. Structurally dismembered elements of this sequence are exposed in the hills to the east of Yucca Mountain and are likely to be present below the Cenozoic cover along Lines 2 and 3. The Proterozoic and Paleozoic rocks at Bare Mountain are extensively faulted, both by low-angle thrust faults and high-angle normal faults, and folded at kilometer and outcrop scales [Monsen and others, 1992]. Dips near Steve's Pass are relatively steep, and the Proterozoic/Paleozoic section is locally overturned. Similarly, in the Striped Hills southeast of the eastern end of Line 3, the Paleozoic section has been tilted to nearly vertical and extensively faulted [Sargent and others, 1970; Maldonado, 1985]. In the Calico Hills, the upper-plate Paleozoic rocks about 6 km north of the eastern end of Line 3 are also locally overturned and extensively faulted by low- and high-angle faults [McKay and Williams, 1964].

Yucca Mountain itself consists of a thick sequence of Miocene tuffs and lavas of the ~12.8-12.7 Ma Paintbrush Group, produced at the peak of southwest Nevada volcanic field (SWNVF) eruption [Sawyer and others, 1994]. More than 2200 km^3 of magma was erupted during short episodes within 100 k.y. to form the Topopah Spring and Tiva Canyon Tuffs of the Paintbrush Group. Eruption of these units occurred at a rate identified as the highest during the lifetime of the SWNVF [Sawyer and others, 1994]. The caldera source for the Topopah Spring Tuff is buried and the location uncertain, but the Tiva Canyon Tuff was erupted from the Claim Canyon Caldera [Byers and others, 1976; Sawyer and others, 1994] to the north of present-day Yucca Mountain.

According to Spengler and Fox [1989], "the [Miocene volcanic section at Yucca Mountain] consists chiefly of rhyolitic ash-flow tuffs intercalated with thin beds of volcaniclastic rock. The ash-flow tuffs consist of an alternating sequence of nonwelded to densely welded rock, composed primarily of ash and a poorly sorted mixture of pumice, lithic clasts, and phenocrysts. Variability in initial welding compaction is considered the principal factor controlling the distribution of several physical and mechanical properties particularly at shallow depth. Dry bulk density and matrix porosity of the rock mass correlate closely with field estimates of the degree of welding, despite vertical variability in overburden pressure, growth of vapor-phase minerals, and secondary alteration."

The volcanic section at Yucca Mountain forms a wedge-shaped sequence 3.5 km thick at its northern end and progressively thinner to the south [Spengler and Fox, 1989]. The Paintbrush Group is underlain by the Crater Flat Group, comprised of the older Prow Pass, Bullfrog, and Tram Tuffs estimated to total 880 km^3 in erupted magma [Sawyer and others, 1994]. The Bullfrog Tuff, dated at 13.25 Ma, is thought to originate from a caldera north of Yucca Mountain, but the origin of the two other tuffs is uncertain [Sawyer and others, 1994]. The Crater Flat

Group, like the Paintbrush Group, consists of nonwelded to densely welded tuffs, with units ranging from lithic-poor to lithic-rich [e.g., Spengler and others, 1981; Scott and Castellanos, 1984]. Pronounced variations in rock density, and by inference, seismic velocity, within the Prow Pass and Bullfrog Tuffs [Nelson and others, 1991] are presumed to produce seismic reflections imaged in our lines.

The Miocene tuffaceous sequence is broken by a series of high-angle north-trending normal faults into a series of intact but fault-bounded blocks [Scott and Bonk, 1984; Spengler and Fox, 1989]. The geologic complexity of this sequence and resultant scattering of seismic energy have limited earlier attempts to acquire high-quality seismic reflection data [McGovern and Turner, 1983]. Megascopic voids (lithophysal cavities) which comprise up to 30 percent of some parts of the Topopah Spring Tuff [Spengler and Fox, 1989] formed during early stages of crystallization of the ash-flow tuffs and may influence physical properties of the rock and its resultant seismic response.

Cenozoic nonmarine sedimentary rocks and volcanic rocks rest unconformably or in fault contact on the upper Proterozoic and Paleozoic continental-shelf rocks in the mountains surrounding the Amargosa Desert. Oligocene sedimentary rocks [Hinrichs, 1968; Maldonado, 1985], which have been erroneously correlated with the Miocene Horse Spring Formation [Barnes and others, 1982], are the oldest Tertiary rocks known in the area. Alluvial, fluvial, and lacustrine deposits with sparse beds of volcanic ash form the lower and middle Miocene section in the eastern Amargosa Desert. Within the Nevada Test Site these rocks have been informally designated as the rocks of the Pavits Spring Formation [e.g., Barnes and others, 1982]. Locally, massive tongues of monolithologic carbonate breccia derived from lower Paleozoic strata are intercalated in Tertiary basin deposits [Swadley and Parrish, 1988; Swadley and Carr, 1989]. In the vicinity of Timber Mountain, about 25 km north of Yucca Mountain, Miocene sedimentary deposits intertongue with coeval ash-flow tuff units erupted from calderas [Barnes and others, 1982].

DATA ACQUISITION PARAMETER TESTING

Three days of field testing were conducted to determine optimal parameters for the acquisition of seismic reflection data along Lines 2 and 3. This testing was performed in Crater Flat between Stations 673 and 833 along Line 2, northeast of well USW VH-1 (fig. 1B). This test location was chosen to minimize logistical problems as well as to attempt to sample conditions close to Yucca Mountain and Crater Flat during the testing. Reflections observed during the parameter testing, such as the event at 0.8 s twtt along this part of the line (fig. 10), permitted focusing of the acquisition parameters. The testing was conducted along a fairly straight and gently inclined gravel road.

During parameter (noise) testing, three individual receiver arrays (lines in I/O System Two nomenclature), each containing a different geophone-group array pattern, were compared side-to-side. Each array (line) was 4 km long and consisted of 160 individual group arrays spaced at 82.5-ft (25-m) intervals. The first geophone-group array pattern consisted of 12 geophones placed within a circle of about 1-m radius (often called a potted array because it acts as a point receiver). Another geophone-group array pattern was 165 ft (50 m) long and consisted of a nonlinear array of 24 geophones weighted on the pin flag as was used for Line AV-1 (fig. 2A) [Brocher and others, 1990]. The last geophone-group array pattern consisted of 24 geophones inline in a linear array 165 ft (50 m) long (fig. 2B). All geophones were 10-Hz Geospace Model 20D.

The large number of channels (481) used in parameter testing required about a day and a half to deploy and retrieve. A long test spread, however, was considered necessary due to the lack of existing regional reflection data near Yucca Mountain and consequent uncertainty about data quality and where reflections might occur in space and time. Although testing made clear that

either 165-ft (50-m) array would provide noise cancellation superior to the potted geophone pattern, there was little difference in the output of the two 165-ft (50-m) patterns (figs. 3 and 4). We therefore chose the 165-ft (50-m) linear geophone pattern (fig. 2B) for collection of Lines 2 and 3. All geophones were buried along the test line and Lines 2 and 3 except for a few, limited stretches of the lines.

First-break velocities along the test line were between 2500 and 5000 ft/s for a shallow refractor, and between 7000 and 10,000 ft/s for a deeper refractor. The ground roll had velocities between 2000 and 2500 ft/s and had a predominant frequency of about 10 Hz (fig. 3A). The ground roll was similar to that encountered along Line AV-1 [Brocher and others, 1990]. We attempted to attenuate the ground roll using the 165-ft (50-m) geophone pattern described above.

Several vibrator source parameters were compared during the parameter (noise) testing. All together, 27 vibrator records were collected to compare different vibrator sweep frequencies, sweep lengths, number of vibrator sweeps, and geometry of vibrator patterns (Table 1; Appendix 4). Comparisons of vibrator parameters were made in five different locations along Line 2 between Stations 652 and 834, although more than half of the records were obtained at Station 752. Sweep frequencies between 8 and 120 Hz were compared in three different locations (Tests 1 and 2, 10 and 11, and Line 2 tests 4 and 5 on Table 1). Sweep lengths of 6, 8, 12, 18 and 24 s were compared at Station 752 (Tests 3 to 5, 20 to 21 on Table 1). The number of sweeps was tested at Station 672, where records were obtained with six, eight, and ten sweeps (Tests 12 to 14 on Table 1).

Three main types of vibrator patterns were compared. One was a bumper-to-bumper vibrator array without move-up between sweeps (a stacked pattern). The second vibrator pattern consisted of the four-vibrator 231-ft (70-m) pattern used to acquire Line AV-1, modified here to be 225 ft (69 m) long (see fig. 2F). The third vibrator pattern was a four-vibrator 165-ft (50-m) pattern tested by Brocher and others [1990] in the Amargosa Desert (fig. 2G). Vibrator patterns were compared in Tests 6 and 7, 8 and 9, 15 and 16, and 22 to 24 (Table 1). A halt in the acquisition of Line 2, caused by problems in getting the receiver spread deployed, permitted further testing of vibrator patterns. Tests 1 to 3 on Line 2 compared different 165-ft (50-m) and 195-ft (59-m) vibrator patterns (figs. 2H and 2I). These three patterns on Line 2 yielded very similar records, and, in turn, these records were very similar to those obtained using the production vibrator pattern. These tests suggest that earlier differences noted in records from the 165-ft (50-m) vibrator pattern with only five move-ups (fig. 2G) and the 225-ft (69-m) vibrator pattern with 11 move-ups (fig. 2F) may have resulted primarily from the smaller number of different source array points rather than from the total length of the pattern.

Figure 3 compares records obtained using 10 to 50 Hz sweeps for two different vibrator patterns at station (St.) 752, in the middle of the noise test spread. Figure 3A shows the record obtained using vibrators without move-up. Figure 3B shows the record obtained using the 225-ft (69-m) pattern used to acquire Lines 2 and 3 (fig. 2F). In both Figures 3A and 3B, we show the data recorded by the 165-ft (50-m) weighted inline geophone group array, the potted geophone array, and the 165-ft (50-m) linear geophone group array. The potted geophone group array (fig. 3A) shows the coherent noise which would be generated without either a vibrator or geophone group array. Conversely, the linear group array in Figure 3B shows how the arrays used to acquire Lines 2 and 3 have attenuated the surface wave energy produced by the source.

Figure 4 compares records obtained using 10 to 50 Hz sweeps for two different vibrator patterns at St. 652, about 0.5 km off the end of the spread. Figure 4A shows the record obtained using the 225-ft (69-m) pattern used to acquire Lines 2 and 3. Figure 4B shows the record obtained by a 165-ft (50-m) pattern with move-up between every other sweep (fig. 2G). Note a minor improvement in the quality between Figure 4B and Figure 4A of the reflection observed at about 1.5 s at far offsets.

Table 1. Data Acquisition Parameter Tests

Test #	No. Sweeps	Sweep Length (sec)	Sweep Frequency*	Vibrator Pattern
At Station 752:				
1	12	12	8-40 Hz	Bumper to bumper pattern with no move-up
2	12	12	12-80 Hz	Bumper to bumper pattern with no move-up
3	12	6	10-50 Hz	Bumper to bumper pattern with no move-up
4	12	8	10-50 Hz	Bumper to bumper pattern with no move-up
5	12	12	10-50 Hz	Bumper to bumper pattern with no move-up
6	12	12	10-50 Hz	165-ft pattern with 7.2-ft move-ups. 2 sweeps at each location and 5 move-ups total.
7	12	12	10-50 Hz	225-ft pattern with 8-ft move-ups. 11 move-ups total
At Station 672:				
8	12	12	10-50 Hz	225-ft pattern with 8-ft move-ups. 11 move-ups total
9	12	12	10-50 Hz	165-ft pattern with 7.2-ft move-ups. 2 sweeps at each location and 5 move-ups total
10	12	12	8-40 Hz	Bumper to bumper pattern with no move-up
11	12	12	12-80 Hz	Bumper to bumper pattern with no move-up
12	6	12	10-50 Hz	Bumper to bumper pattern with no move-up
13	8	12	10-50 Hz	Bumper to bumper pattern with no move-up
14	10	12	10-50 Hz	Bumper to bumper pattern with no move-up
At Station 652:				
15	12	12	10-50 Hz	225-ft pattern with 8-ft move-ups. 11 move-ups total
16	12	12	10-50 Hz	165-ft pattern with 7.2-ft move-ups. 2 sweeps at each location and 5 move-ups total
At Station 752:				
17	Poulter Charge			40 lbs over 165 ft
18	Poulter Charge			40 lbs over 82.5 ft
19	12	12	12-70 Hz	165-ft pattern with 7.2-ft move-ups. 2 sweeps at each location and 5 move-ups total
20	12	18	10-50 Hz	Bumper to bumper pattern with no move-up
21	12	24	10-50 Hz	Bumper to bumper pattern with no move-up
At Station 834:				
22	12	12	10-50 Hz	225-ft pattern with 8-ft move-ups. 11 move-ups total
23	12	12	10-50 Hz	165-ft pattern with 7.2-ft move-ups. 2 sweeps at each location and 5 move-ups total
24	12	12	10-50 Hz	Bumper to bumper pattern with no move-up
At Station 757 - Test during Line 2 - 31 October 1994:				
1	12	12	10-50 Hz	195-ft pattern with 7.5-ft move-ups. 11 move-ups total (production parameters).
2	12	12	10-50 Hz	165-ft pattern with 4-ft move-ups with a total move-up 44 ft. 11 move-ups total (production parameters).
3	12	12	10-50 Hz	165-ft pattern with 7.5-ft move-ups with a total move 82.5 ft. 11 move-ups total (production parameters).
4	12	12	12-70 Hz	165-ft pattern with 7.5-ft move-ups. 11 move-ups total with a total move-up of 82.5 ft.
5	12	12	12-120 Hz	165-ft pattern with 7.5-ft move-ups. 11 move-ups total with a total move-up of 82.5 ft.

*Four vibrators, 8-second listen used for all vibrator tests; all patterns centered on the flag.

We chose a 10- to 50-Hz sweep for vibrator acquisition along Lines 2 and 3 after comparing the data resulting from these vibrator tests, plotted as unfiltered and bandpass-filtered common shot records, as well as comparing spectra of these data. Because of the relatively shallow target depth of study, we sought to use high frequencies if possible. Unfortunately, above 50 Hz there appeared to be little signal-generated reflection energy, although there was significant ambient and source-generated noise above this frequency. Based on our field comparisons, we also selected a 12-s-long sweep, 12 sweeps per vibrator pattern, 8-ft (2.5-m) vibrator move-ups, and a total vibrator pattern length of 225 ft (68.6 m; fig. 2F). Throughout our work we used four Mertz Model 18 buggy-mounted vibrators with Pelton Advanced 2 Release 5.0 electronics (see Appendix 2). During vibrator testing, data were recorded as summed and correlated to allow real-time plotting of correlated records in the recording truck. This choice allowed rapid decisions about the choice of vibrator parameters. During acquisition of Lines 2 and 3, however, vibrator data were recorded summed but uncorrelated and plotted as uncorrelated records in the recording truck.

Two different Poulter charges (surface explosive charges [Poulter, 1950]) were compared to determine the optimal pattern length (Tests 17 and 18 on Table 1). Each Poulter charge consisted of 40 lbs (18.2 kg) of Surf-A-Seis explosive distributed over eight wooden stakes, each 6 ft (1.8 m) tall. Both patterns were linear and centered on the station flag: one pattern was distributed over 82.5 ft (25 m) and the other over 165 ft (50 m; fig. 2C and 2D). We selected the shorter Poulter pattern because it provided better suppression of the large-amplitude air blast arrival than did the longer Poulter pattern.

Ideal weather conditions prevailed during the parameter testing. Wind speeds were low and temperatures were warm. Wind speeds were recorded at several locations close to Lines 2 and 3 during our field work, including sites at Yucca Mountain, Coyote Wash, Alice Hill, Knothead Gap, and NTS-60 [Tim Moran, DOE, personal communication, 1994]. The station at Yucca Mountain is located on the crest of Yucca Mountain (Nevada State Coordinates are 558,844E; 766,356N) about 2.3 km north of Lines 2 and 3. During parameter testing wind speeds at the Yucca Mountain station were generally less than 4 m/s (8.9 mi/hr; fig. 5a). Station NTS-60 (Nevada State Coordinates 569,126E; 761,795N) was located about 290 m east of St. 1133 on Line 2. The station at Knothead Gap (Nevada State Coordinates 570,344E; 756,538N) was located within meters of St. 322 on Line 3. Figure 5 presents a plot of wind speeds, in m/s, recorded at Yucca Mountain, NTS-60, and Knothead Gap during our seismic profiling. Values in excess of 12 m/s signify an absence of wind speed data for that time.

ACQUISITION OF SEISMIC REFLECTION LINES 2 AND 3

This section presents a brief narrative describing the acquisition of Lines 2 and 3. Problems encountered during the acquisition are recounted as well as the means by which they were resolved. Those readers more interested in the actual data may skip on to the next sections.

Line 2

Data acquisition along Line 2, totaling 26 km (16.1 mi), began in the Amargosa Desert (fig. 1) on October 27, 1994, using vibrators (see observer's log in Appendix 5). Line 2 trended northeast from the start of line (SOL) at Station 101, crossed State Highway 95 at station 235, and ran through Steve's Pass at Station 338 before it turned and trended across country between Stations 343 and 646 (fig. 1). The line deviated slightly to the south around the southern end of

Red Cone to avoid the lava flows there. Northeast of Red Cone the line straightened and intersected well USW VH-1 near Station 646 (see Table 2). From Station 945 to the end of line (EOL) at Station 1133, the line ran across country over Yucca Mountain, passing near wells USW WT-7, USW UZ-6, USW SD-7, USW WT-2, USW UZ 7-A, USW H-4, and UE-25 UZ-16. These well ties are detailed in Table 2.

The observer's log (Appendix 5) identifies sources of ambient noise along the line. A large noise source was State Highway 95 on the southwest end of the line (Station 235). Other large noise sources were found in the vicinity of Yucca Mountain with drilling activities at a few sites, including USW SD-7, and at Exile Hill, where work on and with the tunnel boring machine (TBM) was in progress.

Acquisition parameters for Line 2 are provided in Table 3. The vibrator source array was rolled into a spread maintaining 240 channels in front of the vibrator sources until it reached the middle of a symmetric split spread with 240 channels on each side of the source. At that point the symmetric split spread was rolled along. No gap was used between the source and receivers. The group interval was 25 m (82.5 ft). Vibrator source points were spaced at 330-ft (100.6-m) intervals between Stations 101 and 945, providing nominal 60-fold data. Vibrator profiling was completed on November 2, 1994.

Table 2. Well Ties to Lines 2 and 3

Well	Northing	Easting	Line, Sta. No.	Distance (ft)	Azimuth*
USW VH-1	743355.5	533625.9	2, 646	130	SE, 153°
USW WT-7	755569.8	553891.3	2, 938	150	NW, 309°
USW UZ-6	759731	558325	2, 1009	1112	NNW, 338°
USW SD-7	758949.89	561240.3	2, 1036	790	NNW, 338°
USW WT-2	760661	561924	2, 1054	620	NNW, 337°
USW UZ 7-A	760692.74	562269.8	2, 1058	530	NNW, 337°
USW H-4	761643.6	563911.1	2, 1079	1050	N, 350°
UE-25 UZ-16	760535	564857	2, 1088	215	S, 170°
USW H-6	763298.9	554074.9	3, 101	67	N, 004°
USW UZ-6	759731	558325	3, 167	150	S, 199°
USW SD-7	758949.89	561240.28	3, 204	60	NE, 45°
USW WT-2	760661	561924	3, 206	1870	N, 19°
UE-25 p#1	756171.2	571484.5	3, 337	9	S, 197°

*Azimuth from seismic line to well, measured clockwise from North.

Table 3. Data Acquisition Parameters for Line 2

Parameter	Description
Recording Instrumentation	I/O System Two with twisted pair cables and 24-bit recording
Vibrator Array	Four Mertz Model 18 buggy vibrators, each providing a peak force of 45,000 lbs with force control and phase loop locking
Vibrator Electronics	Pelton Advance 2 Release 5.0
Vibrator Pattern	Four vibrators in a 12-element pattern, with a pad spacing of 47.9 ft and an 8-ft move-up between sweeps for a total pattern length of 225 ft
Sweep Frequency	10 to 50 Hz upsweep with a 0.2 s taper
Sweep Length	12 s
Listen Time	8 s
Record Length	20 s
Sample Rate	2 msec
Field Filters	Low-cut 3.0 Hz @ 12 db Slope; High-cut (anti-alias) 135 Hz @190 db slope; Notch Out
Number of Sweeps per VP	12
VP Interval	330 ft (~100 m; every 4th flag)
Receiver group spacing	82.5 ft (~25 m)
Receiver pattern	Linear inline pattern of 24 geophones over 165 ft centered on flag
Geophone Model	Geospace 20D, 10 Hz
Receiver spread	481 channel, symmetric split spread, 240 channels each a side of source, ~6 km maximum offset on each side of source, roll into and roll out of full 481 channels on end of line
CDP fold (vibrator)	Nominal 60 at full fold
Recording format	SEG-D at 6250 BPI on 9-track tape; vibrator data recorded summed but uncorrelated
Poulter Charge Pattern	40 lbs of SURF-A-SEIS explosive over 82.5 ft on 8 stakes with 5 lbs/stake centered on flag. Each stake 6 ft high.
Poulter Charge Spacing	165 ft (~50 m; every 2 flags)
Poulter Record Length	8 s
CDP fold (Poulter)	94 maximum fold
Explosive Shot hole Spacing	80 stations (flags) ~2 km
Explosive Shot hole Depths	100 ft for 100 lb shots, 200 ft for 200 lb shots

The heart of the recording system was the I/O System II, a digital telemetry-based system whose primary means for quality control is look-ahead testing of the RSX units deployed along the cable. These RSX units control the signals from three geophone group arrays on each side of the RSX unit, conditioning and digitizing the signals prior to telemetering the data to the recording truck. The look-ahead tests performed on each RSX unit prior to its use are provided in Table 4. This table provides a list of both those look-ahead tests done on a daily basis to verify satisfactory system performance prior to data acquisition, as well as those look-ahead tests that were continuously monitored during data acquisition. The I/O System II, like many current telemetry-based recording units, offers a number of real-time data-quality monitoring functions and automatically halted the acquisition of data for major errors. Over 81 RSX units were in use at any time for the 481-channel spread used for Line 2. Summed but uncorrelated data were digitally recorded at a 2-msec sample interval on 6250 BPI magnetic tapes in SEG-D format [Barry and others, 1975]. The listen time for the vibrator data was 8 s.

A 2- to 8-fold seismic image of the lower crust (5 to 10 s) along Line 2 was obtained using deep shot holes. As the spread rolled through the line, 100- and 200-lbs (45- and 91-kg) charges were fired in shot holes at 2-km intervals along the line. These Vibragel charges, manufactured by DYNO, were loaded into 100- and 200-ft (30- and 61-m) shot holes and tamped with Wyoming bentonite and drilling cuttings. The holes were pre-drilled and cased with 4-in (10-cm) outer-diameter PVC casing. No tamping was blown out, and there was no surface disturbance at any shot hole. Charge lengths were 88 ft (27 m) for the 200-lbs (91-kg) shots and 44 ft (13 m) for the 100-lbs (45-kg) shots. Each shot was recorded by 481 channels for 20 seconds.

Details of the shot holes used for Lines 2 and 3 are provided in Tables 5 to 8. Table 5 gives the location of each shot hole, the depth to the bottom of the PVC casing (and consequently the depth to the bottom of the charge), the charge weight in lbs, the uphole time of the shot, the date, and the approximate local time of the shot. These local shot times are considered accurate to about 10 minutes. The number of the shooting system, shooter(s), and wind conditions for each shot are given in Table 6. Unfortunately, because of the need to maintain data production many of these shots were recorded in gusty and strong wind conditions. Many of the shot hole locations were staked nearly two years prior to the survey, in order to obtain the necessary permits. A comparison of the design (staked) shot hole location versus the final, actual shot hole location is presented in Table 7. These locations were generally very close (within 100 m), apart from shot point 311, and shot point 300, which was not resurveyed. Finally, Table 8 summarizes lithologies encountered in some of the shot holes. Most of the holes encountered a single lithology, although a number of lithologies were encountered in shot points 3 through 7 and 201. Shot hole lithologies are unavailable for the holes not listed in Table 8.

Vibrator production was hampered by the difficulty in deploying the receiver spread up and over Yucca Mountain. Some delay was also introduced by the late arrival of a helicopter to ferry equipment across Yucca Mountain. On October 31 this delay allowed the crew to perform some maintenance on the vibrator trucks and also to perform a series of five additional vibrator tests described in Table 1. High-frequency sweeps were tested as well as vibrator patterns slightly shorter than those used for the production sweep. These tests indicated little difference in record quality for the different vibrator patterns and suggested that little useful additional information could be gathered using higher-frequency sweeps.

Table 4. Look-Ahead Tests (LATs) of the RSX Units

Daily

1. Short Equivalent Input Noise Test (2-s records)
2. Filtered Pulse Test (Limit <7.5% RMS error from Average Pulse)
3. Dynamic Range Test (0 db, 72 db, 84 db, Fx Gain)
4. Harmonic Distortion Test Class I (Limit <0.02%)
5. Seis Channel Gain Calibration (Limits 0.96-1.10)
6. Oscillator Calibration (RMS Limit 6.85 v ± 5%; THD Limit <0.01%)
7. A/D Converter Calibration (Gain Limit 0.816-1.016; Channel Offsets Limit ± 0.138 v)

Continuous Mode LATs

1. Short Equivalent Input Noise Test (2 sec records)
2. Filtered Pulse Test (Limit <7.5% RMS error from Average Pulse)
3. Dynamic Range Test (0 db, 72 db, 84 db, Fx Gain)
4. Harmonic Distortion Test Class I (Limit <0.02%)
5. RSX Calibration

Table 5. Shot hole Information for Lines 2 and 3

	Location						PVC	Charge	Uphole		Approx. Local
	Lat. (°N)	Long.(°W)	Nev. State Coord.				Depth	Size	Time	1994	Time
SP #	(Dg., Mn.,Sc.)	(Dg., Mn.,Sc.)	X (ft)	Y (ft)	Z (ft)	Sta. #	(ft)	(lbs)	(msec)	Date	HrMin
1	36 43 13.86	116 40 18.20	498518	717221	2663	101	201.3	200	41	10/28	1338
3	36 43 59.36	116 39 23.29	502988	721822	2671	178	202.4	200	37	10/28	1423
5	36 44 46.34	116 38 29.43	507371	726574	2736	258	200.0	200	31	10/28	1533
7	36 45 29.12	116 37 33.69	511905	730902	2953	338	198.0	200	26	10/28	1631
9	36 45 58.91	116 36 30.86	517016	733917	2939	410	201.4	200	22	10/29	1401
11	36 46 31.42	116 35 21.07	522691	737209	2999	490	202.3	200	39	10/29	1426
13	36 47 04.03	116 34 11.38	528358	740511	3062	573	201.9	200	41	10/30	1339
201	36 47 36.64	116 33 01.64	534026	743815	3173	653	206.4	200	27	10/30	1658
203	36 48 08.24	116 31 50.58	539801	747018	3364	733	200.0	200	34	10/30	1726
205	36 48 39.50	116 30 42.54	545329	750187	3574	811	191.8	200	30	11/01	1556
205A	36 48 40.72	116 30 41.11	545445	750311	3574	813	191.7	200	37	11/01	1605
205B	36 48 41.87	116 30 39.73	545558	750427	3575	817	191.4	200	38	11/01	1610
207	36 49 15.70	116 29 33.16	550965	753858	3783	895	188.7	200	33	11/02	1153
208.5A	36 49 52.19	116 28 21.35	556795	757559	4249	980	99.9	100	19	11/02	1732
208.5B	36 49 52.21	116 28 21.70	556767	757561	4243	981	100.2	100	17	11/02	1743
211A	36 50 22.48	116 26 58.06	563560	760637	4109	1072	100.0	100	20	11/03	1436
211B	36 50 22.82	116 26 58.50	563523	760671	4113	1072	99.5	100	24	11/03	1434
300*	36 51 22.66	116 32 08.87	538287	766676	---- -	100	201.7	100	38	11/11	0943
302A	36 50 37.99	116 28 35.24	555657	762188	4162	124	100.0	50	25	11/11	0850
302B	36 50 37.56	116 28 34.88	555687	762145	4257	125	100.0	100	18	11/11	0853
305A	36 49 55.38	116 27 01.74	563266	757895	4153	232	100.0	100	12	11/09	1045
305B	36 49 54.95	116 27 01.45	563290	757852	4150	232	100.0	100	12	11/09	1051
307	36 49 38.56	116 25 27.33	570946	756213	3662	330	200.6	200	34	11/11	1016
311	36 49 27.27	116 24 02.44	577850	755090	3357	416	201.5	200	34	11/11	0854

*Latitude and Longitude of SP 300 are taken from GPS coordinates of Shot hole Stakes by Michael J. Moses, USGS, 10/30/92. Estimated Northing and Easting for SP 300 are from a Letter dated 8 Apr. 1993 from C. Thomas Statton, TRW, to Mark Tynan, DOE, YMSCPO, reference LV.SC.JDA.4/94-099. The location of SP 300 was not resurveyed by NGA surveyors.

Table 6. Shot hole Shooting Systems, Shooters, and Wind Conditions

SP #	Location X (ft)	Y (ft)	Z (ft)	Shooting System	Shooter(s)	Wind Conditions
Line 2						
1	498518	717221	2663	M-1	Jason Clark/Dan Malberg	Light
3	502988	721822	2671	M-1	Jason Clark/Dan Malberg	Slightly higher winds
5	507371	726574	2736	M-1	Jason Clark/Kim Wegemeyer	Strong wind from south
7	511905	730902	2953	M-1	Jason Clark/Kim Wegemeyer	Winds less strong than for SP 5
9	517016	733917	2939	M-1	Dan Malberg	Windy
11	522691	737209	2999	M-1	Dan Malberg	Windy
13	528358	740511	3062	M-1	Dan Malberg	Variable, gusty winds
201	534026	743815	3173	M-1	Dan Malberg	Very light winds
203	539801	747018	3364	M-1	Dan Malberg	Calm to light winds
205	545329	750187	3574	M-1	Dan Malberg	Breezy
205A	545445	750311	3574	M-1	Dan Malberg	Breezy
205B	545558	750427	3575	M-1	Dan Malberg	Breezy
207	550965	753858	3783	M-1	Randy Stamey/Oliver Amend	Variable, gusty winds
208.5A	556795	757559	4249	M-1	Randy Stamey/Oliver Amend	Variable, gusty winds
208.5B	556767	757561	4243	M-1	Randy Stamey/Oliver Amend	Variable, gusty winds
211A	563560	760637	4109	M-1	Randy Stamey/Oliver Amend	Strong winds
211B	563523	760671	4113	M-1	Randy Stamey/Oliver Amend	Strong winds
Line 3						
300#	538287	766676	-----	PT400	Greg Brooks/George Berala	Calm to very light
302A	555657	762188	4162	PT400	Greg Brooks/George Berala	Calm to light
302B	555687	762145	4257	PT400	Greg Brooks/George Berala	Calm to light
305A	563266	757895	4153	M-1	Randy Stamey/Oliver Amend	Windy
305B	563290	757852	4150	M-1	Randy Stamey/Oliver Amend	Windy
307	570946	756213	3662	HT600	Oliver Amend/Randy Fortin	Very light
311	577850	755090	3357	PT400	Randy Fortin/Greg Brooks	Light

#Estimated Northing and Easting for SP 300 are from a Letter dated 8 Apr. 1993 from C. Thomas Statton, TRW, to Mark Tynan, DOE, YMSCPO, reference LV.SC.JDA.4/94-099. The location of SP 300 was not resurveyed by NGA surveyors.

Table 7. Comparison of Designed and Actual Shot hole Locations for Lines 2 and 3

	Actual Location (by Extreme Survey)		Design Location (by GPS)#		Actual Location (by Extreme Survey)			Design Location (Estimated)*		
SP #	Lat. (°N) (D., M.,S.)	Long.(°W) (D., M.,S.)	Lat. (°N) D., M.,S.)	Long.(°W) (D., M.,S.)	X (ft)	Y (ft)	Z (ft)	X (ft)	Y (ft)	Z (ft)
Line 2										
201	36 47 36.64	116 33 01.64	36 47 37.56	116 33 01.48	534026	743815	3173	534040	743907	
203	36 48 08.24	116 31 50.58	36 48 09.06	116 31 50.68	539801	747018	3364	539794	747101	
205	36 48 39.50	116 30 42.54	36 48 42.36	116 30 41.38	545329	750187	3574	545424	750476	
205A	36 48 40.72	116 30 41.11	36 48 42.36	116 30 41.38	545445	750311	3574	545424	750476	
205B	36 48 41.87	116 30 39.73	36 48 42.36	116 30 41.38	545558	750427	3575	545424	750476	
207	36 49 15.70	116 29 33.16	36 49 16.76	116 29 32.58	550965	753858	3783	551012	753965	
208.5A	36 49 52.19	116 28 21.35	Not Measured		556795	757559	4249	556582	757516	4228
208.5B	36 49 52.21	116 28 21.70	Not Measured		556767	757561	4243	556582	757516	4228
211A	36 50 22.48	116 26 58.06	36 50 20.10	116 26 55.31	563560	760637	4109	563477	760540	4314
211B	36 50 22.82	116 26 58.50	36 50 20.10	116 26 55.31	563523	760671	4113	563477	760540	4314
Line 3										
300	Not Measured		36 51 22.66	116 32 08.88	Not Measured			538287	766676	----
302A	36 50 37.99	116 28 35.24	36 50 39.36	116 28 34.08	555657	762188	4162	555751	762327	
302B	36 50 37.56	116 28 34.88	36 50 39.36	116 28 34.08	555687	762145	4257	555751	762327	
305A	36 49 55.38	116 27 01.74	36 49 54.40	116 27 04.10	563266	757895	4153	563203	757704	5162
305B	36 49 54.95	116 27 01.45	36 49 54.40	116 27 04.10	563290	757852	4150	563203	757704	5162
307	36 49 38.56	116 25 27.33	36 49 27.50	116 25 27.50	570946	756213	3662	570820	756277	4101
311	36 49 27.27	116 24 02.44	Not Measured		577850	755090	3357	578238	754965	3522

#Latitude and Longitudes taken from GPS coordinates by Michael J. Moses, USGS, 10/30/92.

*Estimated Northing and Easting for SP 300 are from a Letter dated 8 Apr. 1993 from C. Thomas Statton, TRW, to Mark Tynan, DOE, YMSCPO, reference LV.SC.JDA.4/94-099. The location of SP 300 was not resurveyed by NGA surveyors.

Table 8. Shot hole Lithologies for Lines 2 and 3

SP #	Location X (ft)	Y (ft)	Z (ft)	Hole Depth (ft)*	Lithology*
Line 2					
1	498518	717221	2663	0-201	Sand and gravels
3	502988	721822	2671	0-130	Sand and gravels
				130-202	Volcanic tuff
5	507371	726574	2736	0-68	Sand and gravels
				68-110	White Powder
				110-200	Pre-Rainier Mesa tuffaceous rocks
7	511905	730902	2953	0-25	Sand, gravels and Pre-Rainier Mesa tuffaceous rocks
				25-198	Pre-Rainier Mesa tuffaceous rocks
11	522691	737209	2999	0-202	Sands and gravel, unconsolidated rock
13	528358	740511	3062	0-202	Sands and gravel
201	534026	743815	3173	0-40	Sands and gravel
				40-80	Hardpan-Tuff?
				80-145	Tuff
				145-207	Sand and gravel
203	539801	747018	3364	0-171	Sand and gravel
205	545329	750187	3574	95-192	Gravels and cobbles
205A	545445	750311	3574	0-192	Gravels, cobbles, boulders, sand
205B	545558	750427	3575	0-191	Sand, gravel, cobbles, boulders
207	550965	753858	3783	0-145	Sand, gravel, cobbles
Line 3					
300#	538287	766676	-----	0-202	Sand and gravel

*From Drilling Reports, dated August to October, 1994.
#Estimated Northing and Easting for SP 300 are from a Letter dated 8 Apr. 1993 from C. Thomas Statton, TRW, to Mark Tynan, DOE, YMSCPO, reference LV.SC.JDA.4/94-099. The location of SP 300 was not resurveyed by NGA surveyors.

Poulter-charge sources were used on Line 2 over the rugged topography of Yucca Mountain between Stations 941 and 1133. The Poulter charges were spaced at 165-ft (50-m) intervals along this line, yielding a maximum fold of 94. Weather conditions during the acquisition of the Poulter charge data were variable; wind speeds on Yucca Mountain exceeded 10 m/s (22 mi/hr) on November 2 and 3 (fig. 5B), degrading the data. During these windy conditions, it was not possible to trace the first arrivals to offsets of 6 km. Lower wind speeds on Yucca Mountain for November 4, between 2 and 4 m/s (fig. 5B), resulted in much less noisy Poulter-charge data than those data acquired on November 2 and 3.

Weather conditions were mixed during data collection along Line 2. In general, however, the weather turned progressively cooler and windier during the acquisition of Line 2 than it had been during noise testing. Figure 5B shows that wind speeds were generally between 2 and 6 m/s (4.4 and 13.4 mi/hr) at Yucca Mountain, but windier conditions were encountered near the completion of Line 2 when winds exceeded 10 m/s (22 mi/hr). Wind speeds at station NTS-60, near the northeast end of Line 2, generally recorded lower wind speeds than did the station at Yucca Mountain. Except for November 2 and 3, wind speeds at NTS-60 during the acquisition of Line 2 were generally between 1 and 4 m/s (2.2 and 8.9 mi/hr; fig. 5D).

During acquisition of the northern end of Line 2, operations of the tunnel-boring machine at Exile Hill and drilling operations at USW SD-7 were shut down to minimize seismic noise in the data.

Line 3

Line 3, 11 km (6.9 mi) long, trended in an easterly direction from SOL at Station 101 near well USW H-6 in Solitario Canyon (fig. 1). The line utilized a few short sections of existing roads (Stations 101 to 126, 164 to 232, and 311 to 338) but generally was acquired cross country. Due to the rugged topography along the line, three different source types were utilized: vibrators along roads, Poulter charges in very rugged segments up and across Yucca Mountain, and a pattern of shallow charges (miniholes) in off-road segments of the line over Fran Ridge. The line was designed to tie to Line 2 and to well UE-25 p#1 but also passed near wells USW H-6, USW UZ-6, USW WT-2, and USW SD-7 (Table 2). During field operations the line was lengthened eastward two miles, adding Stations 418 to 541, to extend the line across Fortymile Wash and into Jackass Flats (fig. 1). Details of the acquisition and ambient noise sources along Line 3 are provided in the observer's log for this line (given in Appendix 6).

Parameters used to acquire Line 3 are listed in Table 9. Acquisition of vibrator data on the line began November 5 and was completed November 9. Acquisition of Poulter charge data on Line 3 started November 6. Data acquisition along Line 3 was hindered by the slow rate of drilling of the minihole patterns between Stations 331 and 439. Each minihole pattern consisted of five holes spaced over 80 ft (24 m), each 10 ft (3 m) deep and containing 2 lbs (0.9 kg) of Unimax explosive capped with a single fuse (fig. 2C). Drilling of the minihole patterns, using a person-portable drilling rig powered by compressed air, began October 27 and ended November 8. Acquisition of data along Line 3 was maintained by drilling miniholes during the day and acquiring vibrator data at night after the minihole drilling ceased for the day.

Wind conditions were variable during the acquisition of Line 3 (figs. 5C and 5E). From November 5 to November 8, winds at the Yucca Mountain station on the crest of Yucca Mountain were typically between 2 and 6 m/s (4.4 to 13.4 mi/hr). Wind speeds recorded at Knothead Gap (St. 322) were significantly lower, in the range of 1 to 4 m/s (2.2 to 8.9 mi/hr; fig. 5E). November 9 was stormy at both Yucca Mountain crest and Knothead Gap, with gusty winds in excess of 8 m/s (17.9 mi/hr). High winds (up to 10 m/s or 22 mi/hour) and rain precluded data acquisition on the following day, November 10 (fig. 5C). Line 3 was completed on November 11 when much of the Poulter-charge and all of the minihole data for Line 3 were acquired in nearly ideal wind conditions. Wind speeds recorded at Yucca Mountain and Knothead Gap on November 11 were between 1 and 4 m/s (2.2 to 8.9 mi/hr).

Table 9. Acquisition Parameters for Line 3

Parameters are the same as for Line 2 with the following exceptions and/or additions:	
Parameter	Description
VP Interval	165 ft (~50 m; every 2nd flag)
Receiver spread	441 channel, symmetric split spread, 240 channels on a side of source, ~6 km maximum offset on each side of source, roll into and roll out of full 441 channels on end of line
CDP fold	Nominal 100 at full fold
Minihole Pattern	10 lbs of UNIMAX explosive over 80 ft in 5 miniholes each 10 ft deep centered on flag, 2 lbs explosive per hole.
Minihole Record Length	8 s
CDP fold	125 nominal fold

During the acquisition of Line 3, a number of ongoing activities at Yucca Mountain generated high levels of seismic noise. These noise sources included road grading and quarrying operations, drilling and boring activities, light trucks driving along the seismic line, diesel-driven electrical generators on drilling platforms, operations with the tunnel-boring machine (TBM), and helicopters passing near the seismic line. We were successful in shutting down most of these activities during working days, and found that data acquisition at night or on the weekends also eliminated most of these noise sources. When these sources could not be shut down, however, they noticeably degraded the quality of the seismic data.

Surveying of Lines 2 and 3, by Extreme Surveys, Inc., provided horizontal coordinates accurate to a tenth of a foot and vertical elevations to within a hundredth of a foot. The survey coordinates were plotted on 1:24,000 topographic maps and written in standard SEISURV 3.6 format on magnetic floppy disks in DOS format. Normal industry survey closure procedures were employed, resulting in maximum horizontal closure errors of 13.0 and 5.5 m for Lines 2 and 3, respectively, and in maximum vertical closure errors of 0.61 and 0.40 m for Lines 2 and 3, respectively.

Ancillary Data

Field processing of the seismic reflection data was performed by Geophysical Control, Inc., using MicroMAX seismic processing software. The field processing was used to help guide the selection of field parameters used for Lines 2 and 3 as well as to monitor data quality during the acquisition of these lines. In addition to plotting the common shot data, and performing spectra of some of the parameter test data, the field processor also produced brute sections for three portions of Line 2, including (1) a portion at the beginning of the line, (2) a section near the middle of the line in Crater Flat, and (3) the northeastern end of the line containing all of the Poulter-charge data. In addition, the field processor made a brute section of the deep shot hole data along Line 2. The activities, hardware and software, and products of the field processor were detailed by C. Tonish ["Yucca Mountain Project: Seismic data QA/QC and field processing, Oct/Nov 1994", unpublished report, 1994].

A team of University of Nevada/Reno (UNR) seismologists, headed by Dr. Glenn Biasi, recorded absolute shot hole explosion times required for tomographic analysis of the explosion data recorded by the UNR seismic net. Northern Geophysical of America provided an electrical trigger for the UNR recorders whenever a shot tone was transmitted. This trigger was recorded by UNR for all the shot holes. In addition, as a backup, UNR collocated seismic recorders along our geophone array. The travel time of the first arrival to the UNR instruments determined from field plots can be used to determine the absolute shot time (in universal coordinated time, UCT).

Densely sampled potential-field data along the seismic reflection lines were acquired by the USGS subsequent to the seismic work in late November 1994 and February 1995. Data types include coincident ground magnetic stations with a maximum spacing of 25 m and an average spacing of 10 m along the seismic profiles, offset ground magnetic traverses (same spacing) from Amargosa Desert to drill hole USW VH-1 [Langenheim and Ponce, 1995], and aeromagnetic coverage for the remainder of the lines [Sikora and others, 1995]. The ground magnetic data show large anomalies caused by surficial volcanics at Little Cones and Red Cone and at powerlines near St. 240 on Line 2. Correlation of magnetic anomalies and the seismic data are presented later in this report and by Langenheim and Ponce [1995].

Collection of gravity data along the seismic reflection profiles was conducted by Ernie Majer, Ken Williams, and staff from the Lawrence Berkeley Laboratory (LBL) and completed in December 1994 [E.L. Majer, written commun., 1995, in Appendix 1 in LBL Letter Report, April 1995, WBS 1.2.3.11.2 Surface-Based Geophysical Testing]. Gravity stations were made at 100-m spacing along the seismic profiles, tied to the seismic station flags. Gravity data were acquired

using two LaCoste and Romberg Model G gravity meters. Field terrain corrections were not made. All gravity measurements were tied to the absolute gravity station MERCA, located in the USGS Core Library building in Mercury, Nevada [Zumberge and others, 1988]. Data reduction, including removal of solid-earth tide, meter drift correction, Bouguer correction, and topographic correction, was performed by LBL and the USGS. A regional correction using the principle of isostasy was also applied to the data to model and remove long-wavelength effects due to deep compensation for topographic loads [Simpson and others, 1986]. Three inaccurate gravity readings are noted along Line 2, at km 12.3, km 17.4, and km 25 (fig. 19A). One inaccurate gravity reading is noted along Line 3, at km 2.1 (fig. 21A). The data acquired along Lines 2 and 3 fill an important gap in continuous gravity coverage across Crater Flat and Yucca Mountain.

Gravity Modeling

Two-dimensional modeling of the isostatic residual gravity data (reduced at a density of 2.67 g/cm^3) was performed using HYPERMAG [Saltus and Blakely, 1993]. Because of the densities used in this reduction, Yucca Mountain is expressed as a local gravity low (with an amplitude of 6 to 10 mGal). Densities used in the model were derived from seismic refraction data [Mooney and Schapper, 1995] and from density measurements [Snyder and Carr, 1984; Langenheim, written commun., 1995]. Densities do not necessarily reflect lithologies, but in general reflect the increase in density with depth [Snyder and Carr, 1984]. In the model, densities within the Tertiary volcanic section increased from 2.0 to 2.5 g/cm^3. The density of the Paleozoic section was fixed at 2.72 g/cm^3, consistent with Paleozoic densities measured in samples from UE-25 p#1 and on hand samples from Bare Mountain. Two models for each line are shown (figs. 19 and 21). Both pairs of models fit the gravity data equally well but show a different geometry for the eastern boundary of the Crater Flat basin. One set of models fits the gravity data with a single, gently sloping surface on the top of the Paleozoic (figs. 19A and 21A) whereas the other set of models breaks this surface into two steps corresponding to the Solitario Canyon and Ghost Dance faults (figs. 19B and 21B), consistent with the geometry imaged in the seismic reflection data. Under Yucca Mountain, the depth to pre-Tertiary basement derived from gravity modeling is consistent with the depth from the seismic reflection data. The geometry of the basement surface under Crater Flat is similar to that imaged in the seismic reflection data if the thicknesses of the shallower units (for example, the 2.2 g/cm^3 layer) are increased in the region between USW VH-1 and the Solitario Canyon fault. Gravity data along the eastern part of Line 3 indicate that the basement surface is essentially flat. More detailed correlation of the gravity data and the seismic data is presented later in this report.

COMPARISON OF FIELD SHOT RECORDS

As discussed previously, a combination of logistical and environmental requirements led to the hybrid use of vibrator, Poulter surface charge, and minihole sources along Lines 2 and 3. Different sources were overlapped by two source points to allow phase matching of the different sources. These overlaps led to the acquisition of multiple records at the same source point, providing a total of nine comparisons of records obtained using vibrator and Poulter sources and four comparisons of records obtained using vibrator and minihole sources. In addition, there are 14 comparison records obtained using vibrator and deep shot hole sources and two comparisons each of records obtained using Poulter and deep shot hole sources and records obtained using minihole and deep shot hole sources.

We focused our analysis on those records from portions of the lines displaying reflections within the upper 2 s of the seismic sections. This criterion focused our comparison to those parts of the seismic lines which successfully imaged subsurface structure.

Figure 6 compares data recorded by vibrator and Poulter sources on Line 2 at St. 941 (in Solitario Canyon). Poulter charges were the least energetic type of source employed during our survey; during windy conditions they did not provide clear first arrivals out to the maximum offset of 6 km. Under favorable wind conditions, however, Poulter sources provided clear first break arrivals to maximum offsets of 6 km and provided records comparable in quality to those obtained with vibrator sources. In most cases the first breaks of the Poulter data are easier to pick than those of the vibrator sources, permitting better refraction-static models to be developed. Vibrator methods, however, permit better suppression of ambient noise and the air-wave arrival, which can be very large on Poulter-source data. On unprocessed field shot records, the Poulter-source data have a lower frequency than do the correlated field shot records for the vibrator-source data (fig. 6). Spectra indicate that the Poulter sources have significant energy down to about 4 Hz, whereas the vibrator sources with a 10- to 50-Hz sweep have little energy below 11 Hz. The stacked section for Line 2 indicates that the Poulter sources imaged reflections at least 2 s two-way travel time (twtt) below the surface.

Figure 7 compares data recorded using vibrator and minihole sources on Line 3 at St. 416. All the minihole data were acquired in very favorable wind speed conditions. The minihole sources provided clear first breaks out to the maximum offset of 6 km, which were easier to pick than those of the vibrator source. On balance, records obtained using minihole sources compare favorably to those obtained using vibrator sources. The minihole sources produced little if any air wave energy, but did generate larger-amplitude surface waves than did the vibrator sources. On unfiltered field shot records, the minihole data have a lower frequency appearance than do the correlated field shot records for the vibrator data. Spectra indicate that the minihole sources have significant energy down to about 5 Hz.

DATA PROCESSING

Data acquired along Lines 2 and 3 were processed interactively by Texseis, Inc. using ProMAX release 5.1 seismic reflection processing software. A standard data processing flow was used, as detailed in Table 10. This flow included vibroseis correlation and compensation filter for vibrator data to match explosion data, refraction and datum statics, F-K filter (after normal moveout (NMO) to flatten reflection events), constant velocity stacks for functions at 250 ft/s intervals, NMO and mute, surface-consistent residual statics, datum correction, CDP stack, post-stack bandpass filtering, scaling, F-X deconvolution, depth conversion, and Stolt post-stack migration. The nominal fold for Line 2 was 60, although beneath the crest of Yucca Mountain the fold exceeded 90. The nominal fold of Line 3 was 125. Fold ramped up and off the ends of both lines for 3 km. Much of the reflection signal was carried by the low-frequency part of the spectrum; surface-consistent deconvolution tended to eliminate the low-frequency signal and was therefore not applied.

Careful velocity and statics analyses were required by the large topographic relief of Yucca Mountain and spatially varied surficial velocities. Datum statics were applied using a floating datum and a datum velocity of 5000 ft/s. The 5000 ft/s value chosen was selected due to the presence of stacking velocities less than 6000 ft/s along portions of Lines 2 and 3.

Refraction statics were determined from first breaks (refractions) to offsets of 4000 ft. Refraction first breaks were used to derive a two-layer model; the near-surface weathering zone varied from about 300 to 400 ft (90 to 120 m) thick, having velocities between 2000 and 9000 ft/s (600 to 2750 m/s). The underlying layer had velocities between 5500 and 12,000 ft/s (1680 and 3660 m/s). Weathering-layer corrections made using refraction statics were compared to those generated solely using elevations. Refraction-based weathering statics produced slightly superior stacks than did the elevation-based weathering statics, so we applied refraction statics. Plots of both types of weathering statics determined for both lines are typically within 50 msec. Larger misfits of about 100 msec were noted only at the crest of Yucca Mountain.

Iterative passes of velocity analysis and statics analysis were required to optimize the final sections. The sections shown here consist of two passes of velocity analysis and surface-consistent residual statics. Well log data and stacking velocities from Line AV-1 were used to guide velocity selection. Color screen dumps of the stacking velocities, superimposed on the final sections (fig. 8) show that the stacking velocity function varied smoothly over both Lines 2 and 3; more complex velocity functions did not help stack in reflections. The smooth stacking velocity functions indicate that the reflection events imaged in Figures 10 to 17 result from reasonable stacking velocities.

Depth conversions of the final sections were calculated using a velocity function representing a fixed percentage of the stacking velocities. A range of percentages of the stacking velocity function were tested for depth conversion. The value selected for all of Line 3 and most of Line 2, 80%, provided the best fit of the depth of the inferred Paleozoic/Tertiary reflection to the depth to the top of Paleozoic rocks in UE-25 p#1. Within the Tertiary fill along the southwestern end of Crater Flat, however, it was necessary to lower the depth-conversion velocity to 60% of the stacking velocity. This choice provided a better match to the depth of the Tertiary fill estimated from the depth-converted section with previous estimates based on gravity and seismic refraction data [Langenheim, written commun., 1995; Mooney and Schapper, 1995] and is reasonable given the steep dip of reflections from beneath this zone, which require higher stacking velocities than expected for the fill. Using a higher percentage of the stacking velocities in this location, say 80%, leads to thicknesses of Tertiary fill of over 5000 m. This greater thickness is not compatible with either the density modeling or the seismic refraction data. These depth conversions were also compared to those obtained using interval velocities derived from the east-west trending refraction model near Lines 2 and 3 [Mooney and Schapper, 1995]. The refraction velocity model yielded very similar depths to the Paleozoic/Tertiary contact in the Amargosa Desert and the center of Crater Flat but overestimated the depths to the top of the Paleozoic section along Line 3 as judged from UE-25 p#1 and beneath Yucca Mountain on Line 2. The overestimation of depths to Paleozoic rocks in this vicinity using the refraction velocities is probably related to the failure of the refraction method to account properly for the interbedded high- and low-velocity layers within the Miocene tuff sequence (fig. 9), yielding average velocities that are too high. We conclude that the depth conversions achieved using percentages of the stacking velocity are preferable, and based on this comparison with the refraction velocity model and drilling results from UE-25 p#1, provide reasonable depth estimates along both Lines 2 and 3.

Post-stack migration was performed using the Stolt algorithm. Migration velocities of 50%, 60%, 70%, 75%, 80%, 85%, 90%, 95%, and 100% of the stacking velocity were compared; the migration velocity of 70% of the stacking velocity yielded the best results. A choice of higher stacking velocities led to over-migration of the deeper, more steeply dipping reflections and to some defocusing of the seismic image. The migrated sections, although generally low in quality, do provide some important guidance, particularly for the interpretation of the deeper, steeper-dipping structure.

Processing of the low-fold deep shot hole data followed a somewhat different sequence. With the intent of choosing the best shot gathers to make a low- or single-fold section for the lower crustal section (5 to 10 s), data were plotted with and without preprocessing, including bandpass and F-K filtering. These plots revealed no deep-crustal reflections northeast of St. 600, near USW VH-1. Up to 8-fold stacks of the data also revealed no lower crustal reflections beyond this point. Upon this discovery, we made no further attempt to process these data.

Table 10. Data Processing Scheme for Lines 2 and 3

Processing Step	Description
SEG-D to SEGY Conversion	Demultiplex all four sources
Separate Sources	Vibroseis Data Cross-correlate zero phase Design compensation filter from sweep Apply compensation filter Deep-hole dynamite data Tape output 0-8 s Tape output 0-20 s Apply uphole correction Poulter Data Minihole dynamite data
Merge all sources	Use 0-8 s deep-hole dynamite for statics
Build and apply geometry	In place header definition
Trace edit	
Refraction Statics	Pick first breaks using absolute offsets of 1000-5000 ft and all sources
Datum Statics	Processing Datum is Floating 5000 ft/s replacement velocity
F-K Filter	Apply NMO (brute functions) correction Apply and save AGC FK rejection filter +/- 5000 ft/s Remove AGC Remove NMO correction
Constant velocity stacks	250 ft/s increments from 4000 to 23000 ft/s
NMO Correction and Mute	50% Stretch Mute
Residual Statics	Surface Consistent Residual Statics Window 0.5 to 2.3 s Prefilter 5/10 to 35/50 Hz
Constant velocity stacks	For Stack Velocity Functions
NMO Correction and Mute	50% Stretch Mute
Residual Statics	Surface Consistent Residual Statics Window 0.5 to 2.3 s Prefilter 5/10 to 35/50 Hz
Scaling	500 ms sliding gate

Table 10. Continued

Processing Step	Description
Datum Correction	Final Datum is 5000 ft Use replacement velocity of 5000 ft/s
CDP Stack	
Bandpass Time Variant Filter	5/10-40/60 Hz
Scaling	500 ms sliding gate
FX Deconvolution	
Stack Display	Color and black and white
Depth Conversion	Using 80% of Stacking Velocities
Post-stack migration	Stolt Algorithm using 70% of Stacking Velocities

VSPs and WELL LOGS

Vertical seismic profiles (VSPs) for seven wells along Lines 2 and 3 were acquired by Birdwell Well Services, Incorporated under contract between 1981 and 1983, using geophone spacings of 25 ft and 50 ft (7.6 and 15 m) and vibrator sources (15 to 80 Hz) [Fenix and Scisson, Inc., 1986a, 1986b, 1986c, 1987]. VSPs provide a measure of the two-way travel times to known stratigraphic horizons (Table 11). Comparison between these times and those measured from the synthetic seismograms described below indicate that the observed two-way travel times (twtt) are always slightly greater than would be inferred from the synthetic seismograms (Table 12). For example, at UE-25 p#1, the VSP places the top of the Tram Tuff of the Crater Flat Group at 0.52 s twtt, the top of the Paleozoic section at 0.81 s twtt, and the bottom of the hole (at 1798 m) at 0.98 s twtt. These times are approximately 0.04 s greater than those inferred from the synthetic seismograms (Table 12). At USW VH-1, the VSP places the bottom of the hole (at 747 m) at 0.564 s twtt, about 0.1 s twtt deeper than inferred from the synthetic seismograms. Generally, the VSP data show that the synthetics underestimate total two-way travel times by amounts varying only between 0.03 and 0.1 s, providing general support for the times inferred from the synthetics.

Reasonably complete digital borehole compensated-density logs (DBC) are available for seven wells along Lines 2 and 3 (Table 13). These density logs contain gaps at the top of wells yet on average cover more than 90% of each well. Incomplete digital velocity logs (PVEL) are also available for four of these wells, including USW VH-1, USW H-6, USW H-4, and UE-25 p#1. As noted by Nelson and others (1991), velocity logs can only be acquired in liquid-filled boreholes, and the water table is unusually deep in the vicinity of Yucca Mountain, leading to large intervals at the top of the wells which could not be logged with this tool. Both logs were used to generate synthetic, vertical-incidence seismograms using modules LOGINIT and LOGPROC of DISCO Version 9.0 software.

Table 11. VSP Data#

USW VH-1				USW WT-7		
Depth (ft)	TWTT (sec)	Unit*		Depth (ft)	TWTT (sec)	Unit*
0	0.000	QTac		0	0.000	Tpc
95	0.068	Top Tb	395	0.124	Top Tpt	
175	0.088	Top QTac		1390	0.354	SWL
510	0.184	Top Tpc		1430	0.358	Top Tht
600	0.214	SWL		1575	0.396	Top Tcp/Base of VSP
870	0.256	Top Tpt				
1860	0.452	Top Tcp				
2030	0.494	Top Tcb				
2450	0.564	Base of VSP				

USW WT-2				USW H-4		
Depth (ft)	TWTT (sec)	Unit*		Depth (ft)	TWTT (sec)	Unit*
0	0.000	Tpc		0	0.000	Tpc
275	0.111	Top Tpt		215		Top Tpt
1300	0.314	Top Tht		1315	0.343	Top Tht
1590	0.386	Top Tcp		1625	0.414	Top Tcp
1875	0.448	SWL		1700	0.430	SWL
2025	0.474	Base of VSP		2275	0.530	Top Tcb
				2660	0.594	Top Tct
				3815	0.774	Top Tlr
				3975	0.802	Base of VSP

USW H-6				UE-25 p#1		
Depth (ft)	TWTT (sec)	Unit*		Depth (ft)	TWTT (sec)	Unit*
0	0.000	Qac		0	0.000	Qac
25		Top Tpc		130	0.100	Top Tmr
300		Top Tpt		175		Top Tpc
375	0.384	Top Tht		270	0.144	Top Tpt
505	0.412	Top Tcp		1190	0.334	SWL
725	0.462	SWL		1250	0.342	Top Tht
800	0.480	Top Tcb		1420	0.374	Top Tcp
855	0.554	Top Tct		1820	0.446	Top Tcb
880	0.666	Top Tll	2260	0.514	Top Tct	
710	0.780	Top Tlr	2870	0.600	Top Tlr	
950	0.830	Base of VSP		3500	0.711	Top Tta
				3610	0.732	Top Ttc
				3730	0.754	Top Tc
				3840	0.774	Top Tca
				3950	0.788	Top Tcf
				4080	0.806	Top Slm
				5900	0.980	Base of VSP

#From Fenix and Scisson, Inc. [1986a, 1986b, 1986c, 1987].

*From Nelson and others [1991].

Abbreviations: Qac, alluvium; QTac, alluvium and colluvium; Tmr, Rainier Mesa Tuff of the Timber Mountain Group; Tpc, Tiva Canyon Tuff of the Paintbrush Group; Tpy, Yucca Mountain Tuff of the Paintbrush Group; Tpt, Topopah Spring Tuff of the Paintbrush Group; Tht, Rhyolite of Calico Hills Formation; Tcp, Prow Pass Tuff of the Crater Flat Group; Tcb, Bullfrog Tuff of the Crater Flat Group; Tct, Tram Tuff of the Crater Flat Group; Tll, lavas and flow breccias of Crater Flat Group; Tlr, Lithic Ridge Tuff; Slm, Lone Mountain Dolomite; SWL, Static water level.

Table 12. VSP Data versus Synthetic Seismograms

Well Name	Depth to Base of Log (ft)	Calculated Two-way Travel Time To Base of Log (sec)	Base of VSP (ft)	Two-way Traveltime to Base of VSP (sec)	Basal Unit
UE-25 p#1	5910	0.94	5900	0.98	Slm
USW H-6	3980	0.83	3950	0.83	Tlr
USW VH-1	2477	0.46	2450	0.56	Tcb
USW H-4	4004	0.79	3975	0.80	Tlr
USW UZ-6	1856	0.46	1840	0.50	
UE-25 UZ-16	1676	0.37			
USW WT-7	1589	0.33	1575	0.40	Tcp

As previously noted, all the velocity logs lack substantial amounts of data at the top of the well and contain gaps within the logs, and in total lack data for between 25 and 68% of each well (Table 13). Calculation of synthetic seismograms, however, requires complete logs for both density and velocity, as null values in either would generate spurious seismic reflections. It was necessary, therefore, to fill in gaps in the velocity logs using the more complete density logs. Comparison of observed density and velocity values for the four wells that have both logs revealed that Lindseth's formula (velocity (ft/sec) = 3460/(1.0-0.308 x Den)) yielded a more accurate prediction of velocity from density than Gardner's formula (velocity (ft/sec) = (Den /0.23)^4), where Den=Density(g/cm^3). We therefore filled in gaps in the velocity logs using Lindseth's formula.

Further, as noted by Nelson and others [1991], the density logs from the vicinity of Yucca Mountain suffer from two major problems. First, the density-tool compensation algorithm does not work well in air-filled boreholes above water table, yielding noisy logs and consequently noisy calculated-velocity logs. Second, at depth intervals in which the hole is rugose, the density tool may become separated from the rock wall and provide spuriously low density values. For the wells analyzed here, these intervals typically correspond to zones where the caliper values become unusually large, indicating a wide borehole. This second problem was related to constraints on using drilling fluids above the water table. Thus, both problems are restricted to the interval of the holes above water table; below water table there are relatively few problems with the density logs.

Due to these problems, all the well logs required substantial editing prior to the calculation of synthetic seismograms. The density logs were first desampled to a one-ft sample interval from the original 0.5-ft sample interval, extrapolated to the surface, and then used to interpolate missing portions of the velocity logs from Lindseth's formula. For wells USW UZ-6, UE-25 UZ-16, and USW WT-7, Lindseth's formula was used to generate the entire velocity log from the existing density log. Where velocity and density logs both contained gaps, both of these values were interpolated linearly across the gaps in the logs. Where a gravity log existed, as for UE-25 p#1, it was used to predict density values missing from the DBC log. (Gravity logs were obtained in some holes using a downhole gravity meter [Nelson and others, 1991].) Densities less than 1.0 g/cm^3 were increased to a minimum of 1.3 g/cm^3, and corresponding velocities less than 5000 ft/sec were increased to a minimum of 6000 ft/s. Similarly, above the water table, and except for the Tertiary basalt section of USW VH-1, densities above 2.5 g/cm^3 were reset to 2.5 g/cm^3, and their corresponding velocities were reset to 12,000 ft/sec. In some cases, the velocities in gaps

calculated from Lindseth's formula were increased by hand in order to better match velocity values on either side of the gaps.

The final, edited well logs were converted to integer ASCII values and copied to the DISCO system. The final logs contain depth in integer ft, velocity in ft/sec, and density in kg/m^3. The module LOGINIT was used to read the logs into the YUCCA project name area from disk. The module LOGPROC was used to calculate a sonic well log (SON), impedance log (MLT, KEP), a reflection-coefficient series (TDC), and a primary reflection series (RFC, PRI) from the input velocity and density logs. A 30-Hz Ricker wavelet (defined in FIL and chosen for the mid-range of the 10- to 50-Hz Vibrator sweep) was used to filter the primary reflection series shown here. Display (DIS) was made using wiggle plots for the logs, spike plots for reflection coefficients, and trace plots of the synthetics.

Synthetic seismograms for the shallow holes, USW VH-1, USW WT-7, USW UZ-6, and UE-25 UZ-16, provide information above 0.46 s twtt (fig. 9, Table 13). Synthetic seismograms for UE-25 p#1, USW H-6, and USW H-4 yield information above 0.94 s twtt (fig. 9, Table 13). Given the uncertainty in the density and velocity at the top of the logs, it probably is unwise to attribute much significance to the strong reflections produced by the assumed velocities and densities at the top of the logs. Similarly, it is probably unwise to over-interpret the synthetics in the zones where velocities are interpolated solely from the density. Density logs for USW WT-7 and USW UZ-6 are similar (figs. 9B and 9C), however, and predict a reflection from near the base of the log at the contact between the Calico Hills Formation and the Prow Pass Tuff of the Crater Flat Group.

Table 13. Digital Well Log Data for Synthetic Seismograms

Well Name	Density Log Coverage (ft)	Velocity Log Coverage (ft)	Percent of Density Log Missing	Percent of Velocity Log Missing	Two-way Travel Time To Base of Logs (sec)
UE-25 p#1	37-5910	1267-5900	4	25	0.94
USW H-6	312-3980	1907-3975	8	48	0.83
USW VH-1	50-2449	801-2477	9	60	0.46
USW H-4	59-4003	2583-4004	20	68	0.79
USW UZ-6	325-1856	None	17	00	0.46
UE-25 UZ-16	40-1676	None	3	00	0.37
USW WT-7	53-1589	None	3	00	0.33

The synthetic seismograms show reflections that are produced at intervals where both density and velocity logs exist. The synthetic for UE-25 p#1 reveals a reflection from 0.76 s from just above the pre-Tertiary/Tertiary boundary (fig. 9G). Reflections from 1400 to 2000 ft (430 to 600 m) are from the Prow Pass and Bullfrog Tuffs of the Crater Flat Group. A large-amplitude reflection calculated at 0.04 s twtt for USW VH-1 is caused by a high-density, high-velocity Tertiary basalt layer noted in the drilling log (Nelson and others, 1991; fig. 9A). Reflections within the Topopah Spring Tuff of the Paintbrush Group are calculated at 1400 ft (430 m) in USW VH-1. A low-velocity layer in the Prow Pass Tuff of the Crater Flat Group in USW H-6 at about 2000 ft (600 m) produces a reflection at about 0.52 s (fig. 9F). The existence of these low velocities in USW H-6 is uncertain, however, given that they occur over an interval in which there is a large excursion in the caliper log [Nelson and others, 1991].

GEOLOGIC INTERPRETATION OF SEISMIC SECTIONS

In this section we describe and present a preliminary geologic interpretation of seismic reflection Lines 2 and 3. Three versions of the seismic sections are presented because it is useful to examine different presentations of the data to guide the interpretation. For instance, stacked sections provide the sharpest and least processed images of reflections, but the reflections do not represent a geologic cross section since they are presented in terms of two-way travel time rather than depth. The depth-converted sections provide a depth estimate of the reflections, without vertical exagerration, but also do not represent a true geologic cross section because dipping reflections are not correctly located in the subsurface. Depth conversion tends to make deeper reflections, in high-velocity rocks, appear lower-frequency and provides an estimate of the decreasing vertical resolution with depth inherent to seismic reflection data. Only migrated, depth-converted sections represent a true geologic cross section and are the only sections shown interpreted in this report. Migrations of lower-quality data such as Line 2 and 3 often result in considerable defocusing of the image (producing a wormy appearance), and the collapsing of diffracted energy inherent to migration makes some reflections less obvious. Thus, some reflections are actually easier to identify in the stacked, unmigrated sections, although they are not correctly located in the subsurface. Uninterpreted presentations of all sections are provided. Uninterpreted, unmigrated, and non-depth-converted seismic sections for Lines 2 and 3 are shown in Figures 10 and 11. Both seismic sections are displayed with a final datum of 1500 m (5000 ft) above sea level, although a floating datum was used for the velocity analysis. Plots on these sections also show the elevation along the line, the floating datum used for processing, the stacking velocities (in milliseconds and ft/s) at 1-km intervals, and the fold of the stacked section. The time sections are provided to allow comparisons to other existing and future reflection surveys without introducing the uncertainties involved with depth conversions. Times given in this discussion are generally cited as two-way travel time (twtt) relative to 0.0 s on Figures 10 and 11.

Uninterpreted depth conversions of these seismic sections, plotted without vertical exaggeration, are shown in Figures 12 and 13. Most of the depths given below are cited as depth below the final datum at 1500 m (5000 ft) above sea level. Thus, on all of these plots, the start of data indicates the ground surface. Note that depth-converted sections do not properly account for the location of deeper, dipping events, but do provide reasonable approximations to reflector depths for the shallow, flat-lying reflectors.

Post-stack migrations and depth conversions of the sections are provided in Figures 14 and 15 and are interpreted in Figures 16 and 17. The interpretations in Figures 16 and 17 are based primarily on the depth conversions of these sections, but the depth-converted migrations provide more accurate locations of the deeper, dipping reflections. Table 14 provides a list of geographic locations intersected by both lines for geographic reference. Most of these locations are also presented as top labels along the seismic sections shown in Figures 10 to 17. The hybrid sources used to acquire Lines 2 and 3 are listed in Table 15. Note the overlap in station numbers indicating the overlap of sources used to facilitate processing of these data.

Line 2

Line 2 images seismic reflections at depths between 0.04 km and 24 km (corresponding to travel times between 0.05 s and 8 s twtt). Line 2 crosses four major structural domains, including the Amargosa Desert, Steve's Pass, Crater Flat, and Yucca Mountain (fig. 1B). We discuss the observed reflections within these domains in order from southwest to northeast. In general, we first describe the shallowest reflections and work downwards through the section.

Amargosa Desert (St. 101 to 285)

Within the Amargosa Desert a prominent, low-frequency, west-dipping reflection extending about 1 km below the surface is identified as the Paleozoic/Tertiary contact (fig. 16). The primary basis for this identification is the observation that the reflection projects updip to Steve's Pass, near St. 285, close to outcrops of Late Proterozoic and Cambrian clastic units [Swadley and Carr, 1987; Monsen and others, 1992] located about 200 m south and east of the seismic line between St. 280 and 300. The identification of this reflection as the top of the Paleozoic strata also matches density modeling along the line (fig. 19), which defines a southwestwardly thickening Tertiary basin. Up to 400-m down-to-the-west offset of the Paleozoic/Tertiary contact at St. 230 is inferred in Figure 16. This offset is located about 600 m north of an isolated, low, north-trending ridge of Miocene tuffs [Swadley and Carr, 1987], and is inferred to result from a north-trending, down-to-the-west normal fault. Magnetic data along Line

Table 14. Line 2 and 3 Markers

Line 2		Line 3	
Station	Marker*	Station	Marker*
235	Highway 95	101	USW H-6
332	Steve's Pass	140	Solitario Canyon Fault
430	Little Cones	167	USW UZ-6
550	Red Cone	206	USW WT-2
646	USW VH-1	210	Ghost Dance Fault
730	Crater Flat Fault	296	Bow Ridge Fault
810	Windy Wash Fault	326	Midway Valley Fault
865	Fatigue Wash Fault	337	UE-25 p#1
938	USW WT-7	360	Paintbrush Canyon Fault
980	Solitario Canyon Fault	370	Fran Ridge
1054	USW WT-2	452	Fortymile Wash
1056	Ghost Dance Fault		
1079	USW H-4		
1088	UE-25 UZ-16		

*Fault locations taken from Simonds and others [1996].

Table 15. Line 2 and 3 Sources

Line 2		Line 3	
Station	Source Type	Station	Source Type
101-945	Vibrator	101-129	Vibrator
945-1133	Poulter Charge	127-165	Poulter Charge
		164-235	Vibrator
		233-315	Poulter Charge
		313-337	Vibrator
		331-439	Minihole Pattern
		437-541	Vibrator

2 (fig. 20) are also consistent with fault offset of the Miocene tuffs near St. 220 and with north-trending normal faulting near St. 150 [Langenheim and Ponce, 1995].

The seismic sections image only poorly the geometry of the Tertiary fill above the Paleozoic/Tertiary contact along this portion of Line 2, perhaps due to the lower fold of the seismic data there. There is, however, a suggestion of a gentle easterly dip of strata into the inferred Paleozoic/Tertiary contact at St. 250 (fig. 16).

Beneath the Amargosa Desert, reflections from the lower crust were successfully acquired using both vibrator and shot hole sources. The depth to the top of the reflective lower crust just above 15 km (4.8 s twtt; fig. 18) is similar to that imaged by line AV-1 to the southeast [Brocher and others, 1993]. The base of the crust, or Moho, is imaged between 9 and 10 s, corresponding to depths between 27 and 30 km (not shown here). This Moho depth was also reported to the southeast in the Amargosa Desert by Brocher and others [1993].

Steve's Pass (St. 285 to 330)

Little coherent seismic energy is present in the vicinity of Steve's Pass (fig. 16). This observation is consistent with the nearly complete absence of Tertiary rocks over this structural high [Swadley and Carr, 1987; Monsen and others, 1992] and our expectation that few coherent reflections within the highly-deformed Proterozoic and Paleozoic rocks might be obtained. A subhorizontal, low-frequency event at 8000 ft below datum is observed beneath the inferred top of Paleozoic rocks between St. 350 and 370. A prominent gravity high over Steve's Pass is the largest positive anomaly in the gravity data along Line 2 (fig. 19). Density models are consistent with the outcrop of Proterozoic and Paleozoic rocks in this location (fig. 19), although the model slightly underpredicts the gravity field southwest of the pass and overpredicts the field northeast of the pass.

Crater Flat (St. 330 to 910)

Several sets of reflections were observed from Crater Flat, and the data from Crater Flat probably represent the best data acquired during our survey. The data from Crater Flat are notable for the depth to which coherent reflections can be observed as well as the lateral continuity of reflections.

Prominent, subhorizontal reflections about 150 m deep (0.15 s twtt below the surface) may be traced continuously for over 5 km between Little Cones and USW VH-1 (St. 430 and 646; figs. 1B and 16). We interpret these reflections as thin basaltic flows based on the VSP at USW VH-1 (Table 11) and their high-amplitude, low-frequency character. This character is similar to that of reflections inferred to represent shallow basaltic flows along Line AV-1 [Brocher and others, 1993]. The reflections dip gently westward near USW VH-1 but appear nearly unfaulted between Little Cones and Red Cone. Vertical offsets on the inferred basaltic flows are minor, less than 13 m, consistent with the relatively flat character of the ground magnetic field (where not disrupted by magnetic fluctuations caused by the basaltic debris from Little Cones and Red Cone; fig. 20). The apparent continuity of these events is not considered to be an artifact of data processing because surface-consistent residual statics were determined using three different windows between 0.5 and 2.3 s twtt (fig. 10) and were not selected to minimize the apparent structure on this reflection. Basaltic flows intersected at 366 m depth in USW VH-2, located about 2.4 km NNW of St. 602, dated as 11.3 Ma [Carr and Parrish, 1985], may be correlative with the deeper reflector on Line 2. The shallow basaltic flow intersected by USW VH-1, dated as 3.7 Ma [Carr, 1982], may be correlative to the shallower reflector on Line 2. Thus, both reflectors are inferred to be older than Little Cones or Red Cone, which are dated as 1.1 and 1.0 to 1.5 Ma, respectively [Vaniman and others, 1982].

The inferred shallow basaltic reflectors are underlain by coherent reflections which clearly define a thin, asymmetric, west-dipping basin up to 1.2 km (3600 ft) deep between Steve's Pass and USW VH-1 (St. 380 and 650; fig. 16). The base of the basin is defined by reflections from an unconformity at the bottom of the basin. These intersect USW VH-1 (Station 645) at 0.18 s subsurface; this time correlates to VSP and synthetic travel times with the top of the Tiva Canyon Tuff of the Paintbrush Group (Table 11). The unconformity may be traced as far to the northeast as the Fatigue Wash fault where it truncates west-dipping reflections (St. 875) and appears to deepen slightly northeast of USW VH-1 (fig. 16). The shallow reflections above the unconformity do not show significant vertical offset. This basin strongly resembles the shallow basin proposed for this location by Carr and Parrish [1985] based on drilling results from USW VH-2. The existence of this basin was disputed by Hamilton [written commun., 1994], who suggested that the data were also consistent with a tilted block, but its existence may be consistent with low-amplitude folding in Crater Flat produced by N-NE to S-SW directed shortening [Fridrich, written commun., 1995].

Northeast of Steve's Pass, a series of high-amplitude, moderately east-dipping events extend from the surface to 2100 m (7000 ft) below datum (2 s twtt below the surface). These east-dipping reflections project to the surface just northeast of Steve's Pass (between St. 330 and 360), where Monsen and others [1992] inferred three faults beneath surficial cover. For this reason we interpret them as several faults, with the strongest event projecting to St. 330 representing the Bare Mountain fault. On the migrated, depth-converted section (fig. 16) we have interpreted the Bare Mountain fault as truncating a series of prominent, low-frequency subhorizontal reflections on their eastern side. The origin of these subhorizontal reflections is unknown, but based on density models (fig. 19) we interpret them as originating within the Precambrian and Paleozoic section beneath Bare Mountain. Regional gravity data suggest that Line 2 crosses the Bare Mountain fault at a high angle, making it nearly a true dip line in this location [V.E. Langenheim, written commun., 1995]. If so, the depth-converted migration (fig. 16) suggests that the Bare Mountain fault has a dip of about 42° consistent with the density models (fig. 19). The large amplitudes of the reflections are compatible with their origin at the Paleozoic/Tertiary contact.

In the southwestern half of Crater Flat west-dipping reflections extend as much as 3800 m (12,500 ft) below the surface (fig. 16). These west-dipping reflections appear to be truncated by and rotated into the reflection inferred to represent the Bare Mountain fault and are interpreted as reflections from the Tertiary fill beneath Crater Flat. The nearly 4000-m thickness of Tertiary units is in close agreement with the 3300 to 3500 m inferred from seismic refraction and gravity data [V.E. Langenheim, written commun., 1995; Mooney and Schapper, 1995]. Beneath Red Cone we interpret the migrated data as indicating that the basin floor dips westward (fig. 16), contrary to the density models (fig. 19). To the east, west-dipping reflections inferred to represent Tertiary basin fill are underlain by prominent, west-dipping reflections between Red Cone and the Crater Flat fault (St. 550 and 700) at a depth between 15,000 and 8,000 ft (4600 and 2500 m) below datum (twtt between 1.6 and 2.4 sec). These prominent reflections are inferred to represent the Paleozoic/Tertiary boundary due to their large-amplitude, low-frequency character and relative continuity. This interpretation is qualitatively consistent with the density models, which show the Paleozoic/Tertiary contact ramping up eastward at a gentle angle between USW VH-1 and the Windy Wash fault (St. 640 to 820; at km 18 on fig. 19). The density model, however, fails to properly account for the low-amplitude gravity anomalies in this vicinity. The interpretation of the Paleozoic/Tertiary contact shown in Figure 19 in this location is simple, and we acknowledge that additional, small offset structures on this contact could be interpreted in this region (near St. 750).

We interpret a short, subhorizontal reflection between St. 600 and 625 and at a depth of 5300 m (17,500 ft) below datum (3.2 s twtt) lying below this inferred Crater Flat half-graben as occurring within the Precambrian and Paleozoic section. As such, it could represent a stratigraphic boundary in the Precambrian/Paleozoic section or a part of a detachment surface. We acknowledge that this reflection is probably too shallow to represent a postulated detachment

beneath Crater Flat [Scott, 1990]. An alternate model is suggested by seismic refraction data from the base of Crater Flat in this location which show high (6.8 km/s) velocities, as much as 1 km/s higher than adjacent "basement" rocks [Mooney and Schapper, 1995]. Although the 6.8 km/s velocities could represent Paleozoic carbonate rocks (see well log data from UE-25 p#1; fig. 9G), a more interesting speculation is that these velocities could also represent refractions from a thick mafic intrusion into the Precambrian and Paleozoic section. Because mafic sills are known to produce high-amplitude reflections elsewhere in the Basin and Range [Goodwin and others, 1989], and a mafic sill could also provide the deep magnetic source needed to explain the broad magnetic anomaly within Crater Flat (fig. 20), an anomaly which can not be explained by shallower magnetic structures within the Tertiary fill [V.E. Langenheim, written commun., 1995; Langenheim and Ponce, 1995], a mafic intrusion could explain these subhorizontal reflections. Qualitatively, these reflections appear to be in a location and depth expected for the deep magnetic source. A mafic sill is not required, however, because Langenheim and Ponce [1995] suggest that the Devonian Eleana Formation might also be the source of the broad magnetic anomaly.

Deeper reflections are not sharply imaged between the Crater Flat and Fatigue Wash faults (St. 750 and 875). We identify, however, a discontinuous, undulatory, low-frequency reflection at about 3000 m (10,000 ft; 1.8 to 1.9 s twtt) below datum (fig. 16); this event is even clearer in the intermediate section (fig. 18). Based on its character and depth, we infer that it is the Paleozoic/Tertiary boundary. The disrupted character of the reflection (which is more clearly observed in the intermediate level processing of this line (fig. 18) than in Figure 16) probably results from closely-spaced normal faults mapped at the surface (for example, Crater Flat, Windy Wash, and Fatigue Wash faults; fig. 16) and is consistent with magnetic anomaly data (fig. 20) showing fault spacings on the order of 1 to 2 km [Langenheim and Ponce, 1995]. The relatively subdued dip of this horizon is consistent with isostatic gravity anomaly data, which are nearly flat in this region, suggesting that the Paleozoic/Tertiary boundary rises only modestly to the east in this location (fig. 19). We infer that prominent, west-dipping reflections at station 781, about 1500 m (5000 ft) below datum, are produced within the Tertiary section. This reflection may be projected discontinuously westward beneath depths reached by USW VH-1, making this horizon older than the Bullfrog Tuff of the Crater Flat Group.

Lower-crustal reflections can be observed beneath Crater Flat as far northeastward as Red Cone where it resembles those seen in the Amargosa Desert (St. 600; fig. 18; Brocher and others, 1993). Vertical striping of these reflections is attributed to variable near-surface conditions providing windows into the lower crust and are not interpreted as being indicative of the structure of the lower crust. We postulate that northeast of Red Cone (St. 600) the water table was too to couple strongly either the vibrator or shot hole seismic energy into the ground.

Yucca Mountain (St. 910 to 1133)

Reflections from the vicinity of Yucca Mountain are difficult to interpret for several reasons. The most important of these include (1) difficulties created by the strong topographic relief across the mountain, requiring a change of seismic sources and causing large statics and rapid lateral changes in seismic velocities, and (2) problems caused by the highly oblique geometry of the line relative to structural dips. Despite these major difficulties, we believe that very useful and mappable seismic reflections were obtained beneath Yucca Mountain (fig. 16).

An important stratigraphic and structural event is imaged nearly continuously across Yucca Mountain about 500 m (1600 ft) below the surface (time about 0.4 s twtt below the surface). This long, multicyclic event can be correlated to VSPs at wells USW WT-7, USW WT-2, and USW H-4 (Table 11) and originates at or near the top of the Prow Pass Tuff of the Crater Flat Group. The multicyclic character of the reflection indicates that it originates from constructive interference from several units within the Prow Pass and Bullfrog Tuffs. The three cycles which characterize this event thicken slightly to the west, which we interpret as westward stratigraphic thickening

across Yucca Mountain of the Prow Pass and possibly Bullfrog Tuffs also inferred from geologic evidence [Fridrich and others, 1994a]. This observation is geographically restricted to Line 2 between USW WT-7 and UE-25 UZ-16 and is contradicted by the thickness contours of the Prow Pass Tuff by Moyer and Geslin [1995] but not by their data points. Structurally, the event broadly parallels or subparallels topography except between USW WT-7 and the Solitario Canyon fault, where it dips significantly to the west. Scott's [1990] suggestion of wide areas of western dips between pairs of block bounding faults is supported by the observation of local westward stratal dips in Solitario Canyon [D.C. Buesch, oral commun., 1995] but further supported by the reflection line only in the vicinity of the Solitario Canyon fault. We note, however, that detailed mapping elsewhere at Yucca Mountain does not yield westward dips of Miocene strata [Dickerson and Spengler, 1994], nor do we observe western dips in the seismic data elsewhere at Yucca Mountain.

Within the resolution of the seismic reflection data, which is limited by the low frequency of the event to several meters, little if any disruption of the Prow Pass Tuff event is inferred in the vicinity of the Ghost Dance fault, which has important implications for the recent history of this fault [see Spengler and others, 1993, 1994; Simonds and others, 1996]. The Ghost Dance fault, however, does appear to mark a monocline in the Prow Pass Tuff. This monocline may have formed over the simpler offset of the Paleozoic/Tertiary contact beneath it as suggested by Fridrich [written commun., 1995] for Yucca Mountain structures generally but not specifically for the Ghost Dance fault. In fact, given the very small offset of this fault at the surface (very much less than 30 m) any disruption of the Prow Pass Tuff reflection would be surprising. Broadly speaking, there is little if any resolvable vertical offset of the Crater Flat Group across Yucca Mountain, apart for that in the vicinity of the Solitario Canyon fault.

The second widely mappable horizon is the eastward continuation of the deeper, discontinuous, undulose, low-frequency reflection observed over 5 km between St. 700 and 910 at 1.8 s twtt (3000 m below datum). This persistent event may be traced discontinuously over 3.6 km beneath Yucca Mountain (from St. 910 to St. 1090) at nearly the same depth (1.9 s twtt from datum) as to the west. Vertical down-to-the-west offset of this horizon in the vicinity of the Solitario Canyon fault may be as much as 230 m (0.1 s twtt). An apparently more significant component of down-to-the-west displacement occurs just to the west of the mapped location of the Ghost Dance fault, where up to 450 m (0.2 s) of offset is inferred (fig. 16). The event ties to Line 3, where UE-25 p#1 indicates the reflection is at or just below the Paleozoic/Tertiary contact. This interpretation is strengthened by density models indicating that the Paleozoic/Tertiary boundary is located about 2500 to 3000 m beneath the crest of Yucca Mountain (fig. 19). The nearly 1000 m of aggregate offset of the inferred Paleozoic/Tertiary contact on all the faults in the vicinity of the crest of Yucca Mountain is also consistent with gravity data [V.E. Langenheim, written commun., 1995]. More than 500 m of structural relief on the Paleozoic/Tertiary contact in this region has been proposed based on the thickening of Miocene tuffs inferred from well and gravity data [Fridrich and others, 1994a]. A graben is proposed to have formed along this portion of Line 2 from 14 to 13.5 Ma based on these well data [Fridrich and others, 1994a; Fridrich, written commun., 1995]. Perhaps due to declining fold of reflection coverage, this event cannot be traced farther to the east than St. 1100 on Line 2 (fig. 16). Along Lines 2 and 3 in the vicinity of Yucca Mountain the Paleozoic/Tertiary contact produces a reflection signature characterized by a low-frequency, large-magnitude triplet. Because the data were acquired using explosion (impulsive) sources, and the vibrator data was filtered to match the other data, we picked the Paleozoic/Tertiary contact at the top of this reflector triplet.

Lower Crust

As previously described, discontinuous subhorizontal lower-crustal reflections beneath about 15 km (5 s twtt) can be seen only on the southwestern end of Line 2 (St. 101 to 600; fig. 18). These reflections can be observed on shot records obtained using both vibrator and deep shot hole sources. No reflections from the lower crust can be observed northeast of Red Cone (St. 600) on this section, which was confirmed after analysis of the deep shot hole data. The abrupt loss of lower-crustal reflections northeast of Red Cone (St. 600) does not appear to be real. We believe that near-surface conditions in Crater Flat and Yucca Mountain precluded the observation of lower-crustal energy, even from the deep shot hole sources. The water table is over 500 m (1800 ft) deep at Yucca Mountain, and it appears that the seismic energy was lost to due to poor source coupling. The water table in the Amargosa Desert is significantly more shallow than near Yucca Mountain, allowing us to place the shot holes there at or near the water table.

Line 3

Line 3 ran nearly normal to the predominantly north-trending structures across the potential repository area of Yucca Mountain eastward into Jackass Flats (fig. 1B). This line images a number of reflections at depths as shallow as 1600 ft to as great as 20,000 ft (6.1 km or 3 s twtt) below datum (fig. 17). In general, however, few coherent events are observed below 3 s twtt (fig. 11). Our discussion is divided into sections for Yucca Mountain, Jackass Flats, and the lower crust.

Yucca Mountain (St. 101 to 375)

As does Line 2, Line 3 discontinuously images a low-frequency reflection about 500 m (0.4 s or 1600 ft) below the surface between Yucca Crest and Fran Ridge (St. 160 and 400; fig. 17). VSP data at USW H-6 (St. 101), at USW WT-2 (St. 168), at USW H-4 (projected 1.1 km from the north to St. 240), and at UE-25 p#1 (St. 337) indicate that this reflection is at or near the top of the Prow Pass Tuff of the Crater Flat Group (Table 11). Discontinuities in this event make it difficult to determine fault offset. Within the resolution of the seismic data (several meters) little if any offset of this horizon is noted at the vicinity of the Ghost Dance fault, where much less than 30 m of vertical offset has been mapped at the surface where crossed by the seismic line [Scott and Bonk, 1984; Spengler and others, 1993, 1994; Simonds and others, 1996]. Ground magnetic anomaly data, which are sensitive to offset of the Topopah Spring Tuff, apparently show much less offset at the Ghost Dance fault than at the Solitario Canyon fault (fig. 22). It is difficult to determine the offset of this reflection across the Bow Ridge and Midway Valley faults. Both of these regions appear to be complexly faulted zones and have been mapped as imbricate fault zones by Scott [1990], although tunneling results suggest the region near the Bow Ridge fault is not complexly faulted [R.W. Spengler, written commun., 1995].

A second reflection is mapped discontinuously at approximately 2100 to 1800 m depth (1.7 to 1.6 s twtt below datum) between the Ghost Dance fault and Jackass Flats (St. 210 and 510; fig. 17). We interpret this prominent event as the Paleozoic/Tertiary contact based on its high-amplitude, low-frequency signature, structural discordance with overlying reflections, and favorable tie to similar low-frequency reflections along Line 2. This interpretation is strengthened by UE-25 p#1 (St. 337), which intersects this horizon at 1200 m (4000 ft) depth subsurface (0.8 s; Table 11; fig. 9), as well as by density models for the gravity data (fig. 21). We interpret several faults offsetting the Paleozoic/Tertiary contact (fig. 17), although broadly speaking most of these offsets are relatively minor (less than 150 m), in agreement with density models for Line 3 (fig. 21) east of the Bow Ridge. For clarity, several of the faults offsetting this contact are shown as

extending upwards into the Tertiary section (fig. 17) even though the seismic data do not show offset of a Tertiary reflector. The largest offset of the inferred Paleozoic/Tertiary contact is less than 500 m. The westerly dip of the top of the Paleozoic section in the density models west of Bow Ridge is not evident in the seismic reflection data. Note that both density models in Figure 21 fit the gravity data equally well, showing that gravity data alone are not sensitive to the difference between models A and B. Given the presence of only two reflection events, there is considerable uncertainty in the geometry of the interpreted faults shown in Figure 17.

Perhaps the most unusual and unexpected reflection observed during our survey is a moderately east-dipping event that is imaged directly beneath the western flank of Yucca Mountain (stations 121-181), at 1000 to 2000 m (3300 to 6600 ft; 1.0 to 1.8 s twtt) below datum. This event is well above the top of the inferred Paleozoic basement judging from Line 2 and the gravity data (fig. 21). This large-amplitude reflection was imaged using a reasonable stacking velocity of 13,000 ft/s (fig. 8B), but is not observed on Line 2. We therefore interpret this event as representing either a diffraction which has not been properly collapsed during migration, possibly because it is located at the start of the line, or as side swipe from structure outside the plane of the reflection survey. Less plausibly, it may provide evidence for a block of Tertiary rocks rotated by faults in the vicinity of the Solitario Canyon and Ghost Dance faults, and its large structural discordance could be viewed as evidence for listric faulting in this region, probably pre-Prow Pass tuff, as the Prow Pass Tuff reflector is not involved in this tilting. If the reflection represents a processing artifact, however, the need for listric faulting of the pre-Prow Pass tuff would be eliminated. There is no evidence for such a structure in the surficial geologic mapping.

The rocks beneath the inferred Paleozoic/Tertiary boundary produce a number of reflections along Line 3. They show a variety of dips but the reflections are short and are difficult to interpret. This observation is consistent with our expectation that few coherent reflections within the complexly deformed Paleozoic rocks might be obtained.

Jackass Flats (St. 375 to 541)

Jackass Flats is underlain by a series of shallow, gently east-dipping, continuous, high-frequency reflections. We interpret these events as reflections from the Tertiary fill which define an eastward-thickening Tertiary basin section up to 300 m (800 ft) thick. Minor offsets of these reflections may be noted near the eastern end of the line (at St. 515).

Reflections from the inferred Paleozoic/Tertiary contact at 1800 m (1.6 s) below datum show a number of structures extending nearly to the eastern end of the line. The largest structure lies just east of the Paintbrush Canyon fault. Presuming the line is orthogonal to the structure, we interpret the up to 600 m of apparent offset of the Paleozoic/Tertiary contact there as evidence for a moderate-angle, west-dipping fault which projects upward to the vicinity of Fortymile Wash (St. 451). If Line 3 crossed the fault obliquely, however, the dip of the fault would be steeper than inferred here. In the vicinity of Fortymile Wash the Paleozoic/Tertiary contact has a gentle synclinal structure, and we interpret an offset, down-to-the-east, of 90 m in the Paleozoic/Tertiary contact near Fortymile Wash (fig. 17). Previously acquired gravity and magnetic anomaly data are consistent with the absence of larger (hundreds of meters) structural relief of the Paleozoic/Tertiary contact beneath Fortymile Wash [Ponce and others, 1992]. The absence of larger offset of the inferred Paleozoic/Tertiary contact in the vicinity of Fortymile Wash is also consistent with gravity and magnetic data acquired along Line 3 which show no significant anomaly there (figs. 21 and 22). The interpretation of a relatively flat Paleozoic/Tertiary contact beneath Jackass Flats, coupled with an eastward-thickening Tertiary basin, is consistent with an eastward thinning of the Miocene volcanic section.

Lower Crust

Neither the deep shot hole nor vibrator data successfully imaged the lower crust (5 to 10 s twtt) along Line 3. No reflection events below 6000 m (20,000 ft; 3.1 s twtt) can be identified in the section for Line 3. Almost all of the deep shot holes along Line 3 were acquired in ideal weather conditions (Table 6), suggesting that the failure to observe lower-crustal reflections results from unfavorable near-surface geology. As for the eastern parts of Line 2, the shot holes were detonated more than 400 m above the water table, which may have resulted in poor shot coupling and poor signal propagation. Larger shot holes are necessary to obtain lower crustal data in this location.

DISCUSSION

Yucca Mountain offers many challenges to acquiring high-quality seismic reflection data, and early attempts to do so met with little success [McGovern and Turner, 1983]. Lines 2 and 3 were therefore designed to test modern seismic reflection methods at Yucca Mountain. As stated previously, the objectives of this profiling included (1) tracking the pre-Tertiary/Tertiary boundary beneath Yucca Mountain, (2) mapping reflections above this horizon if possible, (3) determining the geometry of faults in the subsurface, and (4) providing subsurface data to limit the number of structural models for Yucca Mountain. A subsidiary objective was to look for seismic bright spots that could indicate the presence of potential magma chambers in the middle and lower crust. Fair- to good-quality data were obtained during our survey in Crater Flat and Jackass Flats, but useful data, although lower in quality, were also obtained at Yucca Mountain. Lines 2 and 3 intersect about 600 m east of the crest of Yucca Mountain, and in that location, both lines show reflections from at or near the top of the Prow Pass Tuff of the Crater Flat Group as well as from the inferred Paleozoic/Tertiary contact (figs. 16 and 17). (The two lines intersect at Station 1027 on Line 2 and Station 191 on Line 3.) The close match is important, as it indicates success in meeting the first two objectives on both lines. Furthermore, as Poulter charges were used to acquire Line 2 in that region whereas vibrator sources were used to acquire the corresponding part of Line 3, the close match suggests that our use of hybrid seismic sources, demanded by environmental, topographic, and operational constraints, did in fact provide comparable seismic data along the lines.

The offset of the inferred Paleozoic/Tertiary contact beneath Yucca Mountain is compelling evidence against the presence of an active detachment surface near or at the Paleozoic/Tertiary contact as previously proposed [Scott, 1986, 1990; Fox and Carr, 1989]. Although there is some uncertainty of the dip of the moderate- to high-angle faults which offset this contact along Lines 2 and 3, the clear offset of this surface suggests that the faults extend deeper into the crust as suggested by opponents of the shallow detachment hypothesis [e.g., Carr and others, 1986; Hamilton, written commun., 1994; Fridrich, written commun., 1995].

The age of shallow structures in the vicinity of the Ghost Dance fault is of major concern to evaluation of the potential repository site at Yucca Mountain. Coupling the lack of large offset of the reflection inferred to represent the top of the Prow Pass Tuff with the absence of large surficial offsets in the vicinity of the Ghost Dance fault [Spengler and others, 1993, 1994; Simonds and others, 1996], we infer that the large offset of the Paleozoic/Tertiary contact in the vicinity of the Ghost Dance fault formed primarily before the mid-Miocene. Fridrich [written commun., 1995] has documented a large extensional event in Paleozoic and older rocks at Bare Mountain between 18 and 15.2 Ma, which may have extended to Yucca Mountain.

The subsurface geometry of the Bare Mountain range-front fault has similarly been the subject of a long and important debate. The Bare Mountain fault forms the western boundary of the Amargosa Basin structural trough [Wright, 1989; Carr, 1990], and is a major structural feature. Snyder and Carr [1984] modeled the fault as a western boundary of a mid-Miocene caldera,

having a steep, easterly dip of 75°. Oliver and Fox [1993] showed that a shallow-dipping (27°) normal fault model is consistent with the gravity data from Crater Flat. Recently, Langenheim [1995] demonstrated that gravity data are consistent with either (1) a low-angle normal fault, (2) stepped, moderate-angle (45°) normal faults, or (3) a single, moderate-angle (45°) fault with interbedding of high-density alluvium in Crater Flat basin. In part, the variability of these estimates of the dip of the fault appear to reflect the progressive decrease in dip of the fault to the north [Hamilton, written commun., 1994; Fridrich, written commun., 1995]. Results from Line 2, which crosses the fault in a location where it dips most steeply [Hamilton, written commun., 1994], are consistent with the Bare Mountain fault representing a single, moderate-angle (42°) fault to a depth of about 3.5 to 3.8 km and inconsistent with its interpretation as a low-angle detachment fault as suggested by Oliver and Fox [1993] and Hamilton [1988]. The moderate dip inferred for the Bare Mountain fault is consistent with other Basin and Range faults, including the Dixie Valley fault of central Nevada [Okaya and Thompson, 1985].

As suggested by surface mapping by Faulds and others [1994], Line 2 clearly shows that the Tertiary strata beneath southwestern Crater Flat dip westward [Hamilton, written commun., 1994]. Line 2 provides the first subsurface confirmation of these geometrical relations and confirms previous inferences that this portion of Crater Flat underwent the most extension.

Significant contrasts are observed in the eastern and western halves of Crater Flat crossed by Line 2. Northeast of the Crater Flat fault (St. 730), Line 2 is interpreted to show small-scale repeated faulting across Crater Flat and Yucca Mountain. This interpretation is consistent with the disrupted nature of reflectors in this half of Line 2 (fig. 16), with the short-wavelength magnetic anomalies observed there (fig. 20), and with geologic mapping of numerous faults (Crater Flat, Windy Wash, Fatigue Wash, Solitario Canyon, and Ghost Dance faults). Whereas the western half of Crater Flat is generally characterized by low-wavelength magnetic anomalies (apart from high-amplitude anomalies produced by surficial and shallowly buried basaltic flows), its eastern half has a more disrupted magnetic anomaly field (fig. 20).

Strong, shallow reflections observed between Little Cones and Red Cone are thought to correlate to shallow basalt flows. If so, the lack of significant offset on them suggests that this portion of Crater Flat has experienced little faulting since the emplacement of the flows between 11 and 3.7 Ma. No genetic association between Little Cones, Red Cone, and the reflectors can be inferred given their likely age differences [Vaniman and others, 1982].

Lines 2 and 3 also provide important new information on the nature and location of the eastern boundary of the Amargosa Desert structural trough at the latitude of the potential repository site (fig. 1A). The eastern boundary of this structural trough has been previously placed at the eastern end of Line 3 [Brocher and others, 1993] or further east of Line 3 at the Gravity Fault [Hamilton, written commun., 1994; Fridrich, written commun., 1995]. Based on the location of the largest vertical offset of the Paleozoic/Tertiary contact, however, we concur with Carr [1990] that the eastern boundary of the Amargosa Desert structural trough at the latitude of the potential repository site is a diffuse structure extending from the Solitario Canyon fault on the west to the Paintbrush Canyon fault on the east.

Line AV-1 successfully imaged the lower crust (5 to 10 s twtt) along the entire line using both vibrator and deep shot hole sources. Line 2 was similarly successful in imaging the lower crust, but only in the Amargosa Desert and the westernmost part of Crater Flat (fig. 18). In this location, the top of the reflective lower crust is at 4.8 s. The top of the reflective lower crust is commonly interpreted as the top of the ductile lower crust [e.g., Klemperer, 1987; Goodwin and Thompson, 1988], and thus may represent the depth at which high-angle faults merge into pure shear of the lower crust as proposed by Hamilton [written commun., 1994]. The base of the crust, the Moho, is inferred to be between 9 and 10 seconds, implying that the crust is in the vicinity of 27 to 30 km thick. This crustal thickness is identical to that found along Line AV-1 [Brocher and others, 1993], suggestive of a relatively flat Moho in the vicinity of Yucca Mountain. Neither

vibrator nor shot hole sources, however, were successful in imaging the lower crust beneath Yucca Mountain or in Jackass Flats. Due to the failure to obtain lower crustal reflections along most of Lines 2 and 3, it is not possible to make definitive statements about the presence or absence of magma within or at the base of the crust.

Using VSPs at several wells along Lines 2 and 3 we identified a reflection event at 500 m (0.4 s) beneath Yucca Mountain within the Tertiary volcanic section as within or near the top of the Prow Pass Tuff. The northeastern end of Line 2 was located in the vicinity of the 2-km-long shallow Line 1 acquired by the Lawrence Berkeley Laboratory (LBL) in 1993 [Daley and others, 1994]. LBL Line 1 trended west to east between USW WT-2 and UE-25 UZ-16 (in the vicinity of Stations 1054 and 1088 of Line 2), and crossed the Ghost Dance fault. LBL Line 1 apparently imaged a number of reflection events in the uppermost 1200 m (4000 ft) of the section, including events from a unit of the Prow Pass Tuff at about 460 m (1500 ft) and a unit of the Bullfrog Tuff at about 600 m (2000 ft) [Daley and others, 1994] . The apparent difference in the depth of units mapped within the Prow Pass Tuff (500 m on our Line 2 versus 460 m on LBL-1) probably results from the higher-frequency source used on the LBL line. Reflections from stratified rocks are interference phenomena and are sensitive to the frequency content of the source. Thus the two sources most likely mapped different units with the Prow Pass Tuff. The Prow Pass Tuff thus appears to have been imaged by both reflection surveys, each having different acquisition parameters.

Based on the results of our work we offer the following recommendations for future intermediate-depth seismic reflection profiling in the immediate vicinity of Yucca Mountain. Our work, conducted using standard 2-D parameters, indicates that although Yucca Mountain itself is a difficult area in which to acquire high-quality seismic reflection data, useful data can be obtained. These parameters appeared to work well in Crater Flat and in Jackass Flats, yet they did not work as well in the immediate vicinity of Yucca Mountain itself. Based on the data we acquired for shallow targets such as the Paleozoic/Tertiary contact near Yucca Mountain, we recommend the use of shorter group intervals, in the range of 30 to 40 ft, to provide higher fold in the depths of interest. For similar reasons, source-point intervals should be shortened to 60 or 80 ft. The total spread length may be shortened to the range of 3 to 4 km to each side. Using 2-D geophone group arrays may cancel some of the side scatter produced by the numerous fractures and normal faults. Larger explosions, perhaps in the range of 1000 to 2000 lbs, are necessary to image the lower crust near Yucca Mountain where the water table is 1800 ft deep. A separate statics crew may be necessary to determine accurate static solutions.

On the basis of the encouraging results from this study, results from the seismic industry, and the complex geology at Yucca Mountain, we recommend that 3-D seismic data be acquired in the vicinity of Yucca Mountain to more accurately determine structure. Although the 3-D data will not be of high quality, it will have higher quality than the 2-D data due to the ability to remove side scatter from the 3-D images. Industry has repeatedly shown that 3-D seismic data can improve data quality in difficult acquisition areas such as Yucca Mountain [Horvath, 1985; Schimunek and Strobl, 1985; Yilmaz, 1987, p. 385-389]. Poulter charges should be examined as a possible source for the 3-D data acquisition, due to the ability to use the method throughout the survey area, regardless of topography and access to roads. Further field testing of different Poulter sources is recommended given the limited field trials attempted during our study. Furthermore, Poulter-charge sources are susceptible to high winds and will require some allowance for halting data acquisition during high winds.

CONCLUSIONS

Regional seismic reflection lines obtained using hybrid-sources across the Amargosa Desert, Crater Flat, Yucca Mountain, and Jackass Flats provide useful images of the upper crustal structure. Although the seismic reflection data are not high in quality, they provide very useful images of the subsurface near Yucca Mountain. Reflections are correlated to Tertiary volcanic formations and the Paleozoic/Tertiary boundary based on geologic mapping, wells along the lines, and auxiliary geophysical models. Offsets of the Paleozoic/Tertiary contact beneath Yucca Mountain suggest that moderate- to high-angle faults mapped at the surface penetrate the Paleozoic/Tertiary contact, providing compelling evidence against the hypothesis of an active shallow detachment surface beneath Yucca Mountain [Scott, 1986, 1990; Fox and Carr, 1989]. Reflections clearly define an asymmetric fault-bounded basin in Crater Flat, up to 3.5 to 4 km thick, extending beneath the western flank of Yucca Mountain. Moderately (42°) east-dipping reflections northeast of Bare Mountain truncate a series of west-dipping reflections, and based on density models, represent a series of normal faults including the Bare Mountain range-front fault. Tertiary strata within the thickest part of the Crater Flat basin dip westward, as recently proposed on the basis of field mapping [Faulds and others, 1994]. These units are overlain by shallow, thin basalt flows having little or no offset and a gentle westward dip, probably corresponding to flows dated at either 11 or 3.7 Ma. Several hundred meters of down-to-the-west offset of the Paleozoic/Tertiary contact is observed beneath Yucca Mountain along Line 2. A mid-Miocene horizon under Yucca Mountain, probably the Prow Pass Tuff of the Crater Flat Group, exhibits much less significant structural relief than the inferred Paleozoic/Tertiary contact and is sub parallel to surface topography. Most of the offset on the Paleozoic/Tertiary contact across these faults is inferred to have occurred prior to the mid-Miocene (pre-Prow Pass tuff), based on the inferred continuity of mid-Miocene units above the inferred faults, and may have formed during an extensional event from 18 to 15.2 Ma preserved in Paleozoic and older rocks at Bare Mountain [Fridrich, written commun., 1995]. Reflection line 2 demonstrates that the Neogene fill in the Amargosa Desert is thin and floored at shallow depth by Paleozoic and older rocks as previously proposed on the basis of gravity data [Hamilton, written commun., 1994]. Likewise, Line 3 indicates that Jackass Flats contains a thin veneer of east-dipping Neogene sedimentary strata. Better interpretation of the seismic reflection data will require additional deep boreholes along the seismic reflection lines. In particular, deep boreholes sampling the Paleozoic/Tertiary contact are necessary to test the interpretations presented here.

ACKNOWLEDGMENTS

We are grateful to Steve Solokis, Mike Waugh, and Troy McLeod, and the rest of Crew 110 of Northern Geophysical of America, Inc., for their fine work in acquiring the seismic data. Bob Craig and Dan Soeder, USGS Yucca Mountain Logistics Support Group, helped to coordinate the data acquisition with other ongoing activities at Yucca Mountain and guided us through a maze of biological, archeological, safety, and security concerns and regulations at the site. Luckey Johnson, REECo-USGS, of the same group, supervised foreign nationals on the Nevada Test Site. Donna Sinks, SAIC, Golden, performed a helpful audit of Quality Assurance practices during the field work. We are grateful to the biologists and archeologists headed by Mike Stover for clearing corridors for us to work within under very short notice. Tim Sullivan and Mark Tynan of the Department of Energy (DOE), Yucca Mountain Site Characterization Project (YMSCO), Las Vegas; John Savino, SAIC, Las Vegas; and Jim Agnew, Woodward-Clyde, Las Vegas spearheaded the effort to get the explosion shot holes drilled. Tim Sullivan also helped coordinate our activities with other DOE activities at Yucca Mountain, including those of the tunnel-boring machine. Win Wilson/DOE/YMSCO facilitated our field work. John Arnold and

Maureen Corbett, USGS, Denver, served as Contracting Officers for the contract with NGA. Chris Tonish, Geophysical Control, Inc., performed the field data processing and made a number of useful suggestions for the data acquisition. Wind speed records were provided by Tim Moran, DOE, Las Vegas. Processing of the acquired data was performed by Cheri Williams and David Rohr of Texseis, Inc., Houston, Texas. Lynda Carlson, USGS, Denver, served as Contracting Officer for the Texseis contract. L.E. 'bud' Thompson, TRW Environmental Safety Systems, Inc., and Roger Olsen, SAIC, Las Vegas, provided the digital well log data. Eric Geist, USGS, taught us how to use DISCO to generate synthetic seismograms from the well log data. David Ponce, USGS, helped to acquire the ground magnetic data. LBL kindly supplied the gravity data along the lines. We thank Ken Fox, Jr., and Warren Hamilton, both retired USGS, Chris Potter, USGS, Rick Spengler, USGS, and George Thompson, Stanford University, for critical reviews of previous versions of this report.

Funding for this work was provided by the DOE under interagency agreement DE-A108-92NV10874.

REFERENCES CITED

Barnes, H., Ekren, E. B., Rodgers, C. L., and Hedlund, D. C., 1982, Geologic and tectonic maps of the Mercury quadrangle, Nye and Clark Counties, Nevada: U. S. Geological Survey, Miscellaneous Investigations Series Map I-1197, 1:24,000.

Barry, K.M., Cravers, D.A., and Kneale, C.W., 1975, Recommended standards for digital tape formats: Geophysics, v. 40, p. 344-352.

Brocher, T.M., Hart, P.E., and Carle, S.F., 1990, Feasibility study of the seismic reflection method in Amargosa Desert, Nye County, Nevada: U.S. Geological Survey Open-File Report 89-133, 150 p.

Brocher, T.M., and Hart, P.E., 1991, Comparison of Vibroseis and explosive source methods for deep crustal seismic reflection profiling in the Basin and Range Province: Journal of Geophysical Research, v. 96, p. 18,197-18,213.

Brocher, T.M., Carr, M.D., Fox, K.F., and Hart, P.E., 1993, Seismic reflection profiling across Tertiary extensional structures in the eastern Amargosa Desert, Basin and Range, USA: Geological Society of America Bulletin, v. 105, p. 30-46, 1 plate.

Burchfiel, B. C., 1964, Precambrian and Paleozoic stratigraphy of the Specter Range Quadrangle, Nevada: American Association of Petroleum Geologists Bulletin, v. 48, p. 40-56.

Burchfiel, B. C., 1965, Structural geology of the Specter Range Quadrangle, Nevada, and its regional significance: Geological Society of America Bulletin, v. 76, p. 175-192.

Byers, F.M., Jr., Carr, W.J., Orkild, P.P., Quinlivan, W.D., and Sargent, K.A., 1976, Volcanic suites and related cauldrons of Timber Mountain-Oasis Valley caldera complex, southern Nevada: U.S. Geological Survey Professional Paper 919, 70 p.

Carr, M.D., Waddell, S.J., Vick, G.S., Stock, J.M., Monsen, S.A., Harris, A.G., Cork, B.W., Byers, F.M., Jr., 1986, Geology of drill hole UE25p#1: A test hole into pre-Tertiary rocks near Yucca Mountain, southern Nevada: U.S. Geological Survey Open-File Report 86-175, 87 p.

Carr, W.J., 1982, Volcano-tectonic history of Crater Flat, southwestern Nevada, as suggested by new evidence from drill hole USW VH-1 and vicinity: U.S. Geological Survey Open-File Report 82-457, 23 p.

Carr, W. J., 1984, Regional structural setting of Yucca Mountain, southwestern Nevada, and late Cenozoic rates of tectonic activity in part of the southwestern Great Basin, Nevada and California: U.S. Geological Survey Open-File Report 84-854, 109 p.

Carr, W. J., 1990, Styles of extension in the Nevada Test Site region, southern Walker Lane belt: An integration of volcano-tectonic and detachment fault models: *in* Wernicke, B.P., ed., Basin and Range extensional tectonics near the latitude of Las Vegas, Nevada: Geological Society of America Memoir 176, p. 283-303.

Carr, W.J., and Parrish, L.D., 1985, Geology of drill hole USW VH-2, and structure of Crater Flat, southwestern Nevada: U.S. Geological Survey Open-File Report 85-475, 41 p.

Cornwall, H.R., and Kleinhampl, F.J., 1961, Geology of the Bare Mountain quadrangle, Nevada: U.S. Geological Survey Geologic Quadrangle Map GQ-157, scale 1:62,500.

Daley, T.M., Majer, E.L., and Karageorgi, E., 1994, Combined analysis of surface reflection imaging and vertical seismic profiling at Yucca Mountain, Nevada: Lawrence Berkeley Laboratory, LBL-36467, UC-400, 44 p.

Dickerson, R.P., and Spengler, R.W., 1994, Structural character of the northern segment of the Paintbrush Canyon fault, Yucca Mountain, Nevada: American Nuclear Society Proceedings of the Fifth International Conference of High Level Radioactive Waste Management, Las Vegas, v. 2, p. 2367-2372.

Evans, J.R., and Smith, M., III, 1992, Teleseismic tomography of the Yucca Mountain region: Volcanism and tectonism: American Nuclear Society Proceedings of the Third International Conference of High Level Radioactive Waste Management, Las Vegas, v. 2, p. 2372-2380.

Faulds, J.E., Bell, J.W., Feuerbach, D.L., and Ramelli, A.R., 1994, Geologic map of the Crater Flat area, Nye County, Nevada: Nevada Bureau of Mines and Geology Map 101, 1:24,000 scale.

Fenix and Scisson, Inc., 1986a, NNWSI (National Nuclear Waste Site Investigation) hole histories: UE-25 WT #3, UE-25 WT #4, UE-25 WT #5, UE-25 WT #6, UE-25 WT #12, UE-25 WT #13, UE-25 WT #14, UE-25 WT #15, UE-25 WT #16, UE-25 WT #17, UE-25 WT #18, USW WT-1, USW WT-2, USW WT-7, USW WT-10, and USW WT-11: National Technical Information Service Report DOE/NV/10322-10, prepared for U.S. Department of Energy, U.S. Dept. of Commerce, 5285 Port Royal Road, Springfield, VA 22161.

Fenix and Scisson, Inc., 1986b, NNWSI (National Nuclear Waste Site Investigation) hole histories: USW VH-1 and USW VH-2: National Technical Information Service Report DOE/NV/10322-17, prepared for U.S. Department of Energy, U.S. Dept. of Commerce, 5285 Port Royal Road, Springfield,VA 22161.

Fenix and Scisson, Inc., 1986c, NNWSI (National Nuclear Waste Site Investigation) hole history: UE-25 p#1: National Technical Information Service Report DOE/NV/10322-16, prepared for U.S. Department of Energy, U.S. Dept. of Commerce, 5285 Port Royal Road, Springfield,VA 22161.

Fenix and Scisson, Inc., 1987, NNWSI (National Nuclear Waste Site Investigation) hole histories: USW H-1, USW H-3, USW H-4, USW H-5, and USW H-6: National Technical Information Service Report DOE/NV/10322-18, prepared for U.S. Department of Energy, U.S. Dept. of Commerce, 5285 Port Royal Road, Springfield,VA 22161.

Fox, K.F., and Carr, M.D., 1989, Neotectonics and volcanism at Yucca Mountain and vicinity, Nevada: Radioactive Waste Management and the Nuclear Fuel Cycle, v. 13, p. 37-50.

Fridrich, C.J., Dudley, W.W., Jr., and Stuckless, J.S., 1994a, Hydrogeologic analysis of the saturated-zone ground-water system under Yucca Mountain, Nevada: Journal of Hydrology, v. 154, p. 133-168.

Fridrich, C.J., Crowe, B.M, Hudson, M.R., Langenheim, V.E., and Thompson, G.E., 1994b, Structrual control of basaltic volcanism in a region of oblique extension, southwest Nevada volcanic field: EOS, Transactions, American Geophysical Union, Supplement, v. 75, no. 44, p. 603.

Goodwin, E.B., and Thompson, G.A., 1988, The seismically reflective crust beneath highly extended terranes: Evidence for its origin in extension: Geological Society of America Bulletin, v. 100, p. 1616-1626.

Goodwin, E.B., Thompson, G.A., and Okaya, D.A., 1989, Seismic identification of basement reflectors: The Bagdad reflection sequence in the Basin and Range Province - Colorado Plateau transition zone, Arizona: Tectonics, v. 8, p. 821-831,

Greenhaus, M. R., and Zablocki, C. J., 1982, A Schlumberger resistivity survey of the Amargosa Desert, southern Nevada: U. S. Geological Survey Open-File Report 82-897, 150 p.

Hamilton, W., 1988, Detachment faulting in the Death Valley region, California and Nevada: *in* Carr, M.D., and Yount, J.C., eds., Geologic and hydrologic investigations of a potential nuclear waste disposal site at Yucca Mountain, southern Nevada, U.S. Geological Survey Bulletin 1790, p. 51-86.

Healey, D. L., and Miller, C. H., 1965, Gravity survey of the Amargosa Desert area of Nevada and California: U. S. Geological Survey Technical Letter NTS-99, 32 p.

Healey, D. L., Wahl, R. R., and Oliver, H. W., 1980, Bouguer gravity map of Nevada, Death Valley sheet: Nevada Bureau Mines and Geology, Map 69, scale 1:250,000.

Hinrichs, E.N., 1968, Geologic map of the Camp Desert Rock quadrangle, Nye County, Nevada: U.S. Geological Survey Geologic Quadrangle Map GQ-726, scale 1:24,000.

Horvath, P.S., 1985, Effectiveness of 3-D offshore seismic surveys: Case study: Geophysics, v. 50, p. 2411-2430.

Klemperer, S.L., 1987, A relation between continental heat-flow and the seismic reflectivity of the lower crust: Journal of Geophysics, v. 61, p. 1-11.

Langenheim, V.E., and Ponce, D.A., 1995, Ground magnetic studies along a regional seismic-reflection profile across Bare Mountain, Crater Flat and Yucca Mountain, Nevada: U.S. Geological Survey Open-File Report 95-834, 33 p.

Maldonado, F., 1985, Geologic map of the Jackass Flats area, Nye County, Nevada: U.S. Geological Survey, Misc. Inv. Series Map I-1519, 1:48,000.

McGovern, T.F., and Turner, D.W., 1983, An evaluation of seismic reflection studies in the Yucca Mountain area, Nevada Test Site with an Introduction by L.W. Pankratz and H.D. Ackermann: U.S. Geological Survey Open-File Report 83-912, 58 p.

McKay, E.J., and Williams, W.P., 1964, Geology of the Jackass Flats quadrangle, Nye County, Nevada: U.S. Geological Survey Geologic Quadrangle Map GQ-368, scale 1:24,000.

Monsen, S.A., Carr, M.D., Reheis, M.C., and Orkild, P.P., 1992, Geologic map of Bare Mountain, Nye County, Nevada: U.S. Geological Survey Investigation I-2201, scale 1:24,000, 6 p.

Mooney, W.D., and Schapper, S., 1995, Seismic refraction studies (Chapter 5) *in* Oliver, H.W., Ponce, D.A., and Hunter, W. Clay, eds., Major results of geophysical investigations at Yucca Mountain and vicinity, southern Nevada: U.S. Geological Survey Open-File Report 95-74.

Moyer, T.C., and Geslin, J.K., 1995, Lithostratigraphy of the Calico Hills Formation and Prow Pass Tuff (Crater Flat Group) at Yucca Mountain, Nevada: U.S. Geological Survey Open-File Report 94-460, 59 p.

Nelson, P.H., Muller, D.C., Schimschal, U., and Kibler, J.E., 1991, Geophysical logs and core measurements from forty boreholes at Yucca Mountain, Nevada: U.S. Geological Survey Map GP-1001.

Okaya, D.A., and Thompson, G.A., 1985, Geometry of Cenozoic extensional faulting: Dixie Valley, Nevada: Tectonics, v. 4, p. 107-126.

Oliver, H.W., and Fox, K.F., 1993, Structure of Crater Flat and Yucca Mountain, southeastern Nevada, as inferred from gravity data: American Nuclear Society Proceedings of the Fourth Annual International Conference on High Level Nuclear Waste Management, April 26-30, 1993, Las Vegas, NV, v. 2, p. 1812-1817.

Ponce, D.A., Kohrn, S.B., and Waddell, S., 1992, Gravity and magnetic data of Fortymile Wash, Nevada Test Site, Nevada: U.S. Geological Survey Open-File Report 92-343, 33 p.

Poulter, T.C., 1950, The Poulter seismic method of geophysical exploration: Geophysics, v. 15, p. 181-207.

Saltus, R.W., and Blakely, R.J., 1993, HYPERMAG--An interactive 2- and 2 1/2-dimensional gravity and magnetic modeling program, Version 3.5: U. S. Geological Survey Open-File Report 93-287, 39 p.

Sargent, K.A., McKay, E.J., and Burchfiel, B.C., 1970, Geologic map of the Striped Hills quadrangle, Nye County, Nevada: U.S. Geological Survey Geologic Quadrangle Map GQ-882, scale 1:24,000.

Sawyer, D.A., Fleck, R.J., Lanphere, M.A., Warren, R.G., Broxton, D.E., and Hudson, M.R., 1994, Episodic caldera volcanism in the Miocene southwestern Nevada volcanic field -- revised stratigraphic framework, $^{40}Ar/^{39}Ar$ geochronology, and implications for magmatism and extension: Geological Society of America Bulletin, v. 106, p. 1304-1318.

Schimunek, K., and Strobl, E., 1985, A combined dynamite-Vibroseis 3-D survey in the subalpine Overthrust zone of Austria: First Break, v. 3, p. 9-15.

Scott, R.B., 1986, Extensional tectonics at Yucca Mountain, southern Nevada: Geological Society of America Abstracts with Programs, v. 18, no. 5, p. 411.

Scott, R.B., 1990, Tectonic setting of Yucca Mountain, southwest Nevada, *in* Wernicke, B.P., ed., Basin and Range extensional tectonics near the latitude of Las Vegas, Nevada: Geological Society of America Memoir 176, p. 251-282.

Scott, R.B., and Castellanos, M., 1984, Stratigraphic and structural relations of volcanic rocks in drill holes USW GU-3 and USW G-3, Yucca Mountain, Nye County, Nevada: U.S. Geological Survey Open-File Report 84-491, 121 p.

Scott, R.B., and Bonk, J., 1984, Preliminary geologic map of Yucca Mountain, Nye County, Nevada with geologic sections: U. S. Geological Survey Open-File Report 84-494, scale 1:12,000.

Seismic Methods Peer Review Panel, The, 1991, Final recommendations of the Peer Review Panel on the use of seismic methods for characterizing Yucca Mountain and vicinity: 36 p.

Sikora, R.F., Campbell, D.L., and Kucks, R.P., 1995, Aeromagnetic surveys across Crater Flat and parts of Yucca Mountain, Nevada: U.S. Geological Open-File Report 95-812, 7 p.

Simonds, F.W., Whitney, J.W., Fox, K.F., Ramelli, A.R., Yount, J.C., Carr, M.D., Menges, C.M., Dickerson, R.P., and Scott, R.B., 1996, Map showing fault activity in the Yucca Mountain area, Nye County, Nevada: U.S. Geological Survey, Misc. Inv. Series Map MI-2520, scale 1:24,000.

Simpson, R.W., Jachens, R.C., Blakely, R.J., and Saltus, R.W., 1986, A new isostatic residual gravity map of the conterminous United States with a discussion on the significance of isostatic residual anomalies: Journal of Geophysical Research, v. 91, p. 8348-8372.

Snyder, D.B., and Carr, W.J., 1984, Interpretation of gravity data in a complex volcano-tectonic setting, southwestern Nevada: Journal of Geophysical Research, v. 89, p. 10193-10206.

Spengler, R.W., Byers, F.M, Jr., and Warner, J.B., 1981, Stratigraphy and structure of volcanic rocks in drill hole USW-G1, Yucca Mountain, Nye County, Nevada: U. S. Geological Survey Open-File Report 81-1349, 50 p.

Spengler, R.W., and Fox, K.F., Jr., 1989, Stratigraphic and structural framework of Yucca Mountain, Nevada: Radioactive Waste Management and the Nuclear Fuel Cycle, v. 13(1-4), p. 21-36.

Spengler, R.W., Braun, C.A., Linden, R.M., Martin, L.G., Ross-Brown, D.M., and Blackburn, R.L., 1993, Structural character of the Ghost Dance fault, Yucca Mountain, Nevada: American Nuclear Society Proceedings of the Fourth Annual International Conference on High Level Waste Management, v. 1, p. 653-659.

Spengler, R.W., Braun, C.A., Martin, L.G., and Weisenberg, C.W., 1994, The Sundance fault: A newly recognized shear zone at Yucca Mountain, Nevada: U.S. Geological Survey Open-File Report 94-49, 11 p.

Swadley, W.C., and Carr, W.J., 1987, Geologic map of the Quaternary and Tertiary deposits of the Big Dune quadrangle, Nye County, Nevada, and Inyo County, California: U.S. Geological Survey, Misc. Inv. Series Map MI-1767, scale 1:48,000.

Swadley, W.C., and Parrish, L.D., 1988, Surficial geological map of the Bare Mountain quadrangle, Nye County, Nevada: U.S. Geological Survey, Misc. Inv. Series Map MI-1826, 1:48,000.

U. S. Geological Survey, 1984, A summary of geological studies through January 1, 1983, of a potential high-level nuclear waste repository site at Yucca mountain, southern Nye County, Nevada: U. S. Geological Survey Open-File Report 84-792, 103 p.

Vaniman, D.T., Crowe, B.M., and Gladney, E.W., 1982, Petrology and geochemistry of hawaiite lavas from Crater Flat, Nevada: Contributions to Mineralogy and Petrology, v. 80, p. 341-357.

Wright, L. A., 1989, Overview of the role of strike-slip and normal faulting in the Neogene history of the region northeast of Death Valley, California-Nevada: *in* Ellis, M. A., ed., Late Cenozoic evolution of the southern Great Basin: Nevada Bureau of Mines and Geology Open-File Report 89-1, p. 1-12.

Wright, L. A., and Troxel, B. W., 1967, Limitations on right-lateral, strike-slip displacement, Death Valley and Furnace Creek fault zones, California: Geological Society of America Bulletin, v. 78, p. 933-950.

Yilmaz, O., 1987, Seismic data processing: *in* S.M. Doherty, ed., Investigations in Geophysics, vol. 2, Soc. Exploration Geophysicists, Tulsa, 526 p.

Zumberge, M.A., Harris, R.N., Oliver, H.W., Sasagawa, G.S., and Ponce, D.A., 1988, Preliminary results of absolute and high-precision gravity measurements at the Nevada Test Site and vicinity, Nevada: U. S. Geological Survey Open-File Report 88-242, 29 p.

APPENDIX 1. Northern Geophysical of America Crew 110

Name	Title
Stephen John Solokis	Field Supervisor
Michael J. Waugh	Party Manager
Michael L. Allred	Assistant Party Manager
Michael Fitz Maurice	Environmental Health and Safety Manager
Kim Wegemeyer	Safety Coordinator and Assistant Party Manager, Shooter
John F. James	Field Service Engineer
Troy McLeod	Observer
Dan Malberg	Observer, Shooter
Jason T. Clark	Junior Observer, Shooter
Bruce Tankersly	Electronic Technician
William W. Everett	Electronic Technician
Joe Montee	Mechanic
Steve March	Mechanic
Louise Sandberg	Permit Agent
Greg Brooks	Head Linesman
Randall J. Stamey	Linesman, Shooter
Oliver Amend	Shooter
Jon Spuhler	Truck Driver
Wayne Eckersley	Truck Driver
Jeff Loveless	Truck Driver
Randy Fortin	Crew Boss, Shooter
George Berela	Crew Boss, Shooter
Ray Trafelet	Layout Technician
Mike McNamee	Layout Technician
Jeremy Buckham	Layout Technician
Allen Burnnett	Layout Technician
Douglas Pagel	Layout Technician
Schuyler Schaff	Layout Technician
Keith Kepp	Cable Technician
Stuart McCarron	Cable Technician
Dennis Hurst	Cable Technician
John Paoli	Cable Technician
Mike Daugherty	Cable Technician
Carl Beck	Cable Repair Technician
Dennis Maliszewski	Assistant Cable Repair Technician
Caryn Ludwick	Clerk

Northern Geophysical of America Crew 110 Subcontractors

Alpha Explosives

Randy Dale Ladd	Explosives Handler

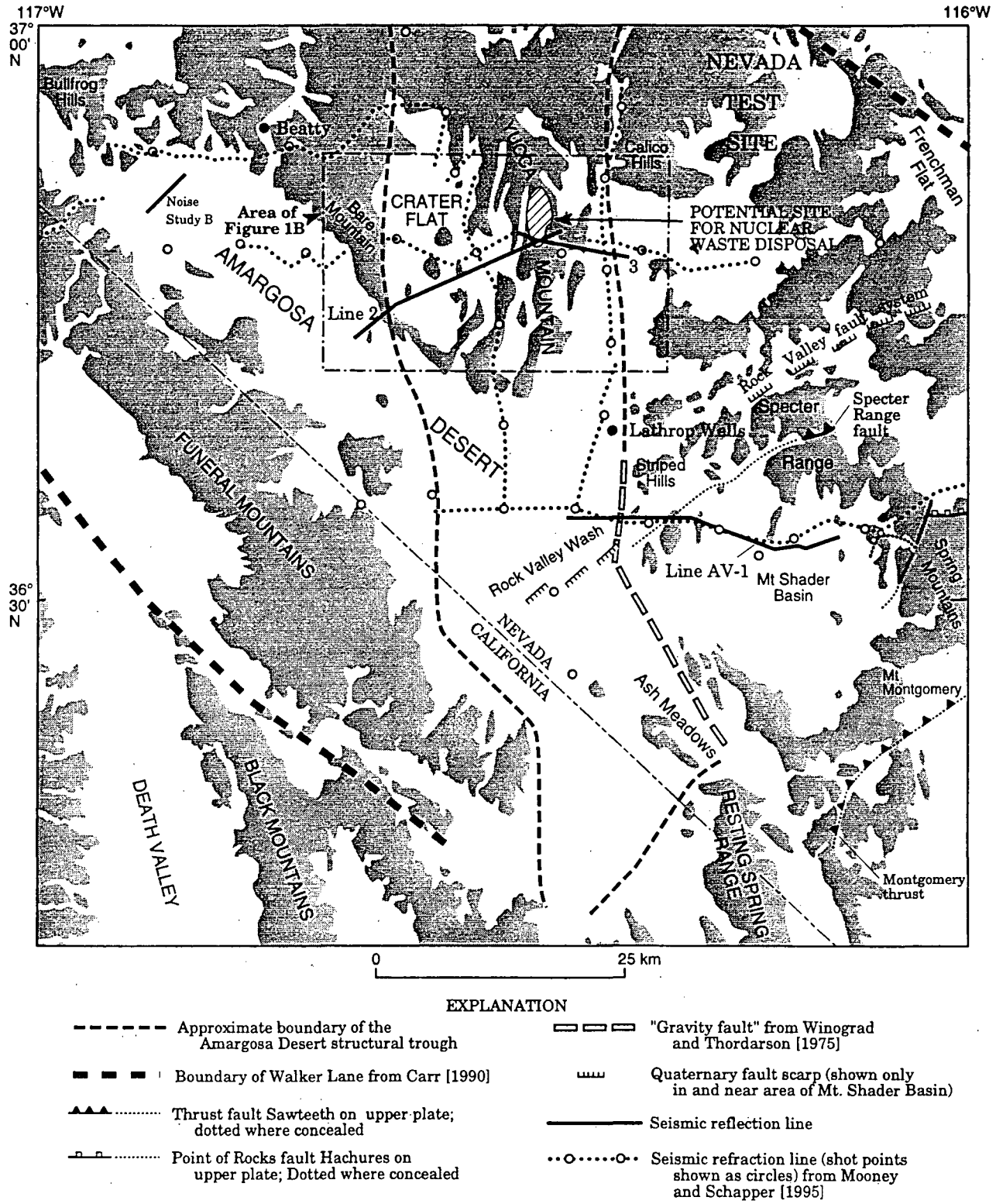

Figure 1A. Regional map of Yucca Mountain area, Nevada, showing seismic lines 2 and 3 and line AV-1 in the Amargosa Desert relative to Yucca Mountain and other structures described in the text. Map modified from Brocher and others [1993]. Outcrops of pre-Pliocene rocks are shaded.

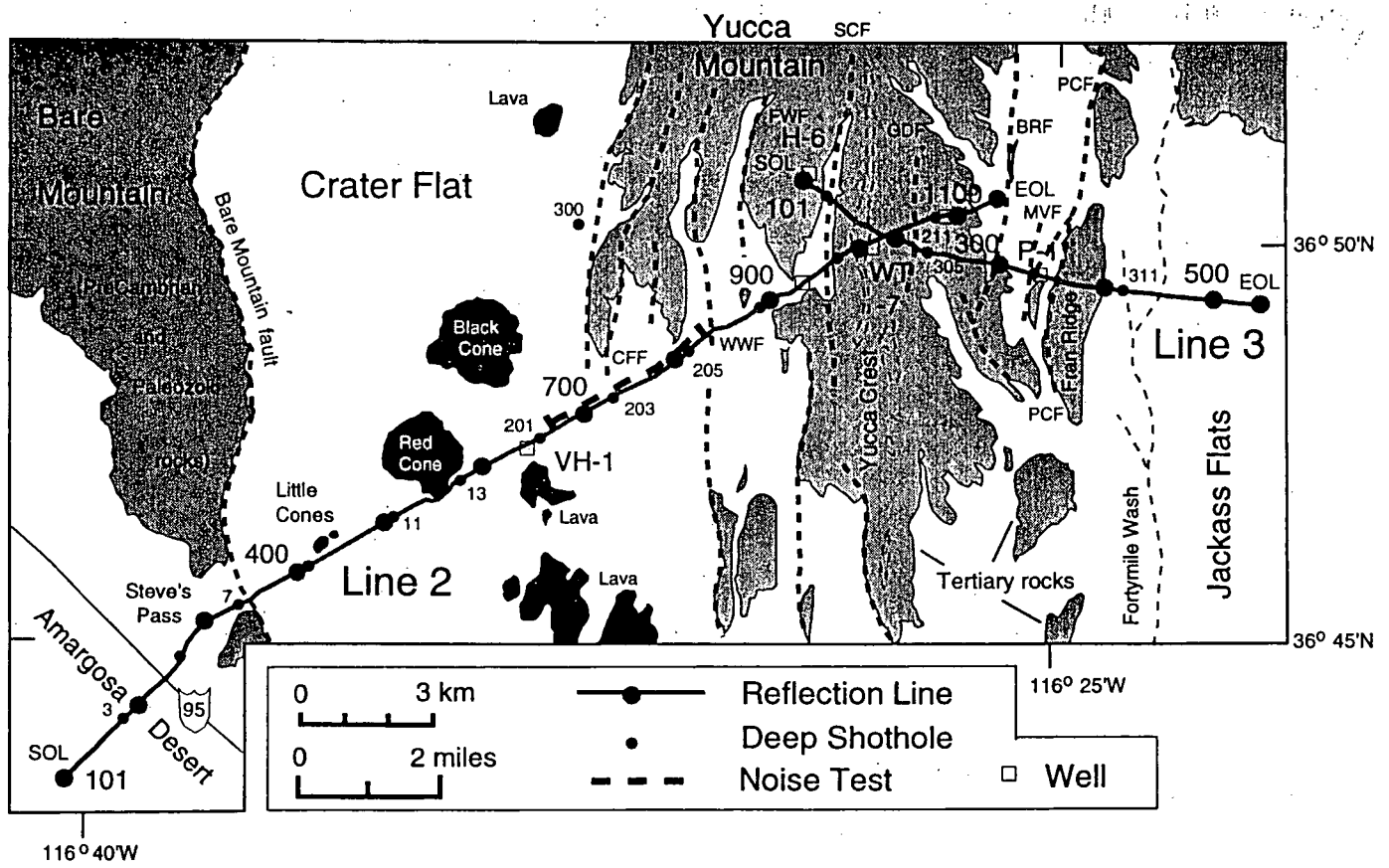

Figure 1B. Map of the vicinity of Yucca Mountain showing location of seismic lines 2 and 3. Larger numbers along lines provide station numbers, smaller numbers provide shothole locations. Dark shaded features in Crater Flat show lava flows and basaltic cones. Selected faults are shown, including the Crater Flat fault (CFF), the Windy Wash fault (WWF), the Fatigue Wash fault (FWF), the Solitario Canyon fault (SCF), the Ghost Dance fault (GDF), the Bow Ridge fault (BRF), the Midway Valley fault (MVF), and the Paintbrush Canyon fault (PCF). Drill holes USW VH-1, USW WT-7, USW H-6, and UE-25 p#1 are also shown.

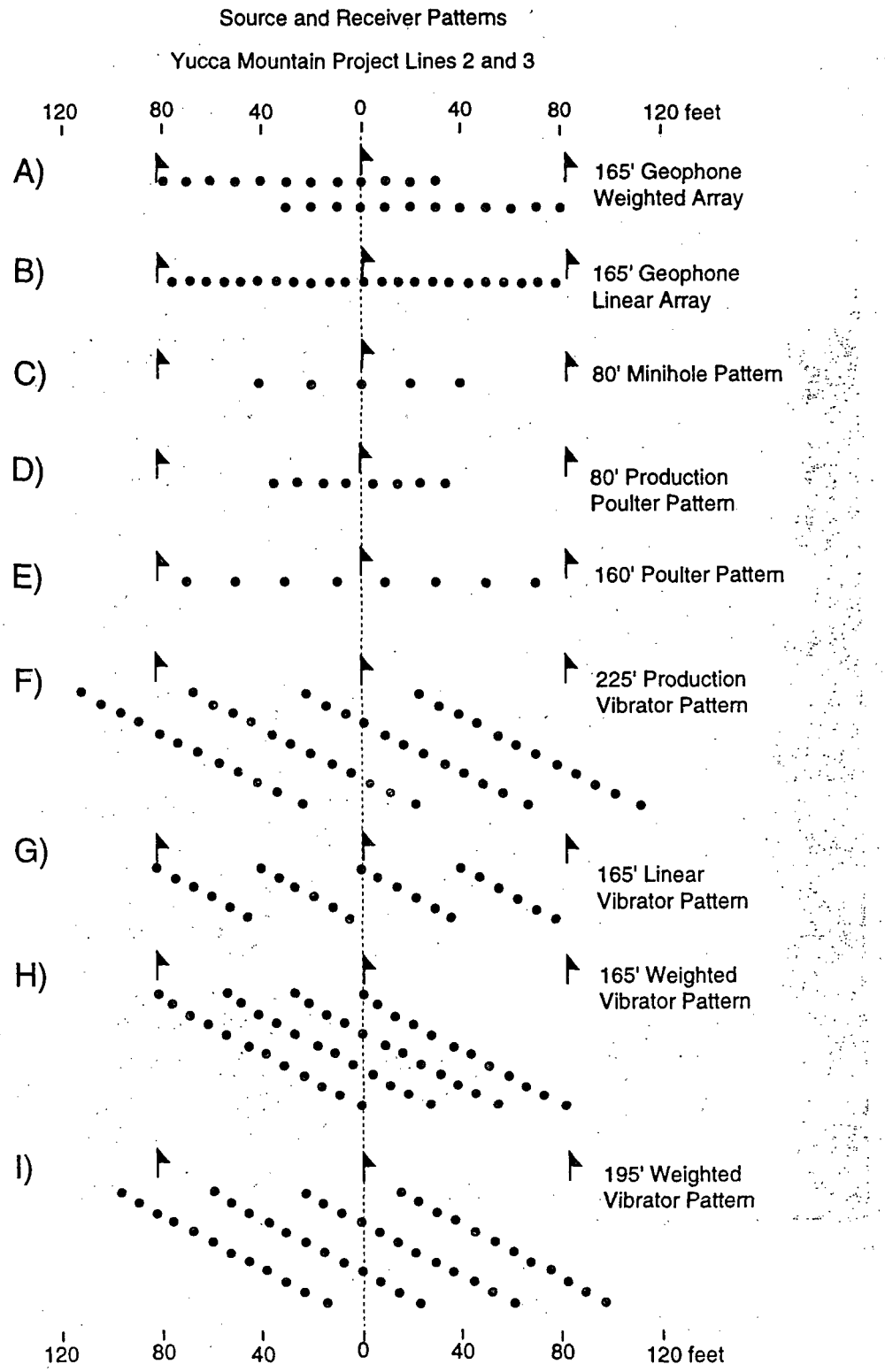

Figure 2. Geophone and source patterns tested during the noise study and used during the acquisition of Lines 2 and 3. Patterns B, C, D, and F were used during the acquisition of Lines 2 and 3. Station flag for each pattern is at 0 feet.

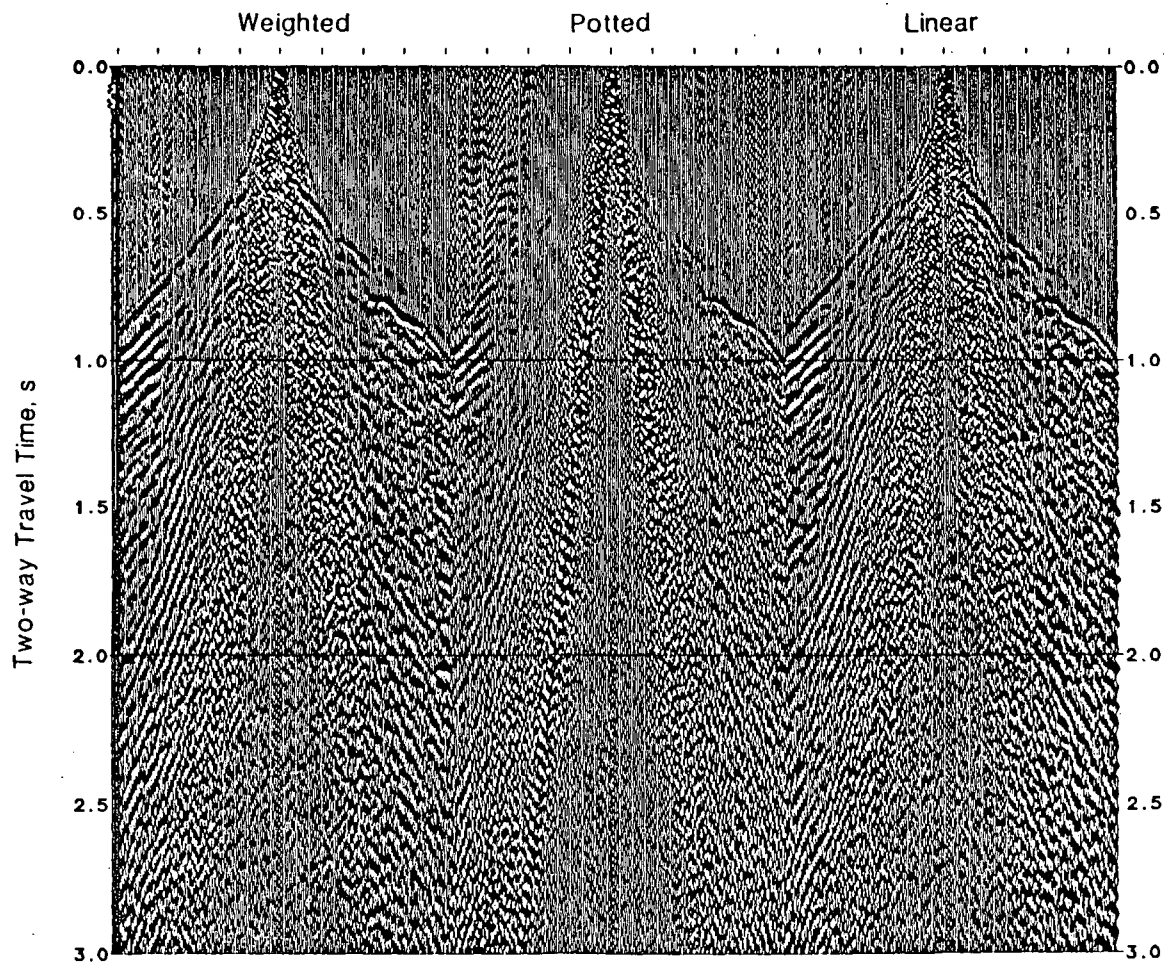

A)

Figure 3. Common source gathers from parameter testing from Vibrator Points (VPs) at (A and B) St. 752. Each source gather shows the output recorded by the three geophone arrays tested: weighted inline array, potted geophones, and linear inline array. Figures 3A and 3B compare bumper-to-bumper vibrator array without move-up versus the 225-ft-long production pattern with 11 move-ups. Each record was obtained using 12 sweeps, 10 to 50 Hz, and 12 s sweeps. Data were recorded summed and correlated but are otherwise unprocessed.

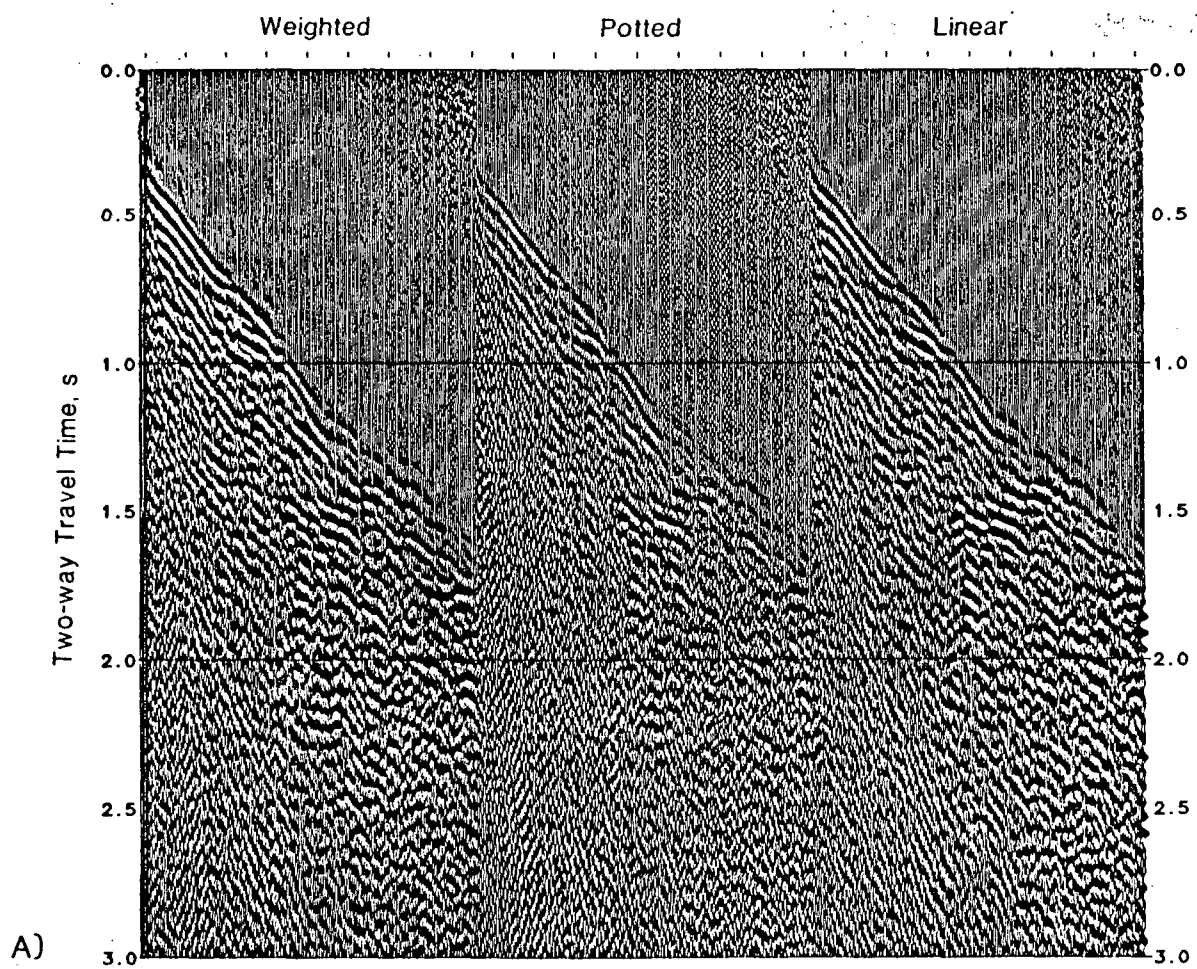

Figure 4. Common source gathers from parameter testing from Vibrator Points (VPs) at (A and B) St. 652. Each source gather shows the output recorded by the three geophone arrays tested: weighted inline array, potted geophones, and linear inline array. Figures 4A and 4B compare a 225 ft vibrator pattern with move-ups between each sweep with a 165-ft-long vibrator pattern with move-up after every other sweep. Each record was obtained using 12 sweeps, 10 to 50 Hz, and 8 s sweeps. Data were recorded summed and correlated but are otherwise unprocessed.

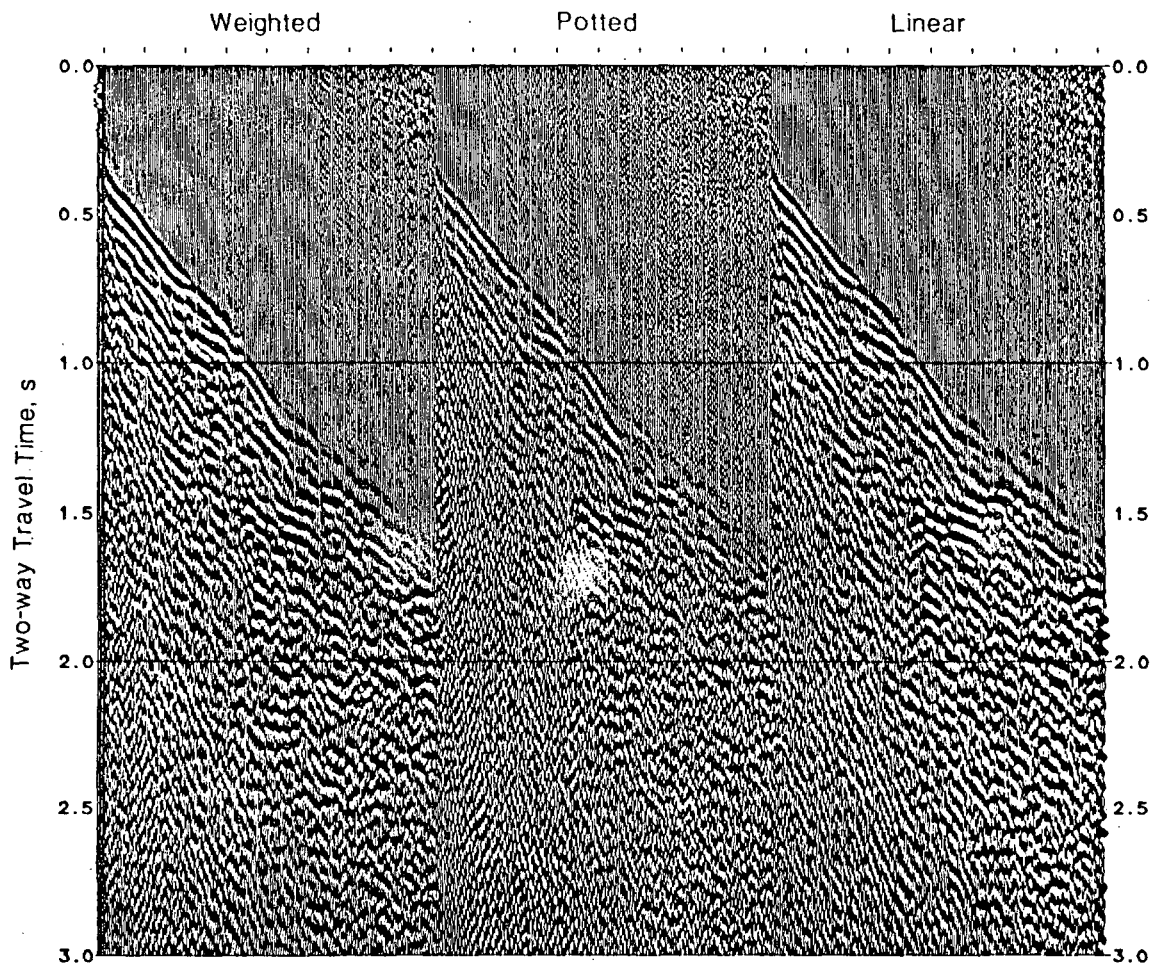
Weighted
Potted
Linear
Two-way Travel Time, s
0.0
0.5
1.0
1.5
2.0
2.5
3.0

B)

Fig. 4

A)

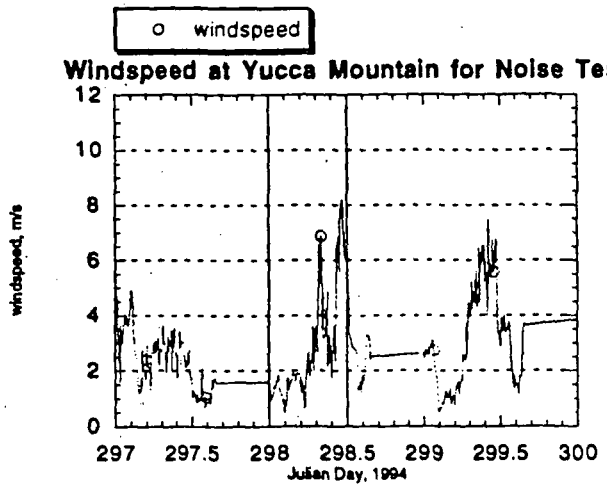
windspeed
Windspeed at Yucca Mountain for Noise Test
windspeed, m/s
0
2
4
6
8
10
12
297
297.5
298
298.5
299
299.5
300
Julian Day, 1994

B)

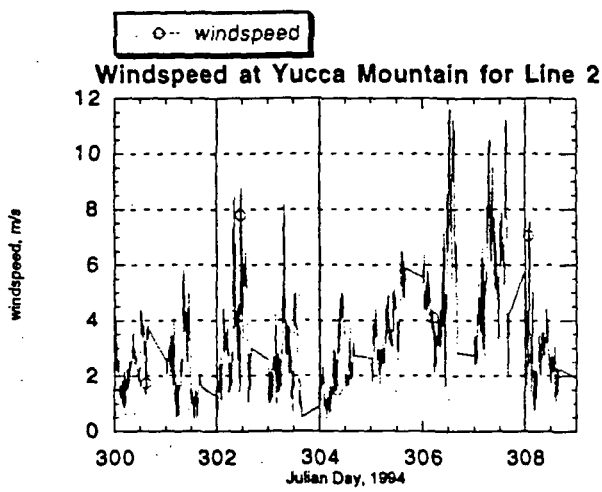
windspeed
Windspeed at Yucca Mountain for Line 2
windspeed, m/s
0
2
4
6
8
10
12
300
302
304
306
308
Julian Day, 1994

C)

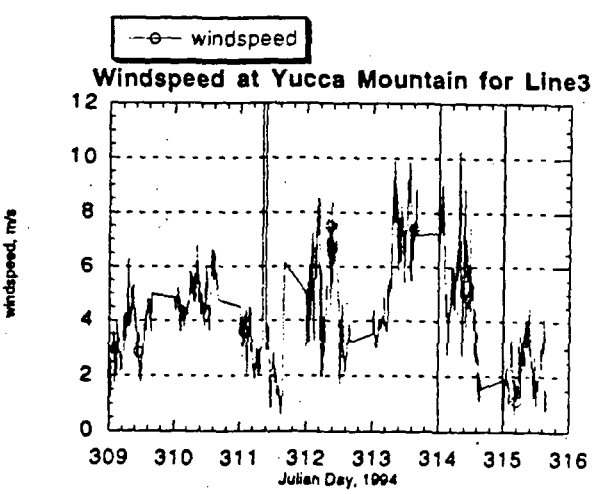
windspeed
Windspeed at Yucca Mountain for Line3
windspeed, m/s
0
2
4
6
8
10
12
309
310
311
312
313
314
315
316
Julian Day, 1994

Fig. 5

D)

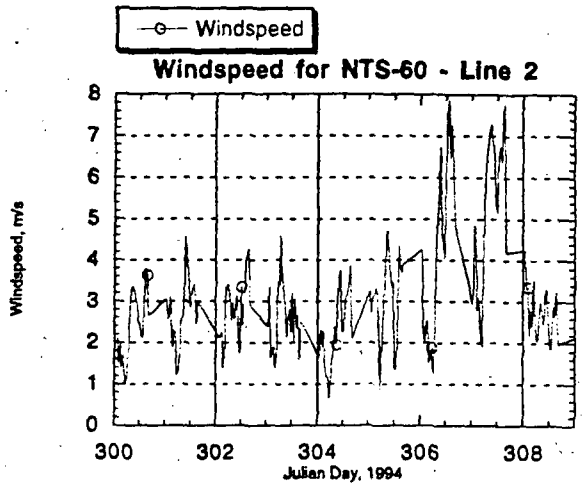

E)

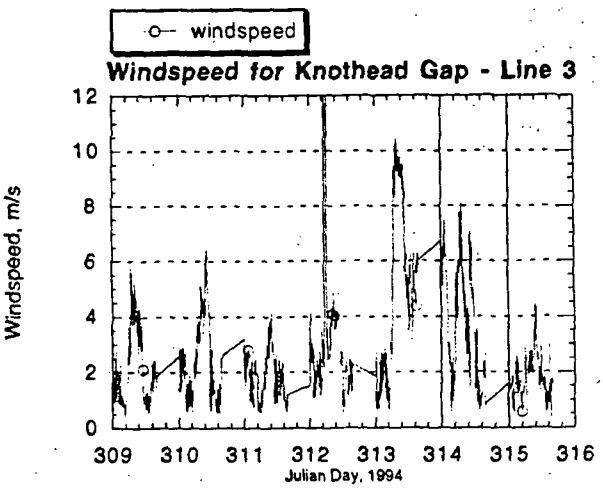

Figures 5A to 5E. Wind speed data (in m/s) recorded at Yucca Mountain (figs. 5A to 5C), NTS-60 (fig. 5D), and Knothead Gap (fig. 5E) during seismic field work. Data for each seismic line are plotted against Julian day; corresponding calendar days are also indicated. Data at Yucca Mountain and Knothead Gap were recorded at 10 minute intervals; data at NTS-60 were recorded hourly. Wind speed values in excess of 12 m/s indicate missing wind speed data for that time.

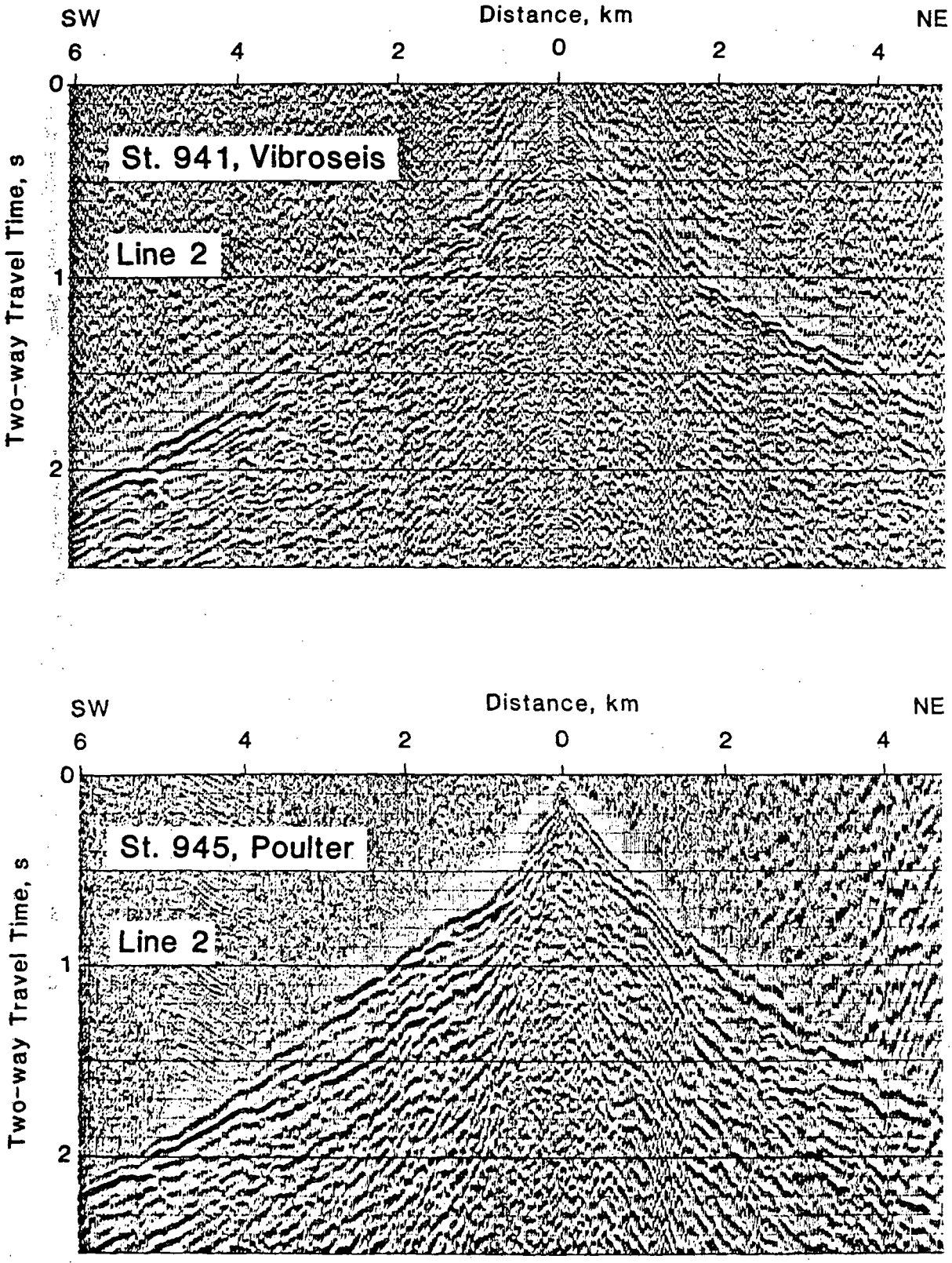

Figure 6. Comparison of shot records obtained using vibrator and Poulter sources at St. 941 on Line 2. Records are unprocessed apart from vibroseis correlation.

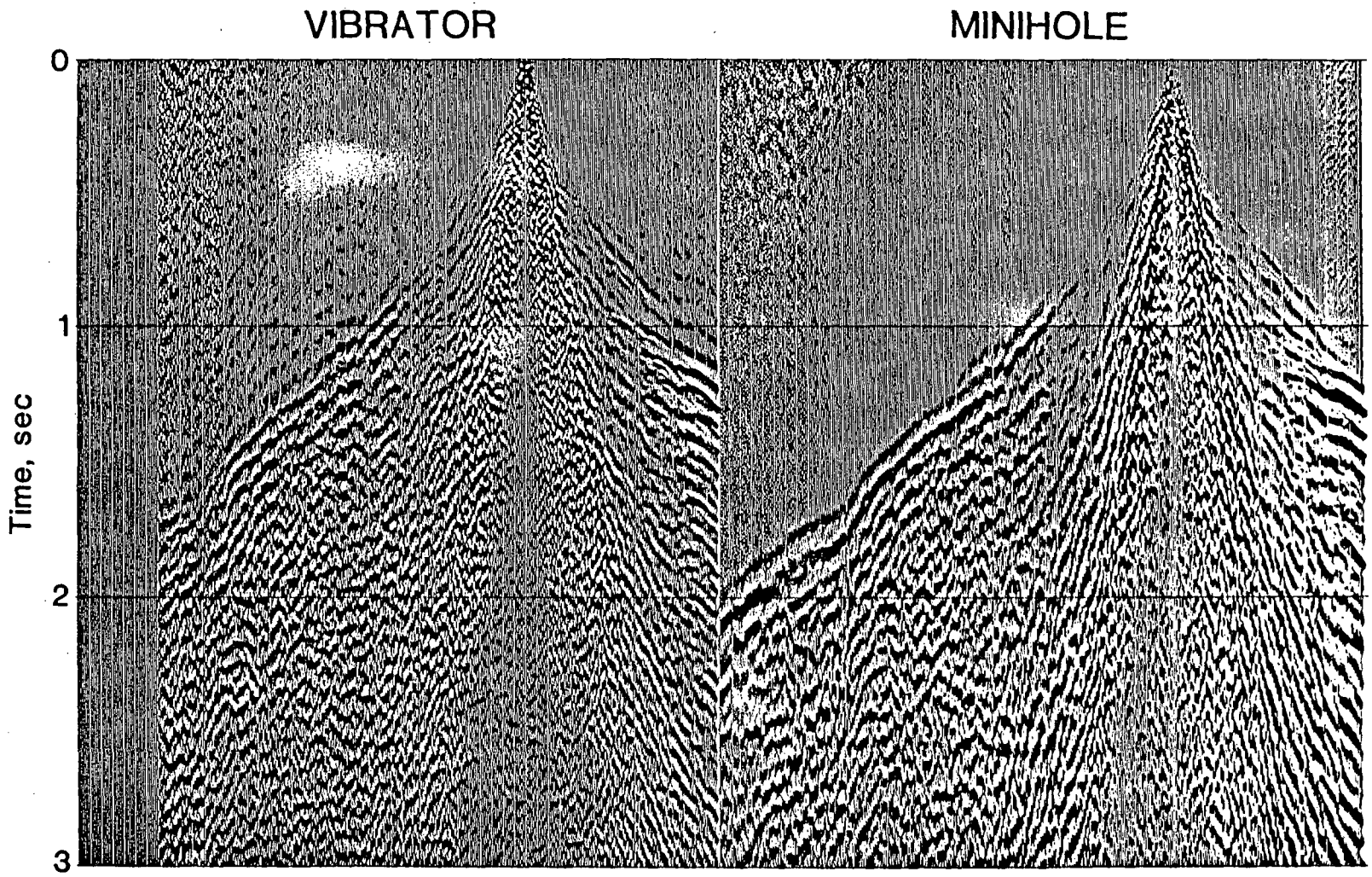

Figure 7. Comparison of shot records obtained using vibrator and minihole sources at St. 416 on Line 3. Records are unprocessed apart from vibroseis correlation.

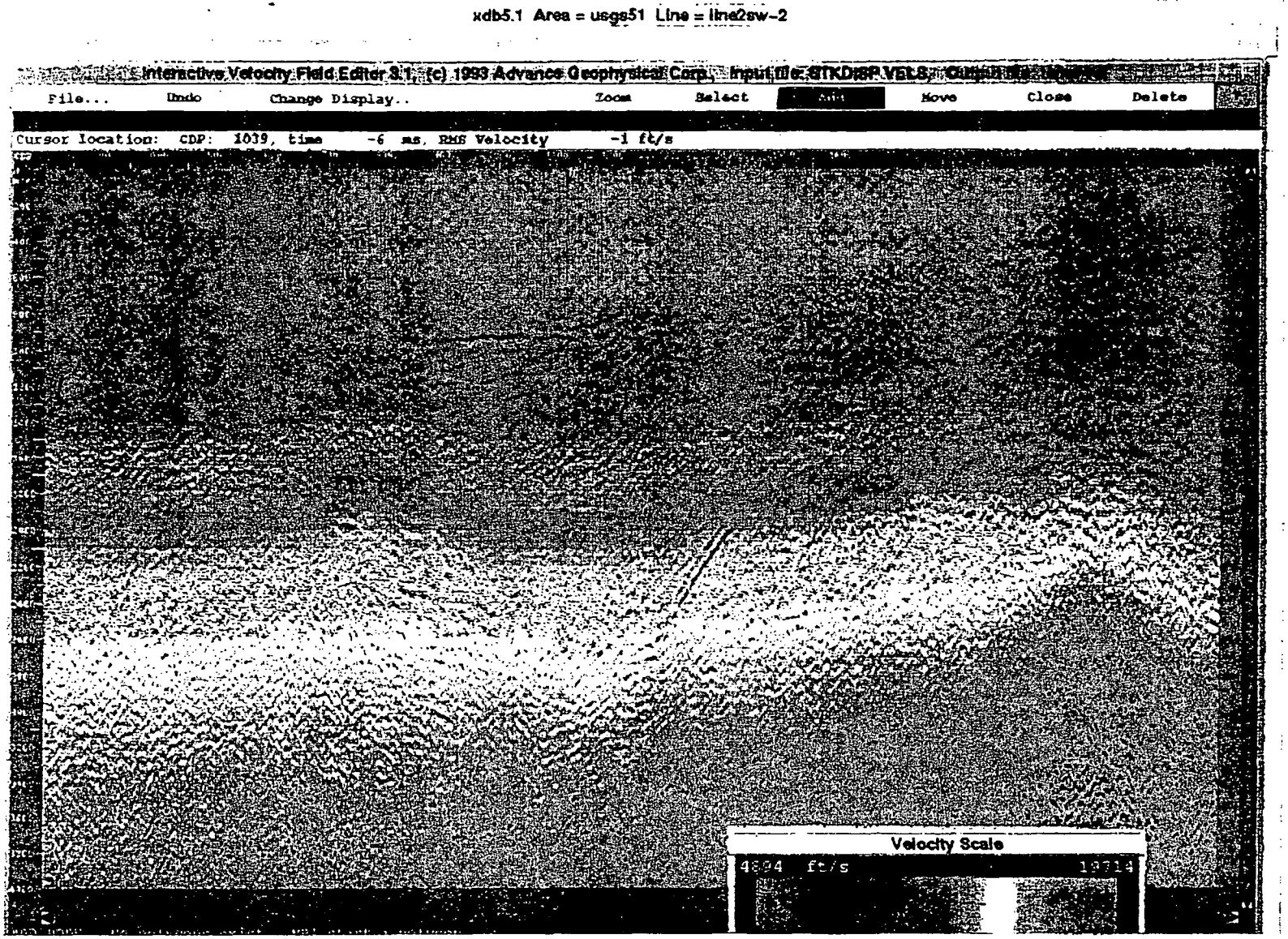

Figure 8A. Stacking velocities used for (A) Line 2, and (B) Line 3, superimposed on the final section of each line. Velocities are shown in terms of two-way travel time and CDP number. 80 CDPs equal one km.

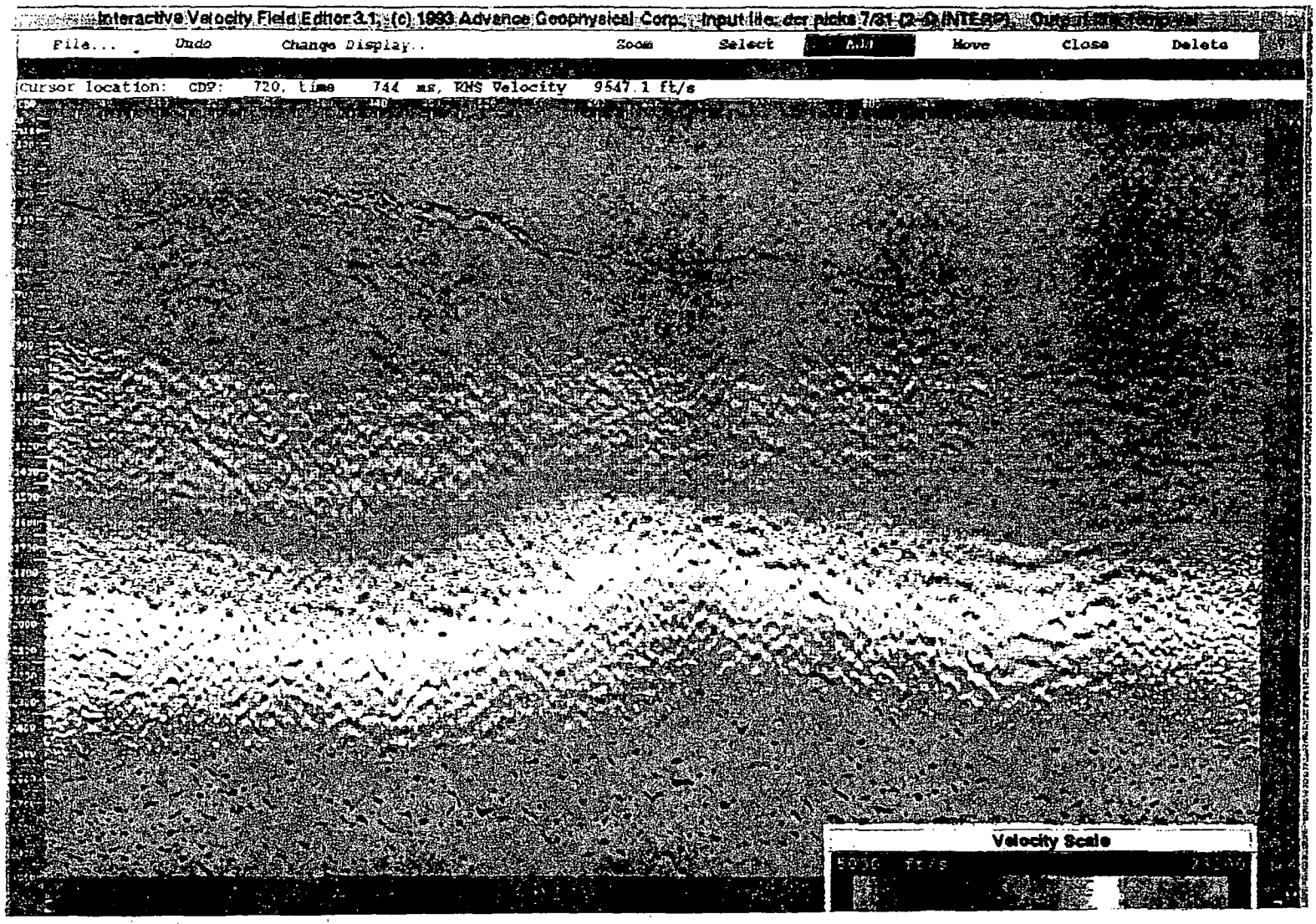

Figure 8B. Stacking velocities used for (A) Line 2, and (B) Line 3, superimposed on the final section of each line. Velocities are shown in terms of two-way travel time and CDP number. 80 CDPs equal one km.

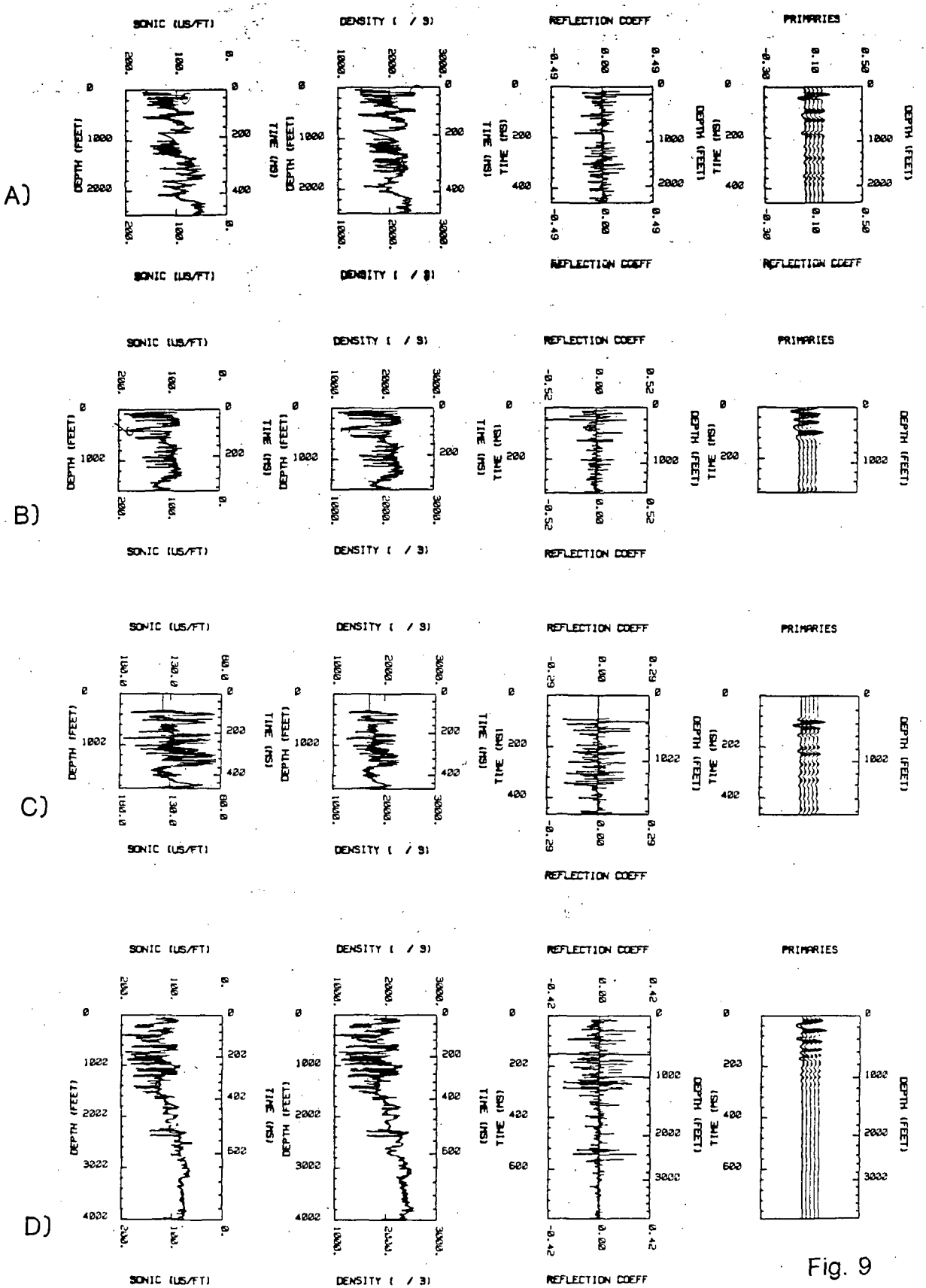
A)
B)
C)
D)
SONIC (US/FT)
DENSITY (/ 3)
REFLECTION COEFF
PRIMARIES
DEPTH (FEET)
TIME (MS)

Fig. 9

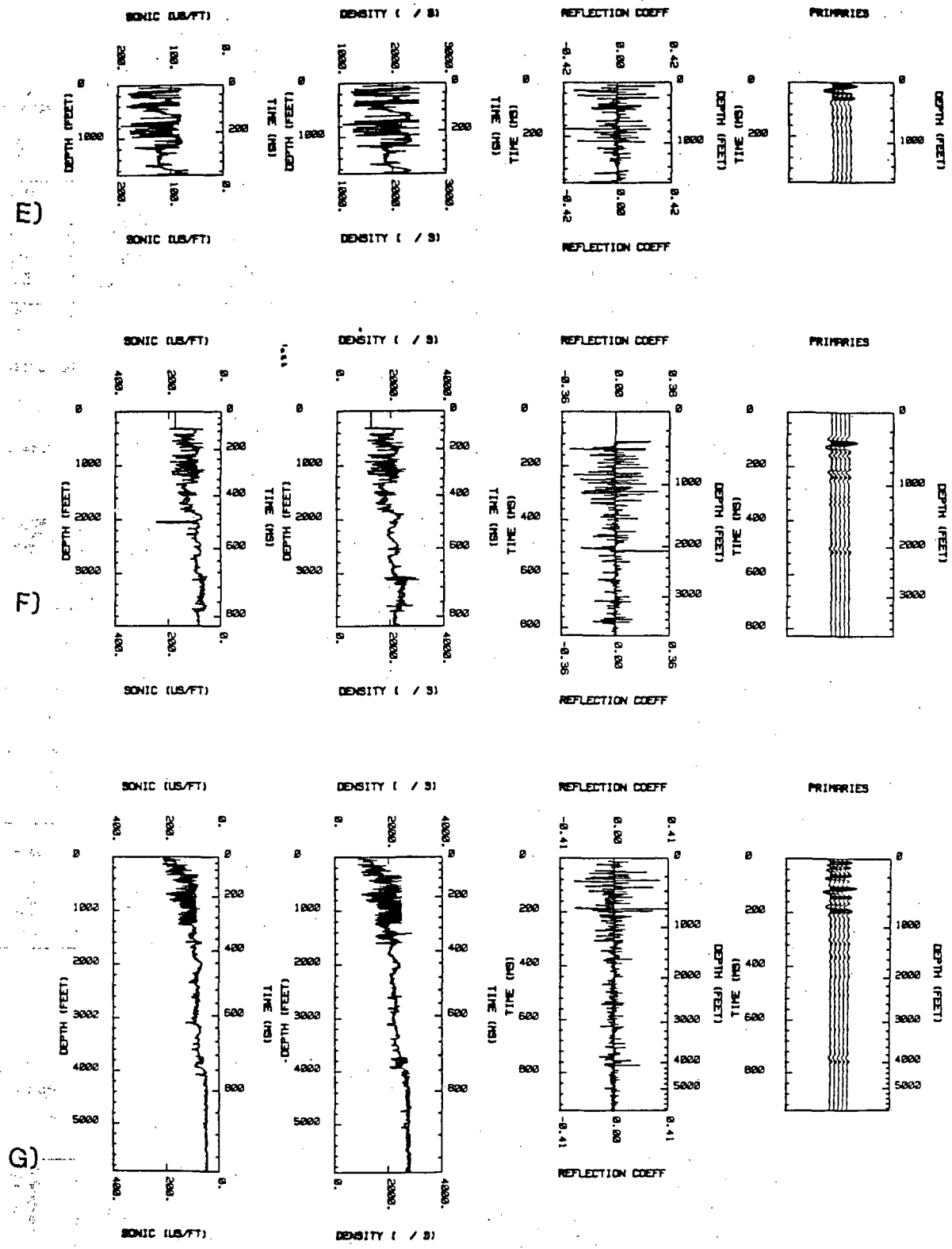

Figure 9. Well logs and synthetic seismograms for seven wells along Lines 2 and 3. For each well the sonic log (in microseconds/ft), density log (in kg/m^3), reflection coefficients, and synthetic seismograms are provided both as functions of two-way travel time and depth. Seismograms were calculated using a 30-Hz Ricker wavelet. Wells are: (A) USW VH-1, (B) USW WT-7, (C) USW UZ-6, (D) USW H-4, (E) UE-25 UZ-16, (F) USW H-6, and (g) UE-25 p#1.

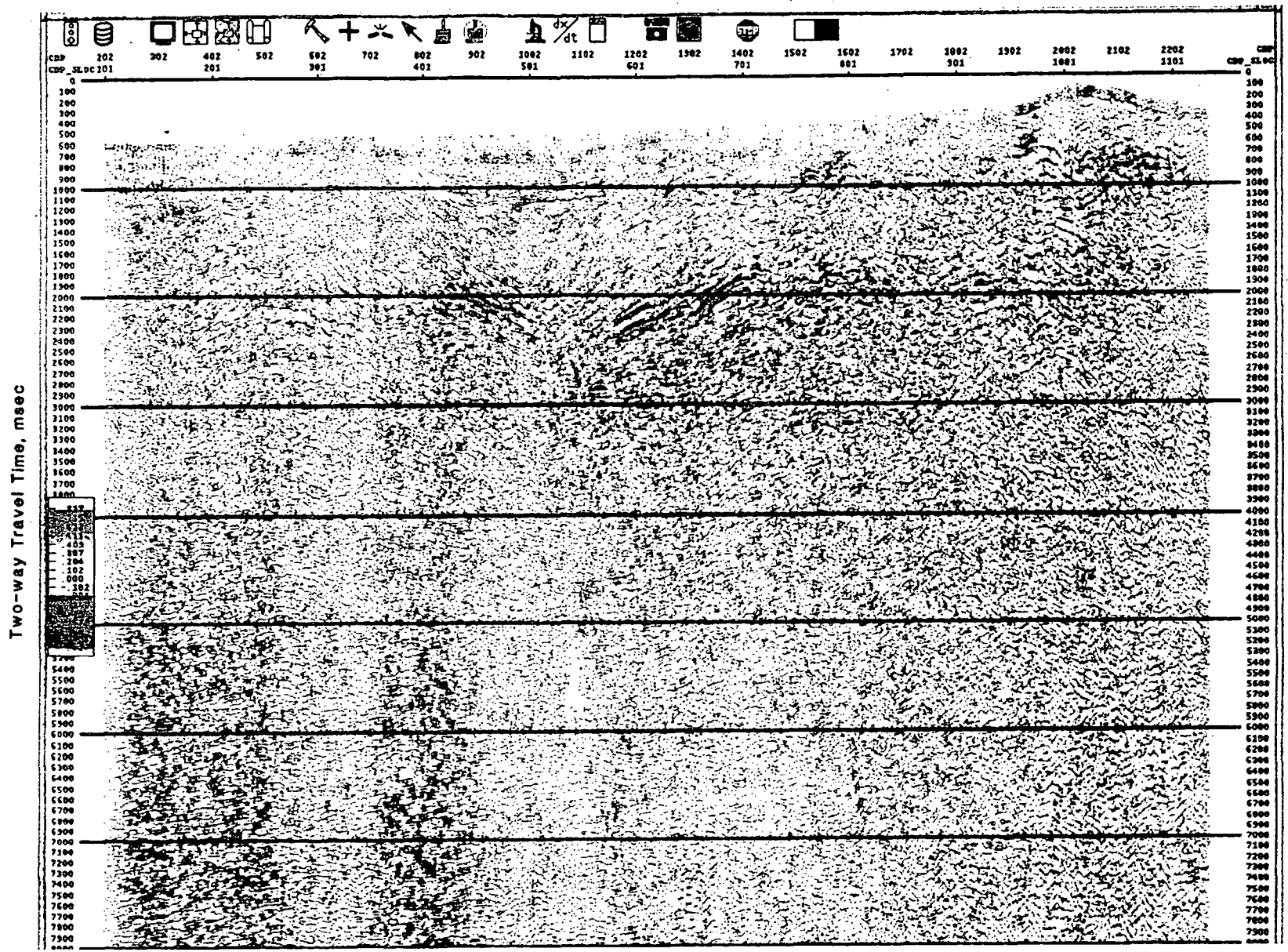

Figure 18. Uninterpreted section produced by intermediate processing of Line 2 showing section down to 8 s. This section has not been depth-converted and does not include final stacking velocities and statics. 40 stations (80 CDPs) equal one km.

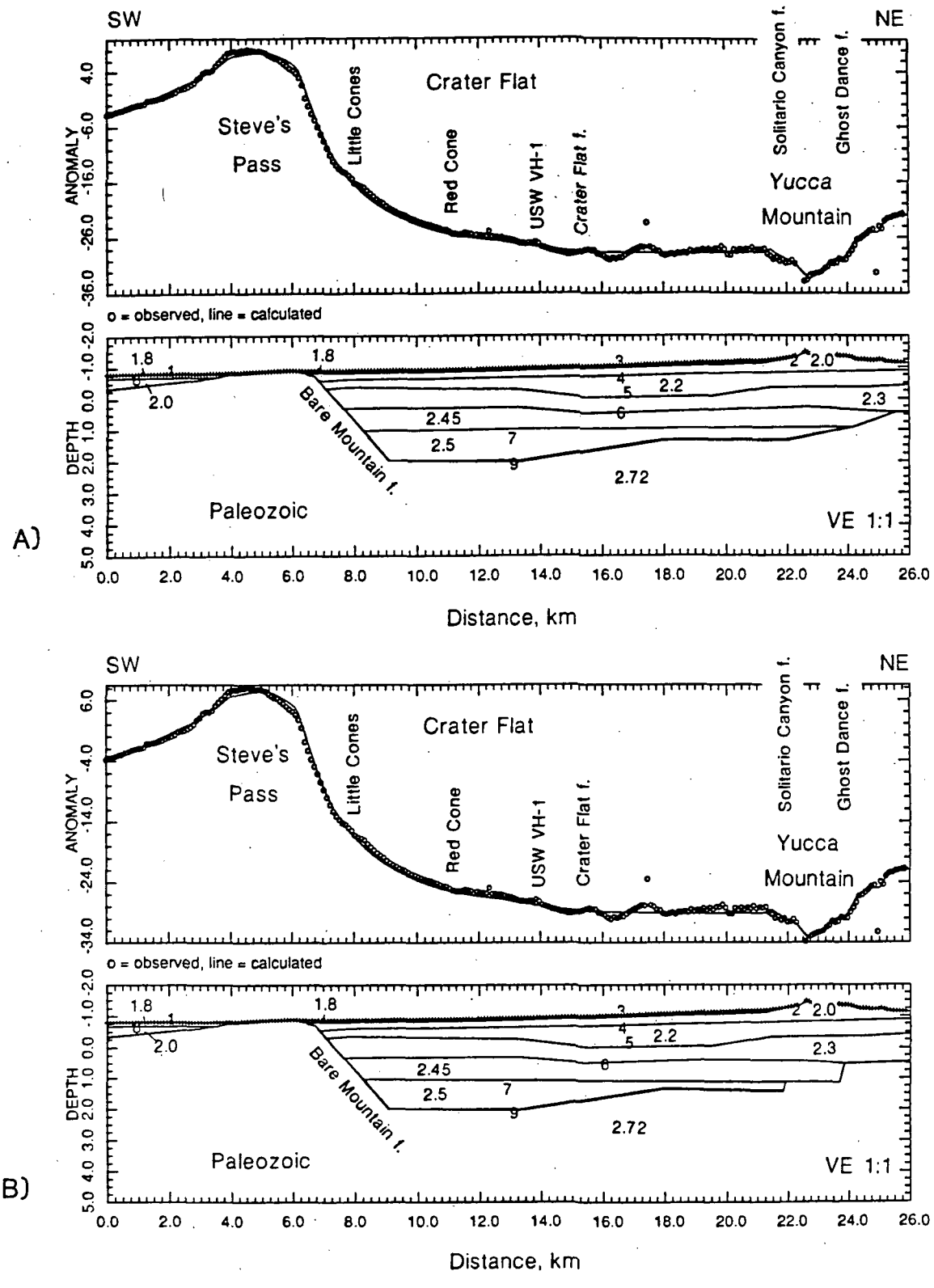

Figure 19. Isostatic gravity anomaly model for Line 2. The start of the seismic line (St. 101) is at model km 0, the end of the seismic line (St. 1133) is at km 26. Models include: (A) a single step in the top of Paleozoic basement beneath Yucca Mountain, and (B) two steps in top of Paleozoic basement beneath Yucca Mountain. Layer densities are given in g/cm^3. Zero elevation on the depth model corresponds to sea level. Geographic and borehole features are given for reference; fault is abbreviated as "f".

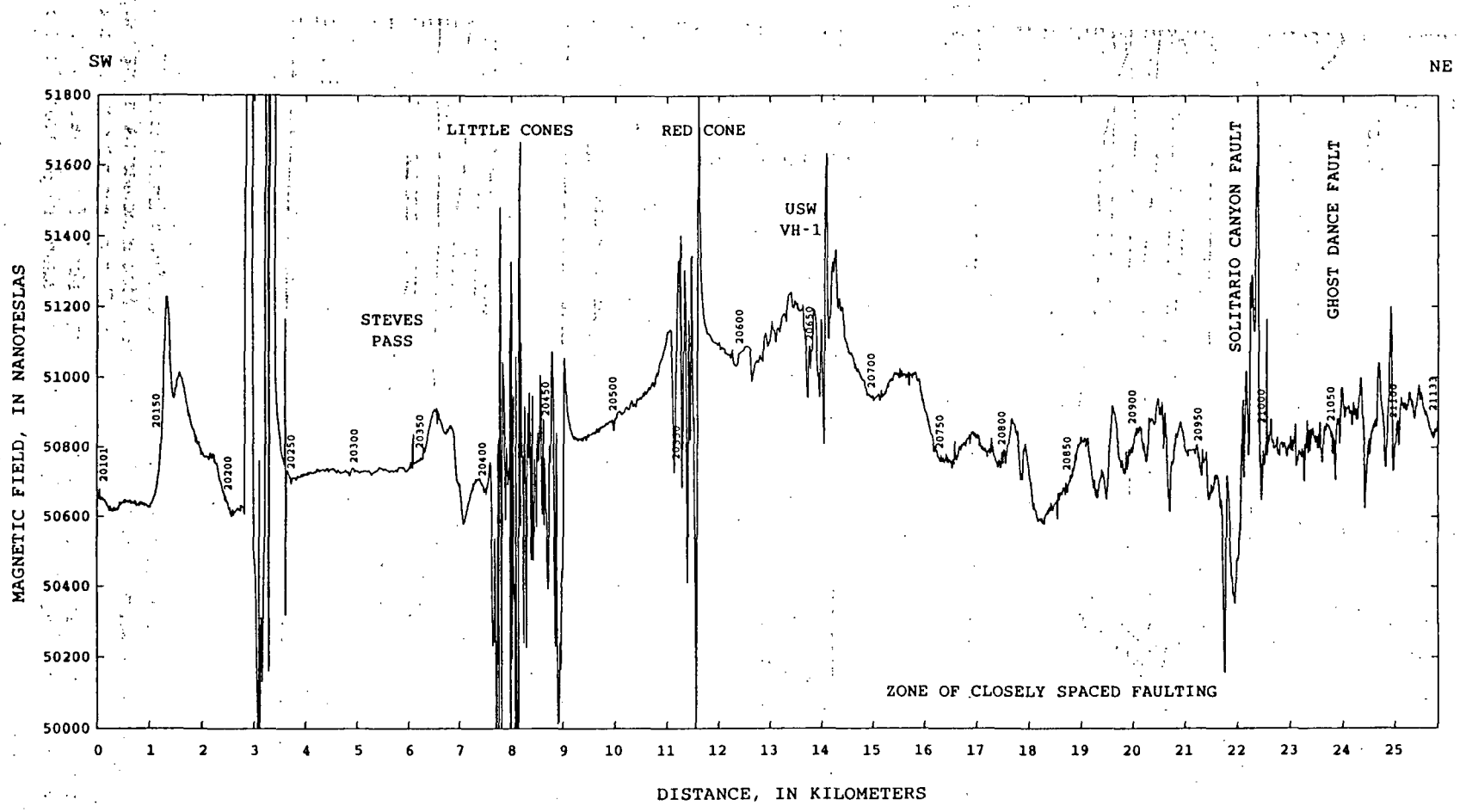

Figure 20. Ground magnetic anomaly data along Line 2. The start of seismic Line 2 is at 0 km, and the end of the line is at km 26. Note the short wavelength anomalies in the eastern half of Crater Flat and at Yucca Mountain. Powerlines near Highway 95 cause large anomalies at km 3.2.

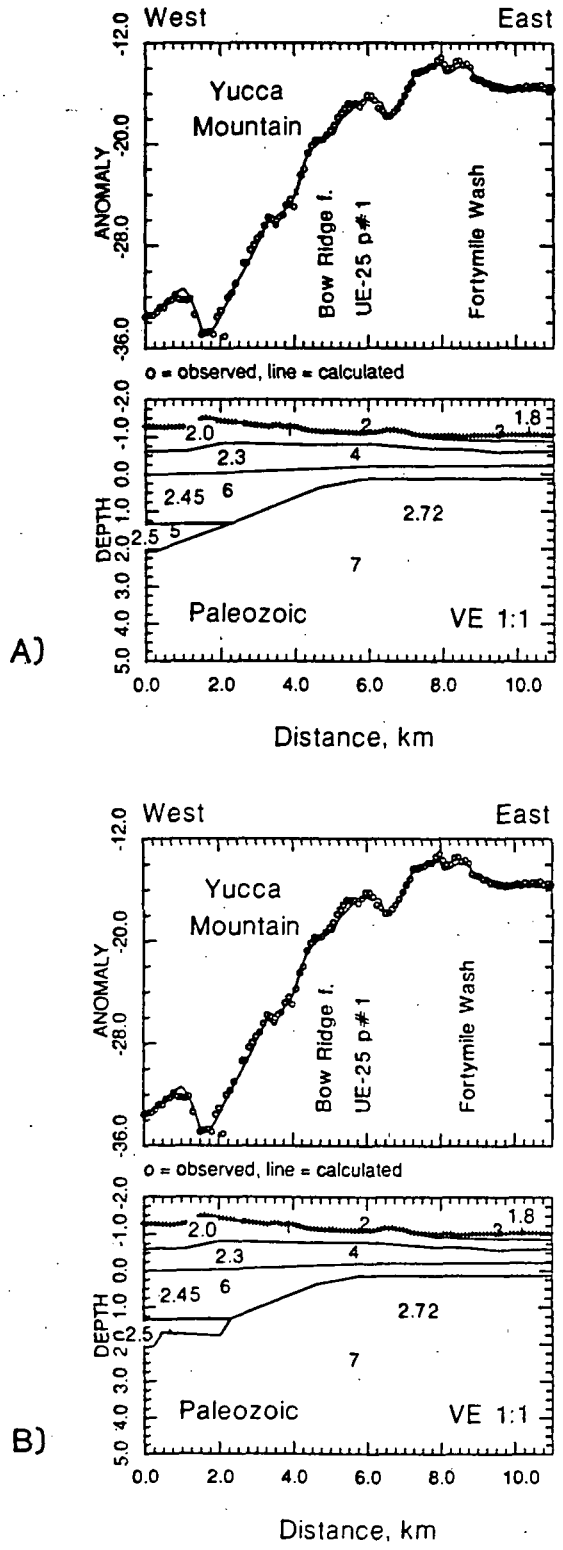

Figure 21. Isostatic gravity anomaly model for Line 3. The start of the seismic line (St. 101) is at km 0, the end of the seismic line (St. 541) is at km 11. Model is constrained by depth to Paleozoic at UE-25 p#1. Models include: (A) a single step in the top of Paleozoic basement beneath Yucca Mountain, and (B) two steps in top of Paleozoic basement beneath Yucca Mountain. Layer densities are given in g/cm^3. Zero elevation on the depth model corresponds to sea level. Abbreviation "f" denotes fault.

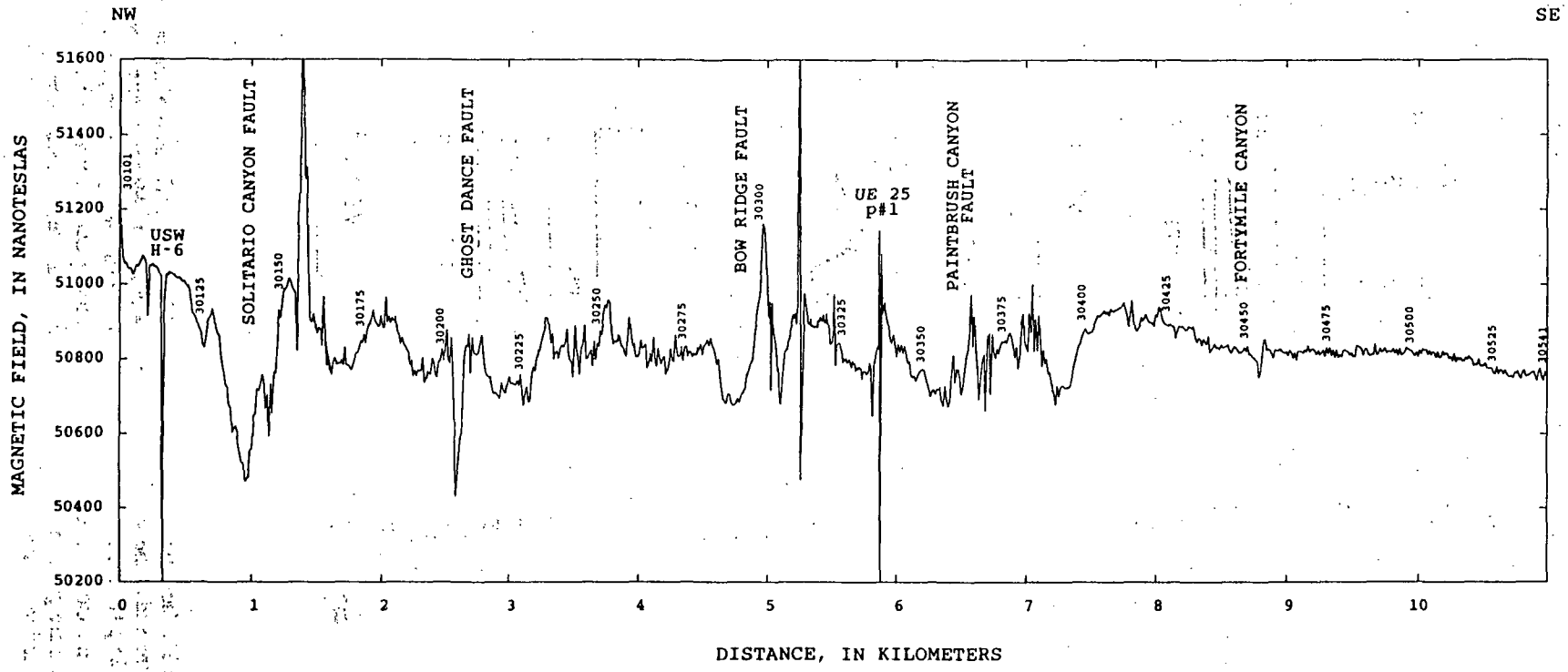

Figure 22 Ground magnetic anomaly data along Line 3. The start of seismic Line 3 is at 0 km, and the end of the line is at km 11. Note the absence of any significant anomaly over Fortymile Wash and presence of anomalies at wells along the line.

Brocher et al. 96

* data collected fall of 1994 ; hybrid mix of seis sours: vibrators, Poulter shots, mini-hole patterns, explosive shot holes
* 37 Km of high-fold seis refl lines; VSPs, well logs (60-125)

Line 2: 26 km NE from Amargosa Desert → Steve's Pass → Crater Flat → Yucca Mtn

Well UE-25 UZ-16

Amargosa Desert: poor in Tv; 1 Km W dipping Σ is Pz/T cont.; 900 m

Steve's Pass: little coherent seis energy – no Tv; few refl in deformed Proterozoic & Paleozoics; lower crust refl. – top @ 15 km

Crater Flat: best data of survey; @ 150 m bs flows; NW dip basin, to 1.2 km deep; @ 3500 m cont r; @ 5300 m r (Pe / Pz); disc low-fre refl @ 3000 m – CFF to FWF Fatigue Wash; Pz T ?; Fair → Good

Yucca Mtn: refl data to inter; some useful mappable seis r. @ 500 m top of Prow Pass Tuff; 3.6 Km Pz/T; 3 K deep; agrees w. grav. 2.5 to 3 Km

inferred top of Paleozoic sec traced discontinuously beneath Yucca Mtn. offset by high mod ∠ fault w/ Crater Flat much more lateral continuity; east bdry is series of antithetic down-to-west normal faults which drop Pz 750 to 1000 m beneath YM.

int. ~500 m W crest YM

Line 3: 11 Km easterly from well USWH-6 → Yucca Mtn → Fortymile Wash → Jackass Flats

Water r @ 500 m

UE-25 p#1

Yucca Mtn: 800

Jackass Flats: good; Pz/T @ 800; Fair to good-JF

GDF & Jackass Flats: 2100 to 1800 m d Pz/T; several small faults, <150 m offset

Tv – Flat

complex faulting imbricate F.Z.

useful, lower quality data

2nd refl mapped discontinuously at ~2100 to 1800 m dept between the Ghost Dan Fault and Jackass Flats as Pz/T contact

"we interpret several faults offsetting the Pz/T <150 m